The Pennsylvania State University

The Graduate School

College of Engineering

DEVELOPMENT OF A WET GRID MODEL FOR TWO – PHASE DISPERSED FLOW FILM BOILING PHENOMENA

A Thesis in

Mechanical Engineering

by

Sriram Goverapet Srinivasan

© 2010 Sriram Goverapet Srinivasan

Submitted in Partial Fulfillment

of the Requirements

for the Degree of

Master of Science

December 2010

The Thesis of Sriram Goverapet Srinivasan was reviewed and approved* by the following

Fan Bill Cheung

Professor of Mechanical and Nuclear Engineering

Thesis Advisor

Savas Yavuzkurt

Professor of Mechanical Engineering

Karen A. Thole

Department Head

Mechanical and Nuclear Engineering Department

*Signatures are on file in the Graduate School

ABSTRACT

The present study focuses on the development of a Wet Grid Model to describe the wet grid phenomenon observed during the reflood stage of a postulated Loss of Coolant Accident (LOCA) in a nuclear reactor. At high flooding rates, it has been observed that the spacer grids at elevations above the quench front undergo rewetting much earlier than the fuel rod. A consequence of this is the establishment of a liquid film on the surface of the spacer grid. Liquid droplet sizes found downstream of a wet grid are larger than those found upstream of the grid indicating a distinctly different mechanism of droplet generation as compared to a dry grid scenario for which the droplets decrease in size as they pass through the grid. In this study, a possible mechanism is postulated and a mathematical model is derived for the same.

The wet grid phenomenon is postulated to be consisting of four individual processes. Firstly, the deposition of droplets from the dispersed two phase mixture onto the spacer grid surface, then the establishment of a liquid film of equilibrium thickness on the surface of the spacer strap, thirdly, the entrainment of liquid ligaments from the liquid film due to the shear action of the steam flow and finally the breakup of these ligaments into a number of fine droplets downstream of the grid. A mathematical model is formulated for each of these processes which can be used to predict the droplet diameter downstream of a wet grid, given the flow and system conditions upstream of the grid. In addition, a numerical based correlation is proposed to obtain the downstream to upstream ratio of the sauter mean diameter of droplets in a wet grid situation.

The flow of superheated steam through the span of a wet spacer grid results in a significant de – superheating and acceleration of the steam due to the evaporation of the liquid film on the surface of the wet spacer grid. The simultaneous effect of steam de – superheating and

acceleration greatly enhances the heat transfer rate from the surface of the nuclear fuel rod, downstream of a wet grid. A mechanistic model is proposed to determine the Grid Enhanced Heat Transfer (GEHT) downstream of a wet grid. The numerical solution to the model equations shows that over a void fraction range of 0.99 to 0.999, the equilibrium film thickness varies between 0.12 and 0.1 mm while the average liquid film velocity varies between 0.7 and 0.1 m/s. The downstream to upstream ratio of the sauter mean diameter of the droplets was found to vary between 2.75 and 0.8. A reduction of around 100 deg. C in the steam temperature was obtained as it flows through the span of the wet spacer spacer grid. A wet grid was found to be more effective in augmenting heat transfer than a dry grid under the same flow conditions. This augmentation was found to be as much as three times higher for void fractions very close to unity. Results obtained from the models, however, are still parametric in nature since no experimental data under wet grid like conditions is available in the literature for model development and validation. Future experiments to obtain the much needed droplet data under wet grid conditions is suggested at the end of this work. Once the present models are validated, they can be implemented directly into best estimate systems analysis codes such as COBRA – TF and TRACE for predicting the rate of cooling of the fuel rods during the reflood transients following a LOCA in a nuclear reactor.

TABLE OF CONTENTS

LIST OF FIGURES

LIST OF TABLES

ABBREVIATIONS

COBRA – TF	COolant Boiling in Rod Arrays – Three Fluid
DFFB	Dispersed Flow Film Boiling
GEHT	Grid Enhanced Heat Transfer
LOCA	Loss Of Coolant Accident
PCT	Peak Cladding Temperature
PWR	Pressurized Water Reactor
RBHT	Rod Bundle Heat Transfer test facility
TRACE	TRAC – RELAP Advanced Computational Engine

NOMENCLATURE

A_{cor}	Area occupied by the Corner Portion of the Liquid Film
A_{film}	Area occupied by the Flat Portion of the Liquid Film
A_i	Droplet Interfacial area available for Heat Transfer
A_u	Cross Sectional Flow Area of a Unit Cell
A_v	Planck Mean Absorption Coefficient of Steam
b	Width of the Spacer Grid
C	Concentration of the Liquid Droplets in the Two Phase Mixture within the Spacer Grid Span
c_1	Fraction of the Spacer Grid Surface occupied by the Flat Portion of the Liquid Film
c_p	Specific Heat Capacity of Superheated Steam
d_0	Sauter Mean Diameter of Droplets Upstream of a Wet Grid
d_{32}	Sauter Mean Diameter of the Droplets formed Downstream of the Wet Grid
$(d_{32})_{ratio}$	Downstream to Upstream Ratio of Sauter Mean Diameter of Droplets in a Wet Grid Scenario
d_{jet}	Diameter of the Liquid Jet Issuing from the Trailing Edge of the Spacer Grid
D_d	Diameter of Droplets formed from the Breakup of the Liquid Sheet
D_{drop}	Diameter of the Droplets Formed from the Breakup of the Cylindrical Jet
D_{lig}	Diameter of the Cylindrical Ligament formed from the Primary Breakup of the Liquid Sheet
D_H	Hydraulic Diameter of the Unit Cell
eff	Relative effectiveness of a Wet Grid in Comparison to a Dry Grid in Augmenting Heat Transfer Downstream of the Spacer Grid
f_{ig}	Interfacail Friction Factor between the Two Phase Mixture and Liquid Film
F_{ij}	View Factor between the i^{th} and j^{th} Surface in Radiation Analysis
g	Acceleration due to Gravity
G_e	Mass Flux of Entrained Droplets

G_v	Mass Flux of Steam
h	Convective Heat Transfer Coefficient at the Liquid Film – Steam Interface
H	Thickness of the Liquid Film on the Surface of the Spacer Grid
J_i	Radiosity of the i^{th} Surface in Radiation Analysis
k	Thermal Conductivity of Steam
k_D	Turbulent Deposition Constant
k_{max}	Wave Number of the Most Unstable Disturbance in the Liquid Sheet
L_m	Mean Beam Length
$\dot{m}_{DE}$	Mass Rate of Liquid Droplet Deposition
$\dot{m}_E$	Mass Rate of Liquid Entrainment from the Liquid Film
$\dot{m}_{EV}$	Mass Rate of Evaporation from the Liquid Film
$\dot{m}_f$	Mass Flow rate of Liquid Droplets Upstream of the Spacer Grid
N_0	No. of Droplets Upstream of the Spacer Grid
N_1	No. of Droplets Downstream of the Spacer Grid that Escaped Through the Gap between the Spcer Grid and the Fuel Rod
N_{32}	No. of Droplets of Diameter d_{32} downstream of a Wet Grid
N_{jet}	No. of Droplets Generated from the Breakup of the Liquid Jet
N_{sheet}	No. of Droplets Generated from the Breakup of the Liquid Sheet
N_T	Total No. of Droplets Downstream of the Wet Spacer Grid
Nu	Nusselt Number
Nu_d	Droplet Nusselt Number
Oh_j	Jet Ohnesorge Number
Oh^*_j	Modified Jet Ohnesorge Number
P	Pressure
Pr	Steam Prandtl Number
q''_c	Convective Heat Flux to the Droplets

q''_w	Convective Heat Flux from the Fuel Rod
$(q''_w)_d$	Convective Heat Flux from the Fuel Rod in a Dry Grid Scenario
$(q''_w)_w$	Convective Heat Flux from the Fuel Rod in a Wet Grid Scenario
Q_{conv}	Convective Heat Transfer Rate to the Liquid Film
Q_{rad}	Radiative Heat Transfer Rate to the Liquid Film
r	Radial Co – ordinate of the Local Polar Co – ordinate System
r_{max}	Maximum Radius Corresponding to the Spacer Grid Surface
r_{min}	Minimum Radius Corresponding to the Liquid Film Interface
R	Ratio of the Steam Velocity to the Increase in Steam Velocity due to Droplet Evaporation in a Dry Grid Scenario
Re_l	Liquid Jet Reynolds Number
Re_{gc}	Gas Core Reynolds Number
R_{ij}	Thermal Resistance between the i^{th} and the j^{th} Surface in Radiation Analysis
S	Slip Ratio between the Droplets and Steam
T_i	Temperature of the i^{th} Surface in Radiation Analysis
T_{sat}	Saturation Temperature of the Liquid Corresponding to System Pressure
T_v	Superheated Steam Temperature
$\vec{u}_{cor}$	Velocity in the Corner Portion of the Liquid Film
$\vec{u}_{film}$	Velocity in the Flat Portion of the Liquid Film
$\bar{u}_{film}$	Average Velocity of the Flat Portion of the Liquid Film
$(u_g)_d$	Steam Velocity Downstream of a Dry Grid
$(u_g)_w$	Steam Velocity Downstream of a Wet Grid
u_{steam}	Velocity of Steam Upstream of the Spacer Grid
$u_z(y)$	Axial Component of the Velocity of Liquid in the Flat portion of the Liquid Film
U	Relative Velocity between the Liquid Sheet and the Co Flowing Steam

v_1	Velocity of the Escaped Droplets Downstream of a Wet Grid
v_{32}	Velocity of Droplets of Diameter d_{32}
V_{gc}	Superficial Velocity of the Two Phase Mixture Upstream of the Spacer Grid
$w(r,\theta)$	Axial Component of Velocity in the Corner Portion of the Liquid Film
$\bar{w}_{cor}$	Average Velocity of the Corner Portion of the Liquid Film
We_j	Liquid Jet Weber Number
x	Mass Quality of the Two Phase Mixture
z	Axial Co – ordinate Direction
Δm_f	Rate of Depletion of Liquid Mass due to Droplet Evaporation
Δm_g	Rate of Increase of Steam Mass due to Droplet Evaporation
ΔT_g	Reduction in Steam Temperature as it passes Through a Wet Spacer Grid
$(\Delta u_g)_d$	Increase in Steam Velocity Due to Droplet Evaporation Downstream of Dry Grid
$(\Delta u_g)_w$	Increase in Steam Velocity Due to Droplet Evaporation Downstream of Wet Grid

Greek Letters

α_e	Void Fraction of the Entrained Liquid Droplets
α_v	Void Fraction of Steam
ε	Spacer Grid Blockage Ratio
ε_i	Emmisivity of the i^{th} Surface in Radiation Calculation
θ	Angular Co – ordinate of the Local Polar Co – ordinate System
λ	Wavelength of the Disturbance Wave with Maximum Growth Rate in the Liquid Jet
μ_g	Dynamic Viscosity of Steam
μ_l	Dynamic Viscosity of Liquid
ν_l	Kinematic Viscosity of Liquid

ν_v	Kinematic Viscosity of Steam
ρ_g	Density of Steam
ρ_{gc}	Effective Density of the Two Phase Mixture
ρ_l	Density of the Liquid
σ	Liquid Surface Tension
τ_i	Interfacial Shear Stress

ACKNOWLEDGEMENTS

Firstly, I would like to express my sincere thanks and deep felt gratitude to my advisor Dr. Cheung for all his time, support, encouragement and guiding me through the course of this work. His immense knowledge in the field of Two Phase flows and Nuclear Reactor Thermal Hydraulics was instrumental in the completion of this work. He has been a constant source of motivation for the past one and half years. Thank you, Professor. I was indeed fortunate to study under you.

Secondly, I would like thank the sponsoring agency, Nuclear Regulatory Commission (NRC), for the financial support they provided without which it would have been impossible to perform this work.

I would like to thank my parents and brother for their constant support and encouragement all through my life. All that I have achieved in my life is mainly because of this support and motivation. Thanks Amma, Appa and Bro. I shall remain greatly indebted to you forever.

I would like to thank my office mate Douglas Miller for a number of insightful discussions we had during the course of this work. It was a great experience to work with you.

I also wish to thank my friends at Penn State who made life at State College such a wonderful experience.

Finally, I would like to thank the Penn State University for giving me the opportunity to pursue graduate studies.

CHAPTER 1

INTRODUCTION

1.1 Wet Grid Phenomena and Grid-Enhanced Heat Transfer (GEHT)

In order to ensure that thermal-hydraulic safety constraints are met in the design and operation of a pressurized water reactor (PWR), it is necessary to understand and model the heat transfer within the reactor fuel assemblies. The most limiting accident that can occur within the primary system of a PWR is the postulated large break Loss Of Coolant Accident (LOCA). In a LOCA event, the major concern is the peak cladding temperature (PCT) that dictates the maximum allowable fuel rod linear power level. During the reflood phase of a LOCA, liquid coolant begins to reach and quench the bottom of the fuel rods. This quenching causes a large amount of heat being transferred from the rods to the coolant, resulting in the production and upward flow of steam which entrains liquid droplets and transports them to higher elevations. The entrained liquid droplets help cool the steam and therefore the fuel rods at these higher elevations reducing the PCTs while allowing the quench front to propagate upward along the rods.

Spacer grids are an intricate part of the fuel assembly design. They provide support for the fuel rods and maintain a constant distance between rods in a tight lattice, secure flow passage, and prevent damage of the assemblies from flow-induced vibration. The environmental condition of a grid spacer has been observed to play an important part in the droplet breakup and liquid re-entrainment processes, as a dry grid versus a wet grid result in significantly different dispersed flows downstream of the grid location. As described in the Letter Report by Cheung and Goverapet Srinivasan (2010), dry grid spacers are found to serve as an effective means of breaking large droplets into smaller droplets, thus substantially increasing the interfacial area

between the liquid droplets and the steam. The reduction in droplet size is known to be dependent upon the Weber number of the incoming droplets, the blockage ratio of the grid spacer, and the volume fraction of the droplets in the dispersed phase. For wet grid spacers, however, the grids appear to act as a potential source of droplets production. Under wet-grid conditions, a liquid film exists on the grid spacer which can be sheared off by the steam flow to form liquid ligaments and large droplets downstream, as evidenced by the experimental data obtained from the RBHT facility. Thus it is necessary to study and model the wet-grid phenomena and the associated wet-grid effects separately from those for dry grids.

During dispersed flow film boiling in the reflood stage of a large-break LOCA, there are several mechanisms of Grid Enhanced Heat Transfer (GEHT) taking place in a rod bundle that could affect the cooling of the fuel rods and thus the resulting PCTs. These mechanisms include:

- Flow acceleration due to flow blockage of the grid
- Flow restructuring and re-development of the velocity and thermal boundary layers through the grid
- Flow mixing and turbulent wakes behind the grid caused by mixing vanes or swirling vanes
- Fine turbulent mixing of the continuous phase caused by the relative motions of the dispersed phase
- Droplet breakup through the grid resulting in a significant increase in the interfacial heat and mass transfer area, thus promoting evaporative cooling
- Grid rewetting and subsequent entrainment of liquid ligaments and droplets downstream of the wet grid

- Two-phase augmentation due to evaporation of droplets that further accelerates the flow while de-superheating the steam
- Direct cooling of the fuel rods by the grid spacers serving as extended surfaces
- Radiative cooling of the fuel rods offered by the grid spacers.

Although the current versions of the transient analysis codes such as COBRA-TF and TRACE (version 6) have included many of the above mechanisms, it fails to adequately accounts for the GEHT due to the dry-grid and wet-grid effects which could have significant impact on the PCTs during the reflood transients. To quantitatively identify and model the dry-grid and wet-grid effects and to implement such models in TRACE is utmost essential to obtain better predictions of the thermal hydraulic response of a reactor core under LOCA scenarios. This work focuses on the wet-grid phenomena and the GEHT due to wet grids.

1.2 Major Objectives of the Present Work

The major objectives of the present work are

- To perform literature review on the droplet deposition, droplet entrainment formation and breakup of liquid ligaments as well as other wet-grid phenomena and prepare a relevant database.
- To develop a physics-based mechanistic model for the generation and entrainment of liquid droplets from a wet spacer grid.
- To develop a mechanistic model for the Grid Enhanced Heat Transfer (GHET) due to a wet grid.
- To identify new data needed for model validation and further development.

CHAPTER 2

LITERATURE SURVEY

The enhancement effects of spacer grids have been studied for many years. Most of the previous studies, however, have been focused on the GEHT for dry grids. Unlike the nuclear fuel rod, the spacer grid structures are unpowered. As a result, their temperatures are much lower than those of the fuel rods. This promotes earlier quenching of the grid structures in comparison to the fuel rods. Once quenched, a potential to develop a thin film on the surface of the grid spacer is established. This liquid film gains mass due to deposition of liquid droplets from the dispersed two-phase steam-droplet mixture while it loses mass by evaporation and shear entrainment from the trailing edge of the grid spacer.

Many experimental studies and empirical correlations have been reported in the literature on droplet deposition and entrainment in annular flows. A brief summary of some of the most important works in this field is provided below.

2.1 Literature Survey on Annular Flow Entrainment

Experimental data and correlations on this topic has been reported by a number of researchers in the past. While developing a database of such correlations and experimental data, particular attention was paid to the research works that utilized steam – water or air – water flow systems.

Keeyes et al [1]

They obtained measurements of liquid entrainment and liquid film flow rate for adiabatic steam – water flow in a vertical 3.7 m long 0.5 in diameter pipe for pressures ranging from 34 to 68 bar. A total mass flux in the range of ~1360 to ~2720 kg/m^{2}s was employed in the study. The entrainment rate was measured using a porous wall device to extract the liquid film flow.

Wurtz [2]

In this work, film flow rates, pressure drop and film thickness were measured for two tubular geometries. Steam – water mixture was used as the flow system and the operating pressure conditions varied between 30 & 90 bar while the mass flux ranged between 500 and 3000 kg/m^2s. The flow quality was varied between 0.08 and 0.6. The liquid film at the wall was extracted using a suction device. Entrained liquid flow rate was calculated at the difference between the total liquid flow rate and the wall film flow rate.

Singh [3]

The author reported liquid film flow rates and pressure drops for co current upward annular flow of steam – water mixture in a tube. The operating pressure varied between 68 and 82 bars. The total mass flux ranged between 272 and 952 kg/m^2s while the exit steam quality varied between 0.3 and 0.92. The test section employed was only 200 L/D long as a result of which the droplet entrainment from the annular liquid film may not be fully developed.

Dallman [4]

In this work, a correlation for the fraction of liquid entrained in fully developed annular gas liquid flows was obtained through the use of an approximate dynamic balance between the rate at which the liquid was atomized from the wall layer and the rate of deposition of liquid back to the wall film. The entrainment rate, local film thickness and pressure drop were measured over a wide range of flow conditions in a horizontal pipe. The effect of flow asymmetry in horizontal two phase flow was included in the development of the correlation.

Ishii &Grolmes [5]

These researchers first developed the inception criteria for droplet entrainment from co-current gas liquid annular flow. They proposed shearing off of the roll wave crests and wave

undercutting as the mechanisms for droplet entrainment for film Reynolds numbers above and below 160 respectively. Experimentally observed change in critical gas velocity for the onset of entrainment at a certain value of the film Reynolds number was explained to be due to the above mentioned change in entrainment mechanism.

Ishii et al [6]

They obtained a correlation for entrainment fraction as a function of three dimensionless groups namely, a dimensionless gas flux, total liquid Reynolds Number and a dimensionless diameter. The derived an expression for the distance necessary to reach quasi developed entrainment state. In the entrance region, they proposed an exponential relaxation form for the entrainment fraction that eventually reaches the fully developed value at the end of the development length. The entrainment model was obtained by considering the shearing off of the roll wave crests by streaming gas flow. The predictions of the correlations compared well with the experimental data in the pressure range of 1 to 4 atm, a liquid Reynolds number range of 370 to 6400 and a superficial gas velocity less than 100 m/s.

Sugawara [7]

The author reported an entrainment model for upward co-current annular flow that was based on a dimensionless gas velocity and a force balance that considers the effects of interfacial shear and surface tension at the wavy interface. A pressure correction factor, polynomial cure fit for the wave height and a logarithmic curve fit for the gas Reynolds number were also used in the model. Validation studies were carried out using the Film Dry out Analysis Code in Sub channels (FIDAS). Though the force balance considered the effect of interfacial shear and surface tension, the effect of gravity was not included.

Hewitt &Govan [8]

The authors presented a correlation for the critical film Reynolds number corresponding to the onset of entrainment based on the density ratio and viscosity ratio of the two fluids. However, this equation did not take into account the effect of surface tension. They also presented a correlation for dynamic droplet entrainment rate based on dimensionless groups and a curve fit to experimental data. Their correlation however had errors as large as one order of magnitude under certain flow conditions.

Nigmatulinet al [9]

The authors reported a correlation for dynamic droplet entrainment rate that accounted for the presence of a critical Weber number below which no entrainment is possible. A separate equation for the critical Weber number corresponding to the onset of entrainment in both laminar and turbulent flow was reported. This equation, for the first time, considered the influence of gravity force vector with reference to the flow direction. Their correlation compared well with the experimental data. In addition, a discussion on the possibility of collisions of depositing droplets resulting in additional entrainment was presented.

Lopez de Bertodano et al [10]

The authors used their air-water and Freon-113 experimental data to develop a correlation based on dimensionless groups like the film Reynolds number, Weber number and a density ratio. A double film extraction technique was used to measure the entrainment rate. The experiments were scaled to approach high pressure steam water flow conditions. The correlation was scaled by a factor to account for the average growth rate of ripples due to Kelvin-Helmholtz instability at the interface. However, the primary means of droplet entrainment in annular flow

(i.e., shearing off of roll wave crests) as suggested by Ishii and Grolmes [5] has not been considered in the development of the correlation.

Sawant et al [11]

The authors reported a correlation for the entrainment fraction based on their experiments using air-water and Freon-113 experiments that accounted for the existence of a critical gas and liquid flow rates below which no entrainment is possible. A new correlation for the minimum liquid film flow rate possible at the maximum entrainment condition was also proposed. Though the correlation compared favorably with air-liquid flow system data reported in the literature, significant differences were found in the prediction of steam-water data.

2.2 Literature Survey on Droplet Deposition

Paleev&Filipovich [12]

The authors performed experiments using air water flow system in a horizontal tube to measure the liquid deposition mass flux and obtained a correlation for the droplet deposition rate in terms of gas Reynolds number and the density ratio by fitting a curve to their experimental data. The experiments were carried out at atmospheric pressure and the local gas Reynolds number varied between $3x10^4$ and $8.5x10^4$. This correlation however does not have any dependence on the droplet size or liquid Reynolds number.

Namie& Ueda [13,14]

The authors obtained experimental data for droplet transfer to the duct walls, distribution of droplet velocity, droplet concentration and gas velocity for annular mist flow through a horizontal duct of rectangular cross section. They utilized air – water flow system with the mean diameter of liquid droplets varying between 27 and 40 microns. They found that the droplet deposition coefficient was affected by both gas velocity and droplet concentration. The velocity

distribution of the droplets was found to be fairly flat. In addition, the eddy diffusivity of the gas was found to reduce with increase in droplet concentration, resulting in a reduced deposition constant.

Issapour& Lee [15]

The authors performed experimental investigation of the droplet deposition from turbulent two phase mist flow onto a parallel vertical wall. They utilized air – water flow system with Reynolds number varying between $1.54x10^5$ and $4.2x10^5$ and a particle sizing two dimensional reference mode Laser Doppler Anemometry technique to obtain the data. A correlation for the droplet deposition coefficient was presented using their experimental data along with a postulated physical mechanism based on the apparent turbulent viscosity of the gas as felt by the particles and the most energetic eddy frequency of the flow.

Trela et al [16]

The authors presented a model for droplet deposition from turbulent gas flow on a vertical plate based on the stopping distance concept allowing for different turbulent diffusivities of the gas and droplets. Experiments were performed in a horizontal duct and the deposition investigation was done on a vertical plate mounted parallel to the duct wall. The experiments used air – water as the flow system at a pressure of 2 atm. The mean gas velocity in the duct varied between 1 and 14.1 m/s. The maximum droplet concentration during the investigation was 0.035 kg/m^3.

Hewitt &Govan [8]

The authors obtained a correlation for the droplet deposition rate based on their air-water experiments using ‘unidirectional deposition method’. They found that the deposition rate was a strong function of the concentration of droplets in the core. However, the influence of gas and droplet velocity on the deposition rate was not taken into account in their work.

Sugawara [7]

A deposition model was developed based on the turbulent droplet diffusion mechanism employing the heat-mass transfer analogy. The effect of concentration of droplets on the core was incorporated by using a curve fit to the non-dimensional deposition constant obtained from a number of experimental runs. Validation studies of the model were carried out using the FIDAS code. The model was however based on a very limited number of air water data obtained at atmospheric pressure. The applicability of the model to high pressure steam water flow systems may be questionable.

Nigmatulin et al [9]

The authors reported a the deposition correlation based on the theoretical analysis of droplet behavior in a turbulent flow and experimental results obtained from unheated air-water and steam-water flow experiments in a vertical tube. This relation takes into account the influence of gas and droplet velocity in the flow core on the deposition rate. The experiments with steam water flow were carried out at a pressure range of 1 to 10 MPa, gas velocity of 4 to 105 m/s and a total mass flow rate of $7x10^{-2}$ to $27x10^{-2}$ kg/s. For the air – water flow experiments the range of pressure was 0.18 to 0.45 MPa, liquid mass flow rate varied between $20x10^{-2}$ and $250x10^{-2}$ kg/s and the droplet volume fraction varied between 0.1 and 0.001.

Okawa&Kataoka [17]

The authors developed a correlation for droplet deposition rate in upward annular flow using the experimental data reported in the literature and physical arguments. It was found that the deposition mass transfer coefficient increases with an increase in the volumetric flux of gas phase at low droplet concentration while it decreases with the increase in droplet concentration at high droplet concentration. Thus the model used the superficial velocity of the gas as the primary

quantity of importance at low droplet concentrations while the droplet concentration itself was the determining factor at high droplet concentrations. Though the model was derived using available air – water experimental data, the authors found good agreement between model predictions and experimental data for high pressure steam – water flows.

Schadel et al [18]

Experiments were performed to measure the rate of deposition and atomization in vertical co current two phase annular flow in a tube of circular cross section. A tracer technique was used to measure the above mentioned quantities based on the rate of change of concentration of the tracer in the wall film. The authors found that at low droplet concentrations, rate of deposition increases linearly with an increase in the droplet mass flow rate while at high droplet concentrations, the droplet deposition rate was independent of the droplet concentration. In addition, they found that the droplet deposition rate was relatively insensitive to the gas velocity. Both of these results are in direct contradiction to the results obtained by previous researchers like Namie& Ueda [13]. The authors attributed their observations to the possibility of the slip ratio between the droplets and the gas being a variable quantity.

Ganic&Mastaniah [19]

In this work, the authors studied, both theoretically and experimentally, the deposition of droplets from a two phase turbulent flow onto to the wall of a smooth tube. They proposed a model for the deposition of particles in the Stokes Regime ($Re_p < 1$) based on turbulent diffusion in the core of the two phase flow followed by a free flight to the wall from the edge of the wall layer. They found that the dimensionless deposition velocity depended only on the particle relaxation time and the tube Reynolds number. Experiments on droplet deposition were performed using air – water flow system in a vertical tube for a tube Reynolds number of 52,500

and 94,600. For the former case, the test section inlet pressure was maintained at 1.15 bar and the droplet concentration varied between $8.5x10^{-3}$ and $62x10^{-3}$ kg/m^3 while for the latter case the inlet pressure was maintained at 1.37 bar and the droplet concentration ranged between $22x10^{-3}$ and $75x10^{-3}$ kg/m^3. The model was found to satisfactorily predict their experimental data and other relevant data reported in the literature.

El – Kassaby&Ganic [20]

In this work, the authors extended the theory of Ganic&Mastaniah [18] to include the theOseen regime ($Re_p < 5$). Once again both theoretical and experimental analysis of droplet deposition onto the wall of a smooth vertical tube was carried out. The main difference from [18] was in the calculation of the particle to fluid diffusivity ratio for which the drag coefficient based on the Oseen regime was employed. Experiments were performed for a tube Reynolds number of 26700, 36000, 43000 and 55200. The inlet pressure varied between 1.09 and 1.254 bar while the droplet concentration varied between $12.7x10^{-3}$ kg/m^3 and $56.8x10^{-3}$ kg/m^3.

From the above review it can be clearly seen that all the correlations and experimental data reported in the literature for both droplet deposition and entrainment have been for developed annular flow scenarios in a duct of circular cross section or flat plates. The flow cross section at a wet grid is considerably different from any of these geometries. The presence of mixing vanes at the top of the spacer grid and dimples within the span of spacer grid further complicates the geometry. In addition, the film thickness on the surface of a wet spacer grid is expected to be very small. As a result, the entrainment from a wet grid is not expected to be similar to the conventional annular flow entrainment mechanisms, namely, shearing off of roll wave crests or wave under cutting. It is anticipated that the shear action of the steam flow would induce a velocity in the liquid film which then issues from the trailing edge of the spacer grid as a viscous

liquid jet. Subsequent breakup of this jet into finer droplets due to aerodynamic and capillary instabilities is expected to be the mechanism for 'entrainment of droplets' appearing downstream of a wet grid. Thus far, there is no experimental data or correlations reported in the literature focusing on liquid entrainment from wet grid like situations.

In the present work, the formation and breakup of liquid ligaments due to the shearing action of the steam flow through a wet grid in a rod bundle during the reflood transient is investigated theoretically. The formation of liquid ligaments is modeled by considering the shearing off of the liquid films on the wet grid. Droplet entrainment into the steam flow is modeled by considering subsequent breakup of these ligaments due to the instabilities in the ligament. The notion of critical Weber number is invoked to establish a stable droplet diameter in the presence of turbulent steam flow. The resulting droplet number density is determined from the conservation of liquid mass of the dispersed phase. Recent experimental data from the Rod Bundle Heat Transfer Test Facility that may be useful for validating the modelis compiled. The physics-based model so developed is intended to be implemented in TRACE to account for the GEHT effects due to a wet grid on drop size and interfacial heat transfer area. However, at the present time, it is not possible to validate the physics-based model owing to the fact that useful wet-grid data is sorely lacking. New data is needed by performing wet-grid-focused bench-top experiments as well as reflood experiments in the RBHT facility. The physics-based model described in this work, once fine-tuned and validated by these new data, can be implemented in TRACE. Assessment of the implemented model can then be done to obtain a better understanding of the GEHT under wet-grid conditions.

CHAPTER 3

WET GRID PHENOMENA OBSERVED IN RBHT REFLOOD TESTS

3.1 Wet Grid Phenomena Observed in the Reflood Tests

The NRC/PSU Rod Bundle Heat Transfer (RBHT) Test Facility was constructed to investigate the flow and heat transfer characteristics within the bundle assembly. The RBHT facility is designed to simulate a portion of a Pressurized Water Reactor (PWR) fuel assembly. The facility consists of a 7 x 7 rod bundle with 45 electrically heated rods, mixing vane grids, and over 500 different channels of instrumentation, which include heater rod and spacer grid thermocouples, sensitive differential pressure cells, and fluid temperature probes. This instrumentation provides detailed measurements for more accurate calculations and a better understanding of the phenomenon that occur within the rod bundle.

One major objective of the RBHT Program is to investigate the effects of grid spacers on the rod bundle heat transfer during reflood transients. A total of 25 reflood experiments have been performed under various flooding-rate conditions in the RBHT facility using the VisiSizer system to determine the effect of spacer grids on the diameters of droplets. In these experiments, the bundle pressure, the flooding rate, the initial rod temperatures, the water inlet temperature, and the peak power level were varied. The laser camera was positioned at a given elevation of the bundle either upstream or downstream of a spacer grid. The VisiSizer system captured high-resolution images of the two-phase mixture and analyzed the images at a rate of seven frames per second, identifying droplets as dark images in front of the laser-illuminated scattering sheet. For each test, a series of droplet measurements were taken at a single elevation. Runs were divided into ten-second periods in which droplet sizes were measured. Statistical analysis of the droplet

data was then performed systematically. Results of importance to the wet-grid phenomena are shown in figures 3-1 and 3-2.

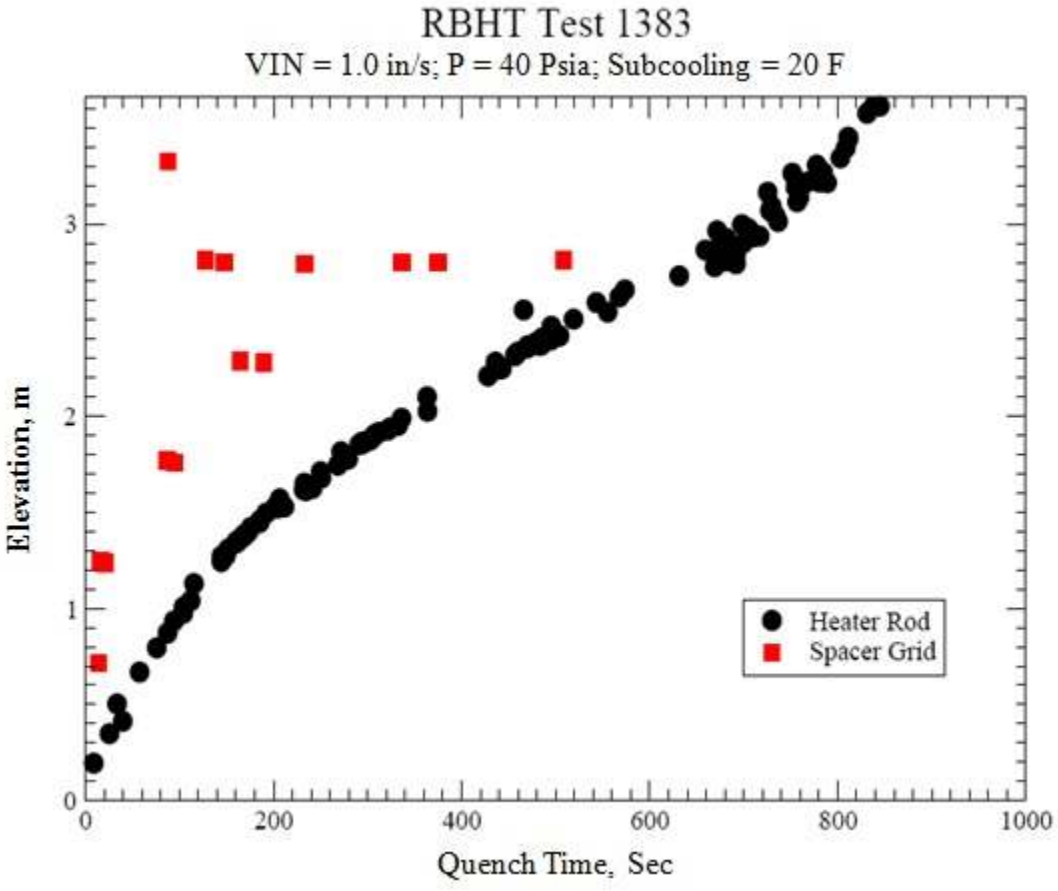

Fig. 3-1.Wet-Grid Formation in the Upper Portion of the Rod Bundle Well Before the Arrival of the Quench Front Observed in RBHT Reflood Test 1383

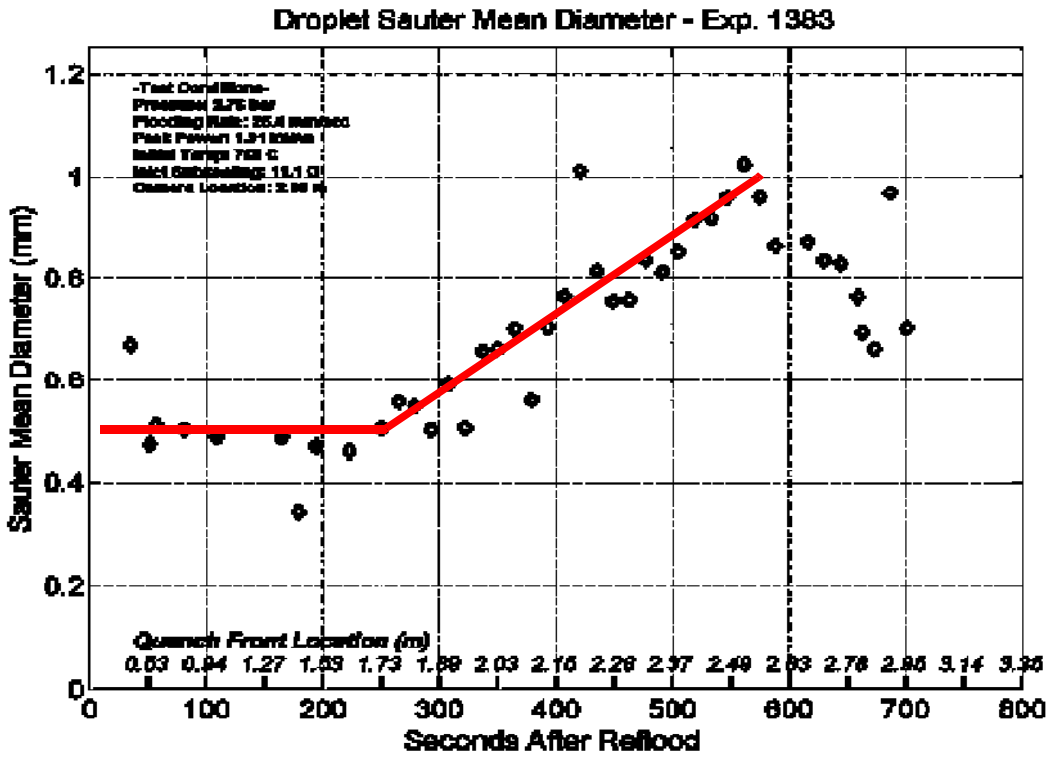

Fig. 3-2.Increasing Droplet Sizes Observed in Grid #6 Located Well above the Quench Front in RBHT Reflood Test 1383

Experimental evidence observed in the RBHT tests clearly indicates that those grids in the upper portion of the rod bundle could become wet well before the arrival of the quench front even under low-flooding-rate conditions as shown in figure 3-1. Moreover, the experimental evidence observed in the RBHT tests (see figure 3-2) clearly shows that the sizes of liquid droplets downstream of a wet grid are considerably larger than those produced by a dry grid, indicating a distinctly different droplet formation mechanism. Evidently, the spacer-grid models currently employed in transient system analysis codes such as COBRA-TF and TRACE which are applicable only for dry grids, cannot be applied under wet-grid conditions.

3.2 RBHT Droplet Injection Wet-Grid Data

To further investigate the grid effects on rod bundle heat transfer, a series of droplet injection experiments have been carried out for a range of constant powers, pressures, inlet sub-cooled droplet temperature, steam quality, and inlet steam flow rate with variable droplet injection flow rates. In these experiments, data was recorded for each set of test conditions once a steady-state time period was maintained and the droplet injection was initiated at the various flow rates. In addition to the various data channels of temperatures and pressures, droplet data was recorded using a high speed camera system with an infrared laser. The droplet data was collected in the regions upstream and downstream of the spacer grid locations within the rod bundle to determine the mixing effects heat transfer enhancement of the grids.

Data from the steam cooling experiments with droplet injection conducted in the RBHT facility provide very detailed insight to the temperature distribution and heat transfer characteristics of dispersed flow film boiling regime during the reflood phase of a LOCA. The information and data required to effectively analyze this regime include: the entrained liquid droplet sizes and velocity, vapor temperature, steam flow rate, and the interfacial heat and mass transfer. Droplet diameter and droplet distribution data were measured at a series of elevations in order to obtain detailed information on the evaporation and breakup of the droplets as they travel upwards through the bundle and pass through the spacer grids. The tests were performed under quasi steady-state conditions to measure the two-phase flow heat transfer effects as compared to previously attained single-phase flow data. Heater rod and bulk flow temperatures were measured axially throughout the rod bundle, and the measured heater rod temperatures were used to determine that steady-state conditions were achieved. Steady-state conditions were considered to be achieved when heater rod temperatures oscillated within ±1 degree Fahrenheit

over a five-minute time period. The upper elevations in the rod bundle were the last to achieve steady-state. Once steady-state steam flow conditions were achieved, droplet injection was initiated and maintained at a fixed rate for several minutes.

Thermocouples within the heater rods, on the grid spacers, and on steam probe rakes provided useful temperature data throughout the rod bundle. Differential pressure cell measurements were also made during the experiments at 23 elevations which include bare bundle and spacer grid spans. High speed camera system imaging of the droplet flow provide useful droplet size measurements axially along the rod bundle. Due to the high temperatures that were reached during the test series, the quartz view windows at the peak power location were not utilized for several tests such that only one test provides droplet data at this elevation. Additionally, it was learned during the testing phase that grid 5 had shifted such that only downstream data could be obtained for that grid location. Therefore, the droplet data for investigating droplet breakup at a spacer grid are nearly entirely based on the upstream and downstream measurements about grid 4 at an elevation of 1.73 m (68 in.).

For heat transfer analysis the Sauter mean diameter (SMD) provides further insight into the effects of the liquid droplet field. For droplet breakup models including that of COBRA-TF, the model is based on the SMD rather than the geometric mean diameter. The Sauter mean diameter accounts for the fact that droplets will not be perfectly spherical, such that it is better suited for modeling the droplet breakup process as the droplet deforms significantly as it traverses and breaks up. The Sauter mean diameter measurements upstream and downstream of grid spacers #4 and #6 within the RBHT facility at elevations of approximately 1.7 m and 2.5 m, respectively, are presented in Table 3-1.

The droplet breakup model is dependent on the Weber number which is a function of the upstream droplet velocity in addition to the droplet diameter. Due to the difficulty and uncertainties in the velocity measurement method of the VisiSizer system, COBRA-TF is utilized to predict the droplet velocities which were missing in the measured data. COBRA-TF input decks were prepared for the RBHT steam cooling with droplet injection tests which provide velocity predictions for the bulk steam flow and the entrained liquid. These velocities provide the maximum and minimum bounds for the actual droplet velocity, such that a range of Weber numbers can also be obtained. The predictions of the droplet velocities by COBRA-TF are presented in Table 3-2.

Table 3-1: RBHT Steam Cooling with Droplet Injection Measured Droplet Diameters

Data File #	ARL Validated Test Designation	Droplet Diameter Upstream of Grid 4 @ 1.69 m (mm)	Droplet Diameter Downstream of Grid 4 @ 1.84 m (mm)	Ratio of Downstream/ Upstream	Droplet Sauter Mean Diameter Upstream of Grid 4 @ 1.69 m (mm)	Droplet Sauter Mean Diameter Downstream of Grid 4 @ 1.84 m (mm)	Ratio of Downstream/ Upstream
4032							
	4032-A	0.88185	0.47406	0.538	0.98610	0.71365	0.724
	4032-B	0.70243	0.41075	0.585	0.85208	0.65600	0.770
	4032-C	0.75362	0.59944	0.795	0.94056	0.86512	0.920
	4032-D	0.67265	N/A	N/A	0.82944	N/A	N/A
	4032-E	N/A	N/A	N/A	N/A	N/A	N/A
	4032-F	0.73682	0.61392	0.833	0.89104	0.81839	0.918
4035							
	4035-A	0.40467	0.34516	0.853	0.70543	0.54939	0.779
	4035-B	0.39666	0.28956	0.730	0.62984	0.52807	0.838
	4035-C	0.48969	0.42153	0.861	0.74045	0.68277	0.922
	4035-D	0.51283	0.40411	0.788	0.73914	0.52832	0.715
	4035-E	0.46894	0.46492	0.991	0.73639	0.64559	0.877
	4035-F	0.47384	0.43086	0.909	0.68942	0.60191	0.873
	4035-G	N/A	N/A	N/A	N/A	N/A	N/A
	4035-H	N/A	N/A	N/A	N/A	N/A	N/A
	4035-I	N/A	N/A	N/A	N/A	N/A	N/A
4037							
	4037-A	0.53069	0.32596	0.614	0.76383	0.56165	0.735
	4037-B	0.50362	0.31479	0.625	0.72565	0.54785	0.755
	4037-C	0.45753	0.28830	0.630	0.67307	0.52739	0.784
	4037-D	0.66625	0.41954	0.630	0.85454	0.76414	0.894
	4037-E	0.56201	0.38376	0.683	0.81322	0.70563	0.868
	4037-F	0.52200	0.36393	0.697	0.71687	0.63099	0.880
	4037-G	N/A	N/A	N/A	N/A	N/A	N/A
	4037-H	0.61401	0.43969	0.716	0.72585	0.72563	1.000
	4037-I	N/A	N/A	N/A	N/A	N/A	N/A
4041							
	4041-A	0.63894	0.32487	0.508	1.00508	0.60655	0.603
	4041-B	0.42012	0.31471	0.749	0.81128	0.65938	0.813
	4041-C	0.48616	0.31801	0.654	0.73406	0.66319	0.903
	4041-D	0.53175	0.29820	0.561	0.77381	0.63957	0.827
	4041-E	0.41821	0.35814	0.856	0.85115	0.67539	0.794
	4041-F	0.46584	0.38938	0.836	0.82233	0.77978	0.948
	4041-G	0.49416	0.34239	0.693	0.82804	0.69774	0.843
	4041-H	0.51511	0.29337	0.570	0.81547	0.57937	0.710
	4041-I	0.51803	0.43332	0.836	0.89967	0.81331	0.904
	4041-J	0.43193	0.41377	0.958	0.85090	0.81839	0.962
	4041-K	0.49695	0.39395	0.793	0.83515	0.75133	0.900
4042							
	4042-A	0.41910	0.47829	1.141	1.10693	0.86904	0.785
	4042-B	0.57944	0.36463	0.629	0.93480	0.73517	0.786
	4042-C	0.55256	0.38312	0.693	0.87297	0.74683	0.856
	4042-D	0.53645	0.33073	0.617	0.81773	0.69491	0.850
	4042-E	N/A	N/A	N/A	N/A	N/A	N/A
	4042-F	0.61132	0.49682	0.813	0.95862	0.91170	0.951
	4042-G	0.56182	0.46132	0.821	0.89675	0.82037	0.915
	4042-H	0.56838	0.41265	0.726	0.86189	0.72074	0.836
	4042-I	N/A	N/A	N/A	N/A	N/A	N/A
	4042-J	N/A	N/A	N/A	N/A	N/A	N/A
	4042-K	0.55569	0.43021	0.774	0.88525	0.72785	0.822
	4042-L	N/A	N/A	N/A	N/A	N/A	N/A

Table 3-1: RBHT Steam Cooling with Droplet Injection Measured Droplet Diameters

Data File #	ARL Validated Test Designation	Droplet Diameter Upstream of Grid 4 @ 1.69 m (mm)	Droplet Diameter Downstream of Grid 4 @ 1.84 m (mm)	Ratio of Downstream/ Upstream	Droplet Sauter Mean Diameter Upstream of Grid 4 @ 1.69 m (mm)	Droplet Sauter Mean Diameter Downstream of Grid 4 @ 1.84 m (mm)	Ratio of Downstream/ Upstream
4049							
	4049-A	0.35772	0.22622	0.632	0.61635	0.33402	0.542
	4049-B	0.45999	0.23446	0.510	0.73677	0.36814	0.500
	4049-C	0.45587	0.23866	0.524	0.72714	0.38842	0.534
	4049-D	0.47455	0.24520	0.517	0.70115	0.39642	0.565
	4049-E	0.51767	0.29731	0.574	0.84218	0.53276	0.633
	4049-F	0.50445	0.29555	0.586	0.81913	0.52207	0.637
	4049-G	0.53063	0.29438	0.555	0.82871	0.54302	0.655
	4049-H	0.55849	0.28913	0.518	0.82870	0.55939	0.675
	4049-I	0.54511	0.33385	0.612	0.85844	0.57193	0.666
	4049-J	0.54000	0.33247	0.616	0.83289	0.60887	0.731
	4049-K	0.54871	0.32460	0.592	0.87872	0.63205	0.719
	4049-L	0.55771	0.31273	0.561	0.86470	0.64306	0.744
4053							
	4053-A	0.43673	0.32339	0.740	0.74429	0.61188	0.822
	4053-B	0.44474	0.41794	0.940	0.70912	0.68986	0.973
	4053-C	0.47074	0.38989	0.828	0.68093	0.79451	1.167
	4053-D	0.37178	0.31090	0.836	0.58983	0.98323	1.667
	4053-E	0.43755	0.41312	0.944	0.80814	0.74715	0.925
	4053-F	0.44971	0.39410	0.876	0.67378	0.71210	1.057
	4053-G	0.41871	0.42211	1.008	0.63285	0.72031	1.138
	4053-H	0.37659	0.38532	1.023	0.68172	0.85242	1.250
	4053-I	0.57642	0.39116	0.679	0.87940	0.68504	0.779
	4053-J	0.42947	0.36855	0.858	0.63194	0.55143	0.873
	4053-K	0.33474	0.28650	0.856	0.55780	0.51302	0.920
	4053-L	0.28242	0.23548	0.834	0.47576	0.59007	1.240
4055							
	4055-A	0.61994	0.44295	0.715	0.98410	0.91640	0.931
	4055-B	0.61979	0.40557	0.654	0.99826	0.80637	0.808
	4055-C	0.58922	0.36741	0.624	0.91649	0.74857	0.817
	4055-D	0.63693	0.46406	0.729	1.10793	0.90949	0.821
4076							
	4076-A	0.55883	0.37389	0.669	0.79518	0.59919	0.754
	4076-B	0.59602	0.48667	0.817	0.89186	0.76937	0.863
	4076-C	0.48000	0.40842	0.851	0.72199	0.85301	1.181
	4076-D	0.42291	0.30759	0.727	0.70790	0.62408	0.882

Data File #	ARL Validated Test Designation	Droplet Diameter Upstream of Grid 6 @ 2.74 m (mm)	Droplet Diameter Downstream of Grid 6 @ 2.89 m (mm)	Ratio of Downstream/ Upstream	Droplet Sauter Mean Diameter Upstream of Grid 6 @ 2.74 m (mm)	Droplet Sauter MeanDiameter Downstream of Grid 6 @ 2.89 m (mm)	Ratio of Downstream/ Upstream
4076							
	4076-A	0.35382	0.23393	0.661	0.60579	0.48997	0.809
	4076-B	0.31318	0.25273	0.807	0.56794	0.5141	0.905
	4076-C	0.30988	0.22784	0.735	0.61951	0.4986	0.805
	4076-D	0.23495	0.19202	0.817	0.37211	0.3015	0.810

Table 3-2: Summary of Velocity Predictions by COBRA-TF for Droplet Injection Tests

Data File #	ARL Validated Test Designation	Steam Velocity Upstream of Grid 4 (m/s) @ 1.69 m	Entrainment Velocity Upstream of Grid 4 (m/s) @ 1.69 m	Upper Bound Weber Number	Lower Bound Weber Number	Droplet Sauter Mean Diameter Upstream of Grid 4 @ 1.69 m (mm)	Droplet Sauter Mean Diameter Downstream of Grid 4 @ 1.84 m (mm)	Ratio of Downstream/ Upstream
4037								
	4037-A	14.12747998	8.296655987	1632.422	893.8551	0.76383	0.56165	0.735
	4037-B	13.90497598	8.165591988	1502.306	822.5585	0.72565	0.54785	0.755
	4037-C	11.89329598	4.651247993	783.0223	247.5503	0.67307	0.52739	0.784
	4037-D	11.98473598	6.89762399	1294.939	691.1872	0.85454	0.76414	0.894
	4037-E	11.56715998	6.72693599	1156.736	625.6146	0.81322	0.70563	0.868
	4037-F	9.884663985	3.270503995	527.2754	130.3569	0.71687	0.63099	0.880
	4037-G	8.549639987	4.788407993	N/A	N/A	N/A	N/A	N/A
	4037-H	7.610855988	7.583423988	712.2155	709.6461	0.72585	0.72563	1.000
	4037-I	7.071359989	7.062215989	N/A	N/A	N/A	N/A	N/A
4041								
	4041-A	14.12747998	8.296655987	2148.01	1176.173	1.00508	0.60655	0.603
	4041-B	13.90497598	8.165591988	1679.585	919.6242	0.81128	0.65938	0.813
	4041-C	12.01216798	4.489703993	849.576	251.554	0.73406	0.66319	0.903
	4041-D	11.89329598	4.651247993	900.2191	284.6018	0.77381	0.63957	0.827
	4041-E	11.98473598	6.89762399	1289.802	688.4452	0.85115	0.67539	0.794
	4041-F	11.56715998	6.72693599	1169.694	632.623	0.82233	0.77978	0.948
	4041-G	9.884663985	3.270503995	609.0436	150.5723	0.82804	0.69774	0.843
	4041-H	9.927335985	3.761231994	649.4239	196.1248	0.81547	0.57937	0.710
	4041-I	8.549639987	4.788407993	680.2555	350.6952	0.89967	0.81331	0.904
	4041-J	7.610855988	7.583423988	834.9165	831.9045	0.85090	0.81839	0.962
	4041-K	7.071359989	7.062215989	709.0435	708.1263	0.83515	0.75133	0.900
4042								
	4042-A	18.12645597	18.12035997	6297.229	6295.111	1.10693	0.86904	0.785
	4042-B	18.75434397	9.939527985	3332.626	1599.557	0.93480	0.73517	0.786
	4042-C	18.82444797	9.781031985	3093.053	1446.499	0.87297	0.74683	0.856
	4042-D	19.07438397	9.747503985	2941.334	1345.694	0.81773	0.69491	0.850
	4042-E	14.49628798	7.717535988	N/A	N/A	N/A	N/A	N/A
	4042-F	14.66087998	7.555991989	2048.811	947.9361	0.95862	0.91170	0.951
	4042-G	14.47190398	7.281671989	1837.479	823.5372	0.89675	0.82037	0.915
	4042-H	14.39875198	7.104887989	1725.7	753.5567	0.86189	0.72074	0.836
	4042-I	7.330439989	3.645407994	N/A	N/A	N/A	N/A	N/A
	4042-J	7.336535989	3.392423995	N/A	N/A	N/A	N/A	N/A
	4042-K	7.546847989	3.392423995	458.7039	176.4557	0.88525	0.72785	0.822
	4042-L	7.482839989	3.227831995	N/A	N/A	N/A	N/A	N/A
4049								
	4049-A	20.64410397	20.64105597	4548.885	4548.213	0.61635	0.33402	0.542
	4049-B	20.93975997	11.21359198	3298.178	1604.616	0.73677	0.36814	0.500
	4049-C	21.04339197	11.05204798	3243.354	1538.343	0.72714	0.38842	0.534
	4049-D	21.36647997	11.03680798	3187.709	1479.27	0.70115	0.39642	0.565
	4049-E	24.32913596	23.22880796	8247.849	7870.61	0.84218	0.53276	0.633
	4049-F	24.52420796	13.31366398	5078.037	2514.766	0.81913	0.52207	0.637
	4049-G	24.89301596	13.30756798	5236.393	2541.848	0.82871	0.54302	0.655
	4049-H	24.96311996	13.13687998	5208.791	2477.031	0.82870	0.55939	0.675
	4049-I	34.62527995	25.70683196	13529.96	9825.546	0.85844	0.57193	0.666
	4049-J	33.95167195	33.91509595	16610.84	16592.94	0.83289	0.60887	0.731
	4049-K	35.01542395	19.32431997	11235.06	5683.404	0.87872	0.63205	0.719
	4049-L	35.20744795	19.15058397	11063.24	5492.614	0.86470	0.64306	0.744

The numerical results obtained using COBRA-TF to simulate the steam cooling with droplet injection tests do not provide significant insight into the droplet breakup phenomenon at dry spacer grids as shown in figure 3-3.

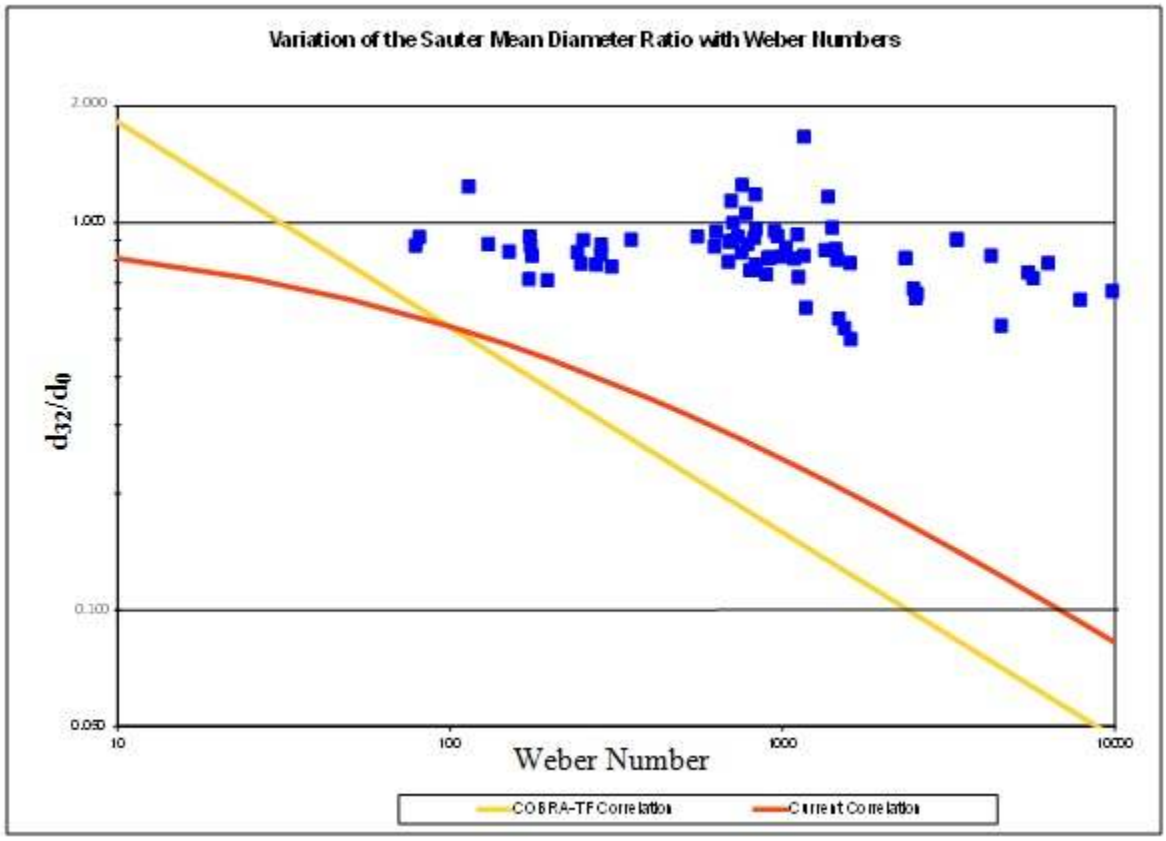

Fig.3-3.Comparison of the Measured Sauter Mean Diameter Ratio with Correlations

The Sauter mean diameter ratios for the droplet injection data are all well above the values predicted by the correlations for a dry grid breakup phenomenon. The ratio is observed in some cases to be greater than one, which indicates that a larger droplet is entrained within the bulk flow downstream of the grid spacer than the incoming droplets which impinged on the grid. This phenomenon is expected for a wet grid rather than a dry grid, and upon review of the spacer grid wall thermocouple temperatures there is indication that the grid was partially wet during the experiment as shown in figures 3-4 and 4-5.

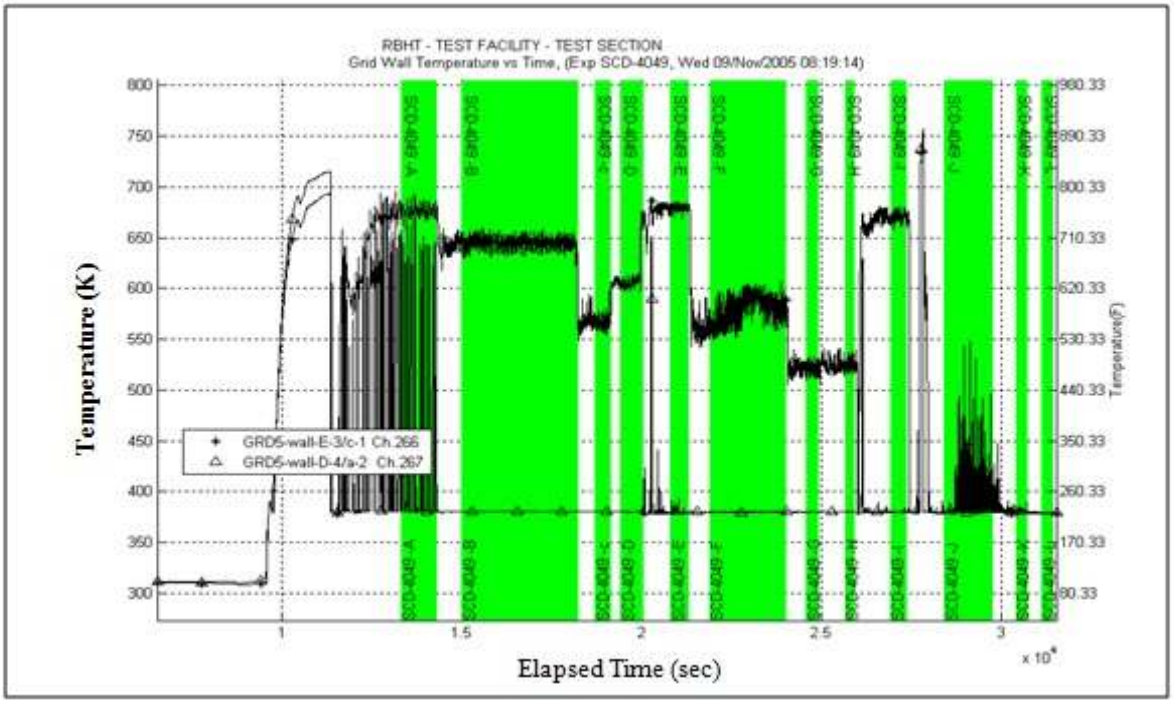

Fig.3-4. Mixing Vane Grid #5 Wall Temperatures

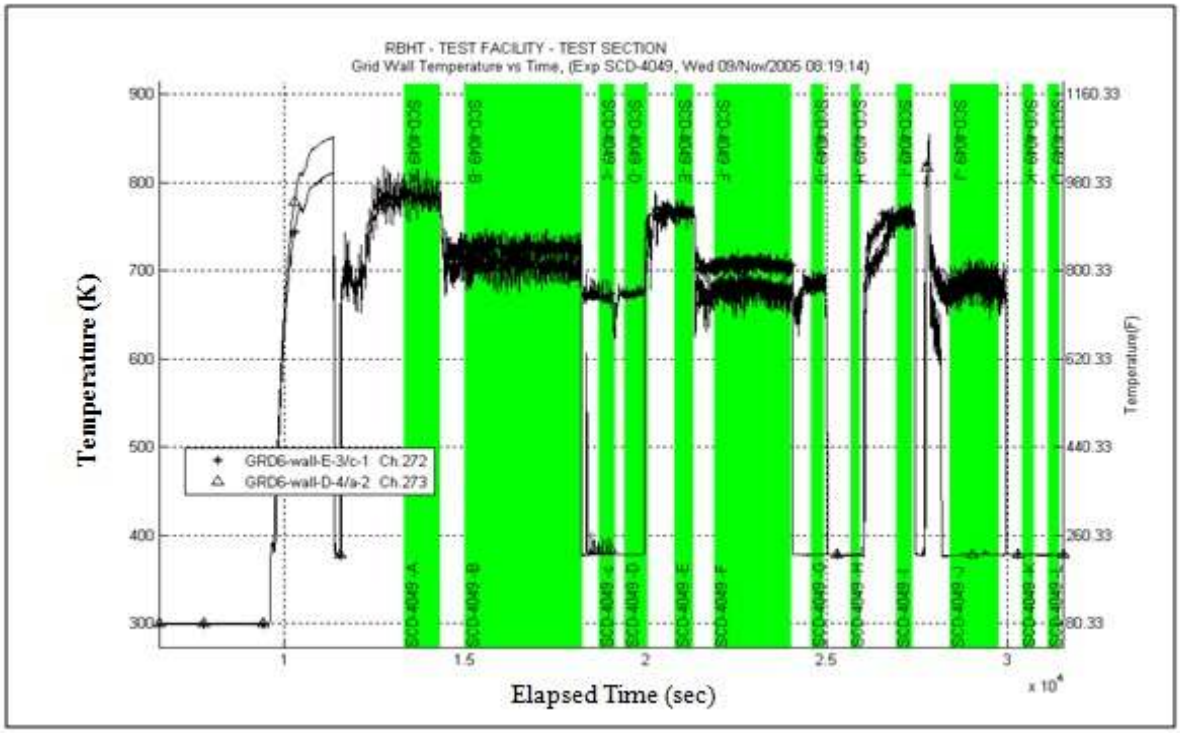

Fig.3-5, Mixing Vane Grid #6 Wall Temperatures

It should be noted that wet grid models accounting for the formation of a liquid film on a wet spacer grid and the entrainment of droplets from the same are entirely lacking. The above data, along with the droplet velocities and Weber numbers calculated by COBRA-TF, should be useful for the development of wet- and partially wet- grid models.

CHAPTER 4

MODEL FORMULATION

4.1 Theoretical Considerations

During the reflood stage of a large-break LOCA, the wet-grid effect could lead to significant enhanced cooling of the fuel rods in the upper portion of the bundle where the PCT usually occurs (see Cheung and Bajorek [21]). Current versions of TRACE and COBRA-TF, however, do not properly account for the wet-grid effect. Specifically, depletion of liquid film that forms on a grid spacer as a result of droplet deposition is assumed to occur only by evaporation. Thinning of the liquid film due to the shear action of the steam flow is not considered. Moreover, entrainment of liquid ligaments from the liquid film and subsequent breakup of the ligaments to form droplets at the trailing edge of the grid spacer are not modeled. The droplet field downstream of a wet grid could be entirely different than those described by the existing correlation employed in TRACE and COBRA-TF. Without incorporating an appropriate wet-grid model, the steam and cladding temperatures could not be accurately predicted during numerical simulations of the reflood transients. Evidently, a new physics-based wet-grid model that adequately accounts for the grid-enhanced heat transfer (GEHT) due to the wet grid effect needs to be implemented into TRACE so as to improve the PCT predictions in numerical simulations and assessments.

Depending on the bundle power and the flooding rate, the spacer grids can be quenched before quenching of the fuel rods by the flow of a dispersed two-phase mixture because the grids are unpowered. Liquid films would form on the grid spacers following quenching of the grid, which could radically change the subsequent droplet formation mechanism. Wet grid could act as a major source for the generation of new droplets especially in the upper portion of rod bundle

where PCT occurs. Contrary to what is being modeled in current versions of TRACE and COBRA-TF, droplet field in the froth region is not as important as the new droplet field downstream of a wet grid. Because the relative velocity of the steam flow to the liquid film is larger, a wet grid would have a higher interfacial heat transfer coefficient than the droplets. This would enhance the liquid evaporation rate. Evaporation of the liquid film in turn increases the steam flow rate while de-superheating the steam. In the meantime, liquid ligaments and new droplets are being entrained from the liquid films on the wet grid in the downstream locations. The combined effects of all these simultaneous processes could greatly enhance the rate of cooling of the fuel rods. This "wet-grid phenomenon" gives rise to significant grid-enhanced heat transfer (GEHT) in the DFFB region, leading to a lower PCT. It should be reiterated that a wet grid could significantly alter the droplet field downstream of the grid as a result of entrainment and subsequent breakup of the liquid ligaments by the shear action of the vapor flow on the liquid films. Thus far, no physics-based model is available describing the wet-grid phenomena.

To adequately account for the wet-grid effect, a physics-based model needs to be developed that includes all the basic elements describing the various processes occurring within and immediately downstream of a wet grid as depicted in figure 4-1. These basic elements should include the following items:

(1) A suitable criterion for predicting the conditions for grid rewet.

(2) A physical model for predicting the "equilibrium" thickness of the liquid film that forms on a wet grid.

(3) A physical model describing the generation of liquid ligaments from the liquid film due to the shearing action of the two-phase flow through the wet grid.

(4) A physical model describing the breakup of liquid ligaments leading to the formation of new droplets downstream of a wet grid.

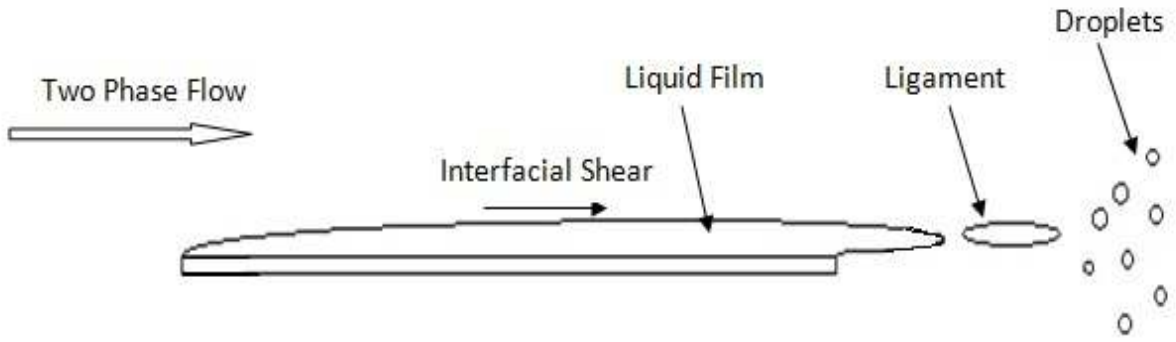

Fig. 4-1. Schematic of the Shear Action of the Steam Flow over a Wet Grid Spacer Resulting in the Formation of Liquid Ligaments and New Droplet Field

(5) A physical model for predicting the droplet number density and size distribution.

(6) A mechanistic model describing wet-grid coolability enhancement accounting for de-superheating of steam and acceleration of the flow due to evaporation of the liquid film within the wet grid and evaporation of the new droplets downstream of the wet grid, both would increase the convective heat transfer coefficient for the cooling of fuel rods and thus reducing the peak cladding temperature.

Among all the individual elements mentioned above, only item (1) has been properly included in transient analysis codes such as COBRA-TF. None of the other elements, i.e., items (2) through (6), have been properly accounted for in the code. It should be noted that separate-effect experiments also need to be performed in order to obtain the much needed data for developing the individual models described in the above items.

For given mass flow rates of the steam and incoming liquid droplets, the "equilibrium" thickness of the liquid film that forms on a wet grid can be determined by balancing the liquid deposition rate and the liquid depletion rate. The latter includes evaporation of the liquid film due to convective heat transfer from the superheated steam and radiative heat transfer from the rods as well as flow-induced thinning of the liquid film as a result of the shear action of the steam flow leading to the formation of liquid ligaments downstream of the wet grid.

Note that the evaporation of the liquid film, along with the blockage of the grid spacer, would greatly accelerate the steam flow. This in turn would result in enhanced shear stresses at the steam-liquid interface leading to the entrainment of liquid ligaments from the liquid film.

Subsequent breakup of these liquid ligaments into droplets occurs when the kinetic energy of the flow exceeds the surface energy required to generate new liquid droplets. The notion of critical Weber number along with the conservation of droplet kinetic and surface energies can be used to establish a suitable criterion for droplet entrainment and breakup. Meanwhile, the size distribution and number density of the new droplet field can be determined by considering the conservation of liquid mass along with other sound physical arguments. Having determined the rate of entrainment of liquid ligament and the size distribution and number density of the new droplet field downstream of a wet grid, the wet-grid-induced coolability enhancement may then be determined to predict the GEHT for the cooling of fuel rods.

From the above discussion, it is evident that a comprehensive physics-based wet-grid model is needed to account for the grid-enhanced heat transfer (GEHT) effects immediately downstream of a wet grid. The model should adequately describe the conditions for grid rewet, the "equilibrium" thickness of the liquid film that forms on the grid, the generation of liquid ligaments from the liquid film due to the shearing action of the two-phase flow through the grid,

the subsequent breakup of liquid ligaments leading to the formation of a new droplet field downstream of the grid, the resulting droplet number density and size distribution,de-superheating of steam and acceleration of the flow due to evaporation of the liquid film within the wet grid and evaporation of the new droplets downstream of the wet grid.

There are, however, very little data relevant to the wet-grid phenomenon occurring during reflood transients are currently available that are useful for model development and code validation. Separate-effect bench-top experiments need to be conducted to simulate the entrainment of liquid ligaments by a shear flow of superheated steam over a thin liquid film on a grid spacer strap and the subsequent formation of a new droplet field. More importantly, wet-grid-focused tests need to be performed subjected to prescribed flow conditions in the RBHT Facility to obtain confirmatory data for assessment of models and validation of TRACE.

4.2 Modeling of the Equilibrium Thickness of the Liquid Film

During the reflood phase of a LOCA, it is recognized that the flow of the coolant at locations well above the quench front is in the dispersed flow film boiling (DFFB) regime wherein numerous tiny liquid droplets (i.e., the dispersed phase) are entrained in the steam flow (i.e., the continuous phase). Being unpowered, the surface temperatures of the spacer grids are lower than those of the fuel rods. The lower temperatures of the spacer grid promote earlier quenching to occur before the quenching of the fuel rods. The rate of propagation of the spacer grid quench front (different from the actual quench front of the rod bundle) can be determined from a combined dry and wet region energy balance. Once the quench front reaches the trailing (top) edge of the spacer grid, the spacer grid structure is completely wetted, allowing the formation of a thin liquid film on the surface of the grid spacer. The equilibrium thickness of the liquid film is

dependent on the rates of mass deposition of liquid droplets and mass depletion of the liquid film.

Deposition of liquid mass onto the surface of the grid spacer occurs by two individual processes, namely, turbulent lateral migration of droplets and direct impingement on the spacer straps. The droplets flowing through a sub channel can either escape through the gap between the spacer grid and the fuel rod or be captured into the liquid film on the grid spacer. The probability for a droplet to be captured into the liquid film is considered equal to the spacer grid flow blockage ratio. Thus it can be assumed that the 'direct impingement' portion of the mass deposited onto the spacer grid is equal to the grid blockage ratio times the mass flow rate of the entrained droplets upstream of the spacer grid, i.e.,

$$(\dot{m}_{DE})_{direct} = \varepsilon \dot{m}_f \tag{4-1}$$

where ε is the grid blockage ratio and $\dot{m}_f$ is the liquid mass flow rate upstream of the grid.

The droplets that escape through the gap between the spacer grid and the fuel rod may get deposited onto the film due to turbulent lateral migration. Conventionally, the turbulent deposition of droplets has been expressed in terms of a deposition constant as

$$(\dot{m}_{DE})_{turb} = k_D C \tag{4-2}$$

where k_D is the deposition constant and C is the concentration of the droplets in the sub channel between the fuel rod and the spacer grid. A number of correlations for k_D have been proposed in the past. The correlation by Nigmatulin et al [9] is utilized in the present study to evaluate the deposition constant since this correlation has been validated over a wide range of experimental conditions and also has the virtue of being one of the more recent correlations reported in the literature. The total mass deposited onto the surface of the spacer grid is given by

$$(\dot{m})_{DE} = (\dot{m}_{DE})_{direct} + (\dot{m}_{DE})_{turb} = \varepsilon \dot{m}_f + k_D C \tag{4-3}$$

The deposition of the liquid droplets results in the formation of a thin liquid film on the surface of the grid spacer whose equilibrium thickness 'H' is dictated by a balance between the liquid mass addition and liquid mass depletion (due to evaporation at the interface and shear thinning by the steam flow). This equilibrium thickness value can be obtained through a combined mass, force and energy balance on the liquid film by invoking the following simplifying assumptions:

(1) The two-phase mixture is well mixed within the spacer grid structure with the flow properties being uniform in the cross stream direction. Specifically, at a given axial location, the pressure across the liquid film is the same as that across the steam core.

(2) The two-phase mixture accelerates as it enters the grid due to the reduction in the flow area. However, within the spacer grid, the steam velocity can be treated as constant. As a first approximation, the acceleration due to vaporization of the liquid film can be neglected.

(3) The liquid film on the spacer grid strap and the strap itself are assumed to be at saturation temperature corresponding to the local pressure.

(4) As a first approximation, the amount of droplet deposition is assumed to be proportional to the grid blockage ratio with the remaining droplets escaping through the spacer grid as the two-phase mixture flowing through the grid.

A unit cell as shown below in figure 4-2 is chosen for the analysis. The liquid film is divided into two regions, namely, a flat film on the spacer strap surface near the edges of the unit cell and a lumped mass at the centre of the unit cell at the corners. For the sake of brevity, only a quarter portion of the unit cell is shown in the figure 4-3. It is anticipated that the liquid issuing from the corner lumped mass would be the source of the larger droplets found downstream of a wet grid whereas the liquid issuing from the flat film would be the source of smaller droplets downstream

of the grid. The flat film of thickness 'H' can be assumed to occupy a fraction c_1 of the spacer grid length. Note that the length $b/2$ of the spacer grid in the sub channel is half its total length b. The lumped liquid mass at the centre of the grid is postulated to take the shape of a quadrant of a circle whose radius is dependent on the equilibrium flat film thickness H and the fraction c_1 as shown in figure 4-3. The velocity distribution in the flat film and the lumped mass at the corner can be obtained through a momentum balance.

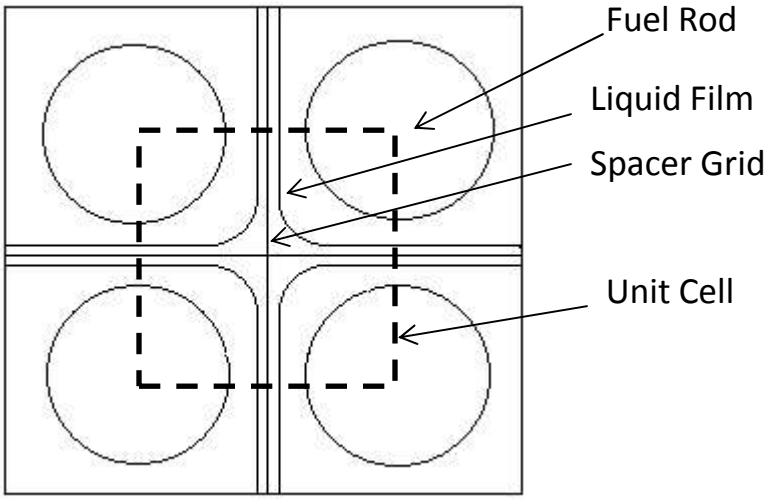

Fig. 4-2. Schematic of the Unit Cell under Consideration

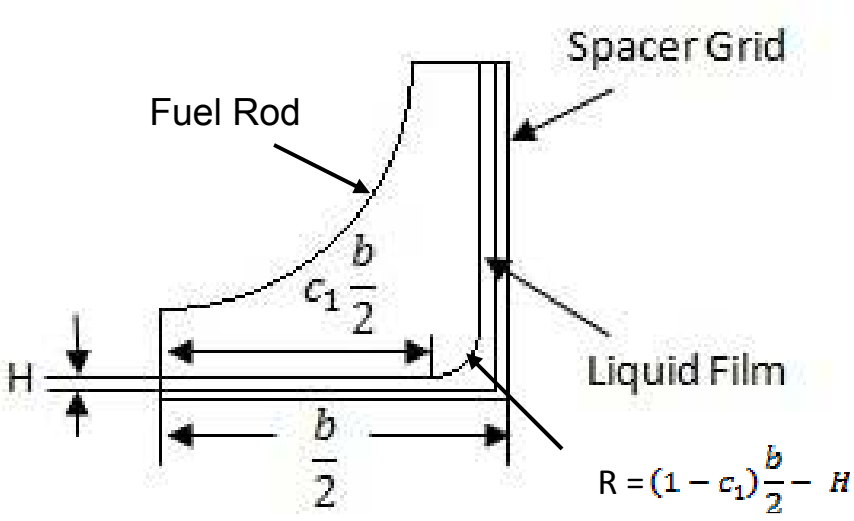

Fig. 4-3. Schematic of the Quarter Unit Cell with Various Length Scales

Two different local coordinate systems, a Cartesian coordinate system and a polar coordinate system, respectively, as shown in figure 4-4 are chosen to carry out the momentum balance analysis. Note that the acceleration due to gravity *g* vector is into the plane of the paper.

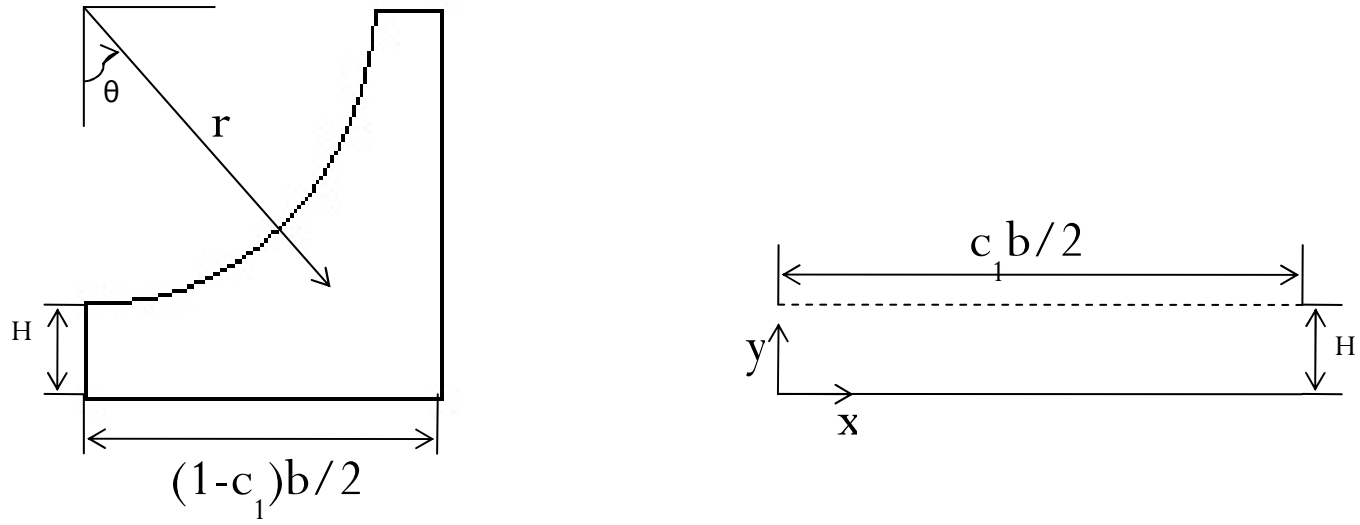

Fig. 4-4.Coordinate Systems Employed in the Analysis

The velocity vector in the flat liquid film with an equilibrium thickness *H* can be assumed to be of the form

$$\vec{u}_{film} = \left(0,0,u_z(y)\right) \tag{4-4}$$

On the other hand, the velocity vector in the corner can be assumed to be of the form

$$\vec{u}_{cor} = \left(0,0,w(r,\theta)\right) \tag{4-5}$$

Since the thickness of the liquid film is expected to be much smaller than the dimensions of the spacer grid structure, the inertia of the flow in the film can be ignored. In addition the velocity of the liquid film can also be approximated to be invariant in the x and z (out of the plane of the paper) directions. Accordingly, the Navier Stokes equation governing the flow of the liquid in the flat film portion of the liquid film can be written as

$$0 = -\frac{1}{\rho_l}\frac{\partial P}{\partial z} + \nu_l \frac{\partial^2 u_z}{\partial y^2} - g \tag{4–6}$$

The above equation can be integrated twice to yield the velocity of the liquid film as

$$u_z(y) = \frac{1}{\mu_l}\left(\frac{\partial P}{\partial z} + \rho_l g\right)\frac{y^2}{2} + A_1 y + A_2 \tag{4-7}$$

The constants A_1 and A_2 can be determined through the no slip and the interfacial shear boundary conditions as given below

$$u_z(0) = 0 \tag{4-8}$$

$$\mu_l \frac{\partial u_z}{\partial y}_{y=H} = \tau_i \tag{4-9}$$

From the above equations, the values of the two constants in equation (4-7) can be obtained and the velocity profile in the flat film becomes

$$u_z(y) = \frac{\tau_i y}{\mu_l} + \frac{1}{\mu_l}\left(\frac{\partial P}{\partial z} + \rho_l g\right)\left(\frac{y^2}{2} - Hy\right) \tag{4-10}$$

Similarly, the inertia of the flow in the corner lumped mass can be ignored. Additionally, the variation of the liquid velocity in the azimuthal (θ) and axial (z) directions can be approximated

to be zero. Accordingly, the Navier Stokes equations in cylindrical coordinates governing the flow of the liquid in the corner can be written as

$$0 = -\frac{1}{\rho_l}\frac{\partial P}{\partial z} + \frac{\nu_l}{r}\frac{\partial}{\partial r}\left(r\frac{\partial w}{\partial r}\right) - g \qquad r_{min} \le r \le r_{max} \qquad 0 \le \theta \le \frac{\pi}{2} \tag{4-11}$$

In spite of the fact that the radial distance r_{max} to the outer boundary corresponding to the solid surface of the spacer is a function of the azimuthal coordinate, at a given angular location the velocity 'w' can be assumed a function of the radial coordinate (r) only, making the problem locally one dimensional in nature. Integrating equation (4-11) twice, the velocity in the corner can be obtained as

$$w(r) = \frac{r^2}{4\mu_l}\left(\frac{\partial P}{\partial z} + \rho_l g\right) + A_3 \log(r) + A_4 \tag{4-12}$$

The constants A_3 and A_4 can be obtained using the no slip and interfacial boundary conditions as given below

$$w(r_{max}) = 0 \tag{4-13}$$

$$\mu_l \frac{\partial w}{\partial r}_{r=r_{min}} = -\tau_i \tag{4-14}$$

The velocity profile in the corner becomes

$$w(r) = \frac{1}{4\mu_l}\left(\frac{\partial P}{\partial z} + \rho_l g\right)(r^2 - r_{max}^2) + A_3 log\left(\frac{r}{r_{max}}\right) \tag{4-15}$$

where r is bounded between r_{min} and r_{max} as

$$r_{min} = (1 - c_1)\frac{b}{2} - H \tag{4-16}$$

$$r_{max} = \begin{cases} (1 - c_1)\frac{b}{2}\sec(\theta) & 0 \le \theta \le \frac{\pi}{4} \\ (1 - c_1)\frac{b}{2}\mathrm{cosec}(\theta) & \frac{\pi}{4} \le \theta \le \frac{\pi}{2} \end{cases} \tag{4-17}$$

In the above expressions, the pressure gradient term can be expressed as a sum of the hydrostatic and interfacial frictional components as

$$\frac{\partial P}{\partial z} = -\rho_V g - \frac{\tau_i}{D_H} \tag{4-18}$$

where D_H is the hydraulic diameter of the unit cell depicted in figure 4-2.

The average liquid velocity in the flat film is given by

$$\bar{u}_{film} = \frac{\int_0^H u\left(c_1\frac{b}{2}\right)dy}{\int_0^H \left(c_1\frac{b}{2}\right)dy} = \left(\frac{\tau_i H}{2\mu}\right) - \frac{H^2}{3}\left[\frac{(\rho_l-\rho_v)g}{\mu} + \frac{\tau_i}{2(w-H)\mu}\right] \tag{4-19}$$

whereas the average liquid velocity in the corner is given by

$$\overline{w}_{cor} = \frac{\int_0^{\frac{\pi}{2}}\int_{r_{min}}^{r_{max}} w(r,\theta) r dr d\theta}{\int_0^{\frac{\pi}{2}}\int_{r_{min}}^{r_{max}} r dr d\theta} \tag{4-20}$$

$$= \frac{1}{A_{cor}}\left[\Delta P\left(-\frac{2}{3}\left((1-c_1)\frac{b}{2}\right)^4 - \frac{\pi r_{min}^4}{8} + r_{min}^2\left((1-c_1)\frac{b}{2}\right)^2\right) + \frac{\pi A_3 r_{min}^2}{8} - \frac{A_3}{2}\left((1-c_1)\frac{b}{2}\right)^2 + \right.$$

$$\left.\frac{A_3 r_{min}^2}{2}\left(\frac{\pi}{2}\log\left(\frac{(1-c_1)\frac{b}{2}}{r_{min}}\right) + 0.1728\right)\right]$$

$$\Delta P = \frac{1}{4\mu_l}\left(\frac{\partial P}{\partial z} + \rho_l g\right)$$

The interfacial shear stress τ_i in the above equations can be expressed by the following correlation proposed by Whally and Hewitt that has been validated over a wide range of flow conditions:

$$\tau_i = \frac{f_{ig}\rho_{gc}V_{gc,sup}^2}{2} \tag{4-21}$$

In the above expression, ρ_{gc} is the gas core density, f_{ig} is the interfacial film friction factor, $V_{gc,sup}$is the superficial gas core mixture velocity. These quantities are expressed as

$$\rho_{gc} = \rho_v\frac{\alpha_v}{\alpha_e+\alpha_v} + \rho_l\frac{\alpha_e}{\alpha_e+\alpha_v}$$

$$V_{gc,sup} = \frac{G_e}{\rho_l} + \frac{G_v}{\rho_v}$$

$$f_{ig} = 0.079 Re_{gc}^{-\frac{1}{4}} \left[1 + 24 \left(\frac{\rho_l}{\rho_v} \right)^{\frac{1}{3}} \frac{H}{D_H} \right] \tag{4-22}$$

$$Re_{gc} = \frac{D_H (G_e + G_v)}{\mu_v}$$

In the above equations, α_e and α_v are the entrained liquid droplet and vapor void fraction respectively. G_e and $G_v$are the mass fluxes of entrained liquid droplets and steam respectively. It is assumed that the same interfacial shear stress is acting on the flat portion of the liquid film and the corner portion of the film. Thus, the same value of τ_i as obtained for the flat portion of the liquid film using the above equations is used in the expression for the average velocity of the corner mass.

The total liquid mass issuing out of the trailing edge of the grid spacer is the sum of the liquid mass issuing out of the flat portion of the liquid film and that issuing out of the corner lumped mass. It follows that the total mass entrained from the liquid film is given by

$$\dot{m}_E = \dot{m}_{film} + \dot{m}_{cor} = \rho_l \left(\bar{u}_{film} A_{film} + \bar{w}_{cor} A_{cor} \right) \tag{4-23}$$

For the unit cell under consideration, the cross-sectional flow areas for the flat film and the corner mass are given respectively by

$$A_{film} = 4 c_1 b H$$

$$A_{cor} = 4 \int_0^{\frac{\pi}{2}} \int_{r_{min}}^{r_{max}} r dr d\theta = (r_{min} + H)^2 - \frac{\pi}{4} r_{min}^2 \tag{4-24}$$

The liquid film on the grid spacer gains mass due to droplet deposition while it loses mass due to evaporation at the interface and liquid entrainment from the trailing edge of the grid spacer. Evaporation at the liquid vapor interface occurs due to the convective heat transfer from the superheated steam and the radiative heat transfer from the nuclear fuel rod. It must be noted that both the grid spacer and the liquid film are assumed to be at the saturation temperature

corresponding to the system pressure. This eliminates conduction heat transfer from the spacer grid surface to the liquid film. The liquid mass evaporated can then be written as

$$\dot{m}_{EV} = \frac{Q_{conv}+Q_{rad}}{h_{lv}} \tag{4-25}$$

where Q_{conv} is the convective heat transfer rate, Q_{rad} is the radiative heat transfer rate and $h_{lv}$is the latent heat of vaporization of the liquid at the local pressure.

The convective heat transfer rate is calculated by

$$Q_{conv} = hA(T_v - T_{sat}) \tag{4-26}$$

where h is the convective heat transfer coefficient, T_v is the superheated vapor temperature and T_{sat} is the saturation temperature corresponding to the local pressure. Since the liquid film is expected to be very thin, the surface area for convective heat transfer is assumed to be the surface are of the grid spacer in the unit cell shown in figure 4-2. This area is given by

$$A = 4Lb \tag{4-27}$$

where L is the height of the spacer grid, b is the length of the grid spacer. For the specific case of the mixing vane spacer grids used in the RBHT facility, the values of L and b are 44.45 mm and 12.6 mm respectively. Again, since the liquid film is expected to be very thin, the liquid film – steam interface is expected to remain smooth, devoid of any disturbance waves. Hence, the same correlation for single phase heat transfer coefficient (i.e., the Weisman correlation) is employed to calculate the heat transfer coefficient in the present case. This correlation is given by

$$Nu = \frac{hD_H}{k} = \left[0.042\frac{P}{D_H} - 0.024\right] Re^{0.8} Pr^{0.4} \tag{4-28}$$

where P is the wetted perimeter, Re is the steam Reynolds number, k is the steam conductivity and Pr is the steam Prandtl number. For the specific case of RBHT facility's mixing vane spacer

grids, $\frac{P}{D_H}$ has a value of 1.3262. Thus the above expression for the convective heat transfer coefficient reduces to

$$h = 0.0317\ \frac{k}{D_H} Re^{0.8} Pr^{0.4} \tag{4-29}$$

It must be noted that the steam velocity to be used to evaluate the Reynolds number in the above expression is the value of the vapor flow within the spacer grid span. Since the spacer grid presents a reduction in the flow area within a sub-channel, steam flowing through the sub-channel is accelerated as it enters the spacer grid span. The velocity of steam within this span can be obtained by mass conservation to be

$$u'_{steam} = \frac{u_{steam}}{1-\varepsilon} \tag{4-30}$$

where u_{steam} is the velocity of steam in the sub channel upstream of the spacer grid and ε is the grid blockage ratio. Then, the Reynolds number to be used in the expression for the heat transfer coefficient is given by

$$Re = \frac{u'_{steam} D_H}{\nu_v} \tag{4-31}$$

The radiative heat transfer to the liquid film can be obtained by performing a simple radiation network balance analysis. By considering a quarter portion of the unit cell shown in figure 4-3, a radiation heat transfer network can be drawn as shown below in figure 4-5.

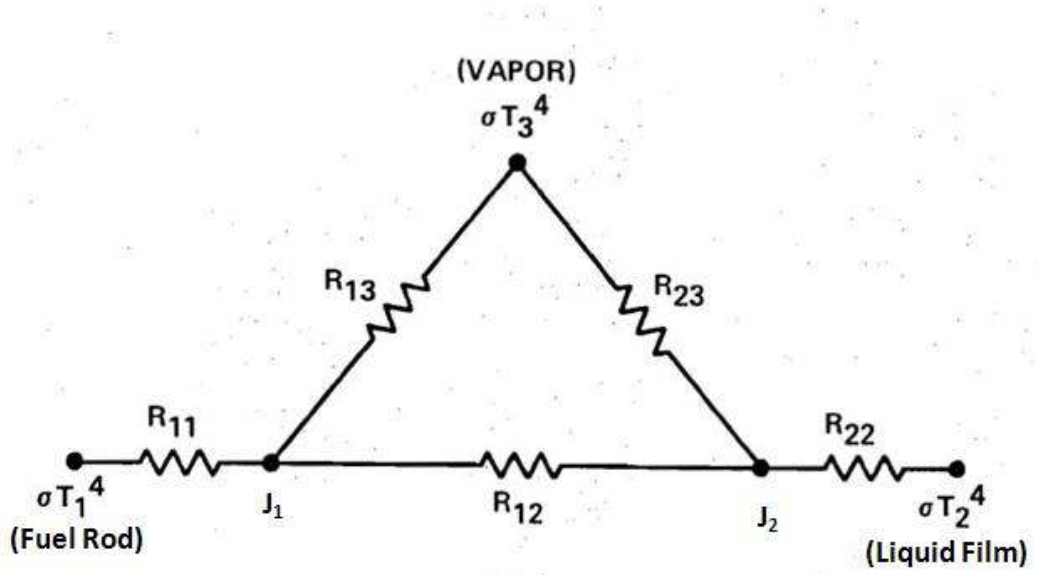

Fig. 4-5. Radiation Network for the Quarter Cell under Consideration

The view factor between the fuel rod and the liquid film in this network is given by

$$F_{12} = \frac{\pi D}{4b} \tag{4-32}$$

From the above network, an expression for the radiant heat flux to the liquid film and the rod can be derived as

$$q_2^{"} = \frac{J_2 - \sigma T_2^4}{A_2 R_{22}} = \frac{J_1 - J_2}{A_2 R_{21}} + \frac{\sigma T_3^4 - J_2}{A_2 A_{23}} \tag{4-33}$$

$$q_1^{"} = \frac{J_1 - \sigma T_1^4}{A_1 R_{11}} = \frac{J_2 - J_1}{A_1 R_{12}} + \frac{\sigma T_3^4 - J_1}{A_1 A_{13}} \tag{4-34}$$

$$R_{11} = \frac{1-\varepsilon_1}{A_1 \varepsilon_1} \quad R_{22} = \frac{1-\varepsilon_2}{A_2 \varepsilon_2} \quad R_{12} = R_{21} = \frac{1}{A_1 F_{12}(1-\varepsilon_3)} \quad R_{13} = \frac{1}{A_1 \varepsilon_3} \quad R_{23} = \frac{1}{A_2 \varepsilon_3}$$

where J_1, $J_2$and J_3 are the radiosities of the rod, liquid film and the vapor respectively, $A_1$and A_2 are the surface areas of the fuel rod (in the quarter cell under consideration) and the liquid film (again, approximated to be equal to that of the spacer grid surface area in the quarter cell), $\varepsilon_1,\ \varepsilon_2, \varepsilon_3$ are the emmisivities of the rod, liquid film and the vapor respectively whereas T_1, T_2 and T_3 are their respective temperatures. The emissivity of vapor can be calculated using

$$\varepsilon_3 = 1 - \exp(-PA_v L_m) \tag{4-35}$$

where P is the pressure, L_m is the mean beam length taken to be 90% of the channel hydraulic diameter and A_v is the mean absorption coefficient of water vapor. The latter can be calculated using the Planck mean absorption coefficient as

$$A_v = 2.146exp\left(-0.345 - T_v(2.961 \times 10^{-3} - 0.444 \times 10^{-6} T_v)\right)$$

The blackbody radiosity of the grid spacer is given by

$$J_2 = \left(\frac{J_1 - \sigma T_1^4}{A_1 R_{11}} - \frac{\sigma T_3^4 - J_1}{A_1 R_{13}}\right) A_1 R_{12} + J_1 \tag{4-36}$$

It follows that the black body radiosity of the rod is

$$J_1 = \frac{C_1 \sigma T_1^4 + C_2 \sigma T_2^4 + C_3 \sigma T_3^4}{C_4} \tag{4-37}$$

where

$$C_1 = A_5 (A_1 R_{12})(A_1 R_{13})$$

$$C_2 = (A_1 R_{11})(A_1 R_{13})(A_2 R_{21})(A_2 R_{23}) \tag{4-38}$$

$$C_3 = (A_1 R_{11})\{(A_1 R_{13})(A_2 R_{21})(A_2 R_{22}) + (A_1 R_{12}) A_5\}$$

$$C_4 = (A_1 R_{11})(A_1 R_{13})(A_2 R_{21})(A_2 R_{23} + A_2 R_{22}) + (A_1 R_{12})[(A_1 R_{13}) A_5 + (A_1 R_{11}) A_5]$$

$$A_5 = (A_2 R_{21})(A_2 R_{23}) + (A_2 R_{22})(A_2 R_{23} + A_2 R_{21})$$

Once the blackbody radiosity of the rod is determined, the blackbody radiosity of the grid spacer can be calculated from the radiation network. The radiation heat flux to the liquid film may then be calculated from (4-34) as

$$q_{rad}^{"} = \frac{J_2 - \sigma T_2^4}{A_2 R_{22}} \tag{4-39}$$

The mass of liquid lost due to evaporation from the surface of the liquid film can be expressed as

$$\dot{m}_{EV} = \frac{Q_{conv} + Q_{rad}}{h_{lv}} = \frac{A(h(T_v - T_{sat}) + q_{rad}^{"})}{h_{lv}} \tag{4-40}$$

Performing a global mass balance on the liquid film, the following relationship must be satisfied:

$$\dot{m}_{DE} = \dot{m}_E + \dot{m}_{EV} \tag{4-41}$$

Substituting for various terms in the above expression, it can be shown that

$$\varepsilon \dot{m}_f = \rho_l \left(\bar{u}_{film} A_{film} + \bar{w}_{cor} A_{cor} \right) + \frac{A(h(T_v - T_{sat}) + q''_{rad})}{h_{lv}} \tag{4-42}$$

The above equation contains two unknowns, i.e., the liquid film thickness H and the fraction of the spacer grid length occupied by the flat portion of the liquid film c_1. Clearly, the value of c_1 which arises from treating the 3-D flow problem by use of a locally 2-D approach as depicted in figure 4-4, needs to be determined separately. Unfortunately, there is no correlation or experimental data available in the literature that provides some kind of a closure relation for c_1. Experiments need to be performed to determine the value of c_1. In the absence of experimental data, the quantity c_1 will be treated as a parameter which leaves the equilibrium film thickness H as the major unknown quantity. Note however that the equation governing the equilibrium film thickness is nonlinear in nature and not amenable to an analytical solution. It must be solved iteratively to obtain the value of H for a given value of the parameter c_1 and the flow conditions.

It is of interest to explore the limiting case of c_1 equal to unity corresponding to the situation in which the flat portion of the liquid film would extend all the way to the center of the spacer grid structure in the unit cell under consideration. Under this limiting condition, the mass balance equation reduces to

$$\varepsilon \dot{m}_f = \rho_l \left(\bar{u}_{film} A_{film} \right) + \frac{A(h(T_v - T_{sat}) + q''_{rad})}{h_{lv}} \tag{4-43}$$

Numerical results for the governing equation will be presented in the next chapter.

4.3 Modeling of the Entrainment of Liquid Ligaments

The flow induced in the liquid film due to the shearing action of the steam causes it to move toward the trailing edge of the spacer strap and eventually leave the solid surface in the form of a liquid jet. These jets would breakup into liquid ligaments which subsequently undergo further

breakup into liquid droplets. The liquid jet leaving the spacer grid can be analyzed by dividing it into two individual components, similar to the way the model was formulated for the equilibrium film thickness in the previous sub-section. It is postulated that the flat portion of the liquid film, extending to a fraction c_1 of the spacer grid length in the unit cell, leaves the trailing edge of the spacer grid in the form of a thin viscous liquid sheet. The corner liquid mass leaves the spacer grid as a distorted column of liquid. However, it is expected that the surface tension forces acting on the column would quickly re-shape the jet into a cylindrical form. Thus, for all practical purposes, the corner liquid mass can be assumed to leave the spacer grid as a cylindrical liquid jet. Further, it is assumed that the average velocity of the liquid in the sheet and the cylindrical jet is the same as the velocity at which they leave the spacer grid. Mass conservation then yields the diameter of the liquid jet issuing from the centre of the unit cell as

$$d_{jet} = 2\sqrt{\left[\frac{4}{\pi}(r_{min} + H)^2 - r_{min}^2\right]} \tag{4-44}$$

Similarly, the thickness of the liquid sheet leaving the trailing edge of the spacer grid is '2H'. It must be noted that, for every unit cell in the rod bundle, there would be 4 liquid sheets and 1 cylindrical liquid jet leaving the trailing edge of the spacer grid. In addition, there are liquid droplets escaping through the gap between the spacer grid surface and the fuel rod.

4.4 Formation of a New Droplet Field Downstream of a Wet Grid

The liquid jet (both the viscous liquid sheet from the flat portion of the liquid film and the round jet from the centre of the unit cell) is inherently unstable to perturbations in the ambient flow field. The aerodynamic forces impressed on the jet due to the steam flow and the surface tension forces tend to break the jet first into liquid ligaments and then into a number of small liquid droplets. Jet breakup has been a subject of study for several decades now. The first mathematical theory for jet breakup was proposed by Lord Rayleigh in 1878. Rayleigh's theory

of cylindrical liquid jet breakup was extended by many other scientists like Bohr, Weber, Ohnesorge, Taylor etc. Ohnesorge classified the jet breakup mechanisms into

(i) Slow dripping from the nozzle under gravity influence (this regime is of no practical significance).

(ii) Cylindrical jet disintegration due to symmetric interface oscillations (Varicose regime).

(iii) Jet disintegration due to asymmetric waves (Sinuous jet breakup).

(iv) Jet atomization due to internal turbulization and surface entrainment.

The size of the particles generated due to the varicose and sinuous breakup of the jet was correlated by Timotika [28] using the equation

$$\frac{D_{drop}}{D_j} = 13Oh_j^{0.5} \tag{4-45}$$

where 'Oh_j' is the Ohnesorge number based on the diameter of the jet. Teng et al [29] correlated the size of the particles resulting from the primary varicose and sinuous breakup of the a jet through

$$\frac{D_{drop}}{D_j} = 1.88\left(1.1303 + 0.0236\log\left(Oh_j^*\right)\right)\left(1 + Oh_j^*\right)^{\frac{1}{6}} \tag{4-46}$$

where Oh_j^* is the modified Ohnesorge number given by

$$Oh_j^* = \frac{3\mu_f + \mu_g}{\left(D_j\sigma\rho_f\right)^{0.5}} \tag{4-47}$$

Faeth [30] correlated particle sizes resulting from jet breakup due to internal turbulization through the relation

$$\frac{D_{drop}}{D_j} = \frac{133}{We_j^{0.74}} \tag{4-48}$$

Kolev [31] suggested that the final size of the droplets after the primary and secondary breakup be taken as the minimum value of the droplet size obtained from all relevant mechanisms. This is because, if inertia fragmentation produces smaller particles, they would be stable in the

environment. On the other hand, if relative velocity method produces smaller particles, the primary entrained droplet would further undergo inertia fragmentation to reach a stable size. Thus, while calculating the final droplet size from the cylindrical liquid jet breakup, the minimum value obtained from the above three correlations was taken to be the stable droplet size.

For the disintegration of the liquid sheet, the physical mechanism proposed by Dombrowski and Johns [32] has been utilized in this work to predict the droplet sizes resulting from the breakup of the viscous liquid sheet. The aerodynamic forces acting on the surface of the liquid sheet causes waves to be generated on the surface of the liquid sheet. Fragmentation of the sheet occurs due to the growth of these waves. Once the amplitude of these waves reaches a critical value, liquid ligaments are torn off from the sheet that deform due to surface tension to form cylindrical ligaments with their axes normal to the flow direction. Capillary forces then cause these ligaments to further breakup into spherical droplets. The most unstable wave number corresponding to the wave with the maximum growth rate was derived to be

$$k_{max} = \frac{\rho_g U^2}{2\sigma} \tag{4-49}$$

In the above equation, 'U' is the relative velocity between the co flowing gas and the liquid sheet. It can be assumed that the ligaments are formed from tears in the sheet twice per wavelength. Then, the diameter of the cylindrical ligament formed is obtained as

$$D_{lig} = \sqrt{\frac{8H}{k_{max}}} \tag{4-50}$$

where H is the half thickness of the sheet, which in the present case happens to the flat film thickness itself. Being oriented transverse to the flow direction, it is expected that the co flowing gas has minimal influence on the breakup of the cylindrical ligament. The process of drop formation from the ligament is primarily governed by capillary instabilities. Following

Dombrowski and Johns [32] again, it can be assumed that the breakup of the cylindrical ligament occurs when the amplitude of the most unstable wave is equal to the radius of the cylindrical ligament. Then, one drop is formed per wavelength. The diameter of this drop is given by

$$D_d = 1.88 D_{lig}(1 + 3(Oh))^{\frac{1}{6}} \tag{4-51}$$

where 'Oh' is the Ohnesorge number based on the diameter of the cylindrical ligament.

It must be emphasized here that there are three individual groups of droplets with different number densities that will observed downstream of a wet spacer grid. These include the droplets that escape through the gap between the spacer grid surface and the fuel rod, the droplets that are formed due to the breakup of the cylindrical jet and the droplets that are formed due to the breakup of the viscous liquid sheet. A convenient physical quantity that can be used to represent these droplets equivalently is the sauter mean diameter, defined as

$$d_{32} = \frac{\sum f_i d_i^3}{\sum f_i d_i^2} \tag{4-52}$$

where f_i is the fraction of droplets in the i^{th} size group and d_i is the diameter of the droplets in the i^{th} size group. Assuming that the droplets that are formed due to the breakup of the cylindrical liquid jet and the liquid sheet are flowing at the same velocity as that of the jet and the sheet respectively, the number density of these droplets can be obtained through mass conservation. The number density of the drops formed from the sheet is given by

$$N_{sheet} = \frac{6A_{film}}{\pi A_u D_d^3} \tag{4-53}$$

The number density of the droplets formed from the cylindrical liquid jet is given by

$$N_{jet} = \frac{6A_{cor}}{\pi A_u D_{drop}^3} \tag{4-54}$$

The number density of droplets upstream of the spacer grid can once again be obtained through a mass balance analysis. If 'α' is the void fraction, the number density of the droplets of diameter 'd_0' is given by

$$N_0 = \frac{6(1-\alpha)}{\pi d_0^3} \tag{4-55}$$

Since it is assumed that the a fraction of the droplets equivalent to the grid blockage ratio gets deposited onto the surface of the spacer grid to form a thin liquid film, the number density of the droplets downstream of a wet grid can be taken to be

$$N_1 = (1-\varepsilon)N_0 \tag{4-56}$$

while the diameter of the droplets can still be assumed to be d_0 (i.e. the droplets undergo negligible amount of evaporation as they flow through the gap between the spacer grid and the fuel rod in the spacer grid span). Then, the sauter mean diameter of the droplets downstream of a wet grid is obtained as

$$d_{32} = \frac{N_{jet}D_{drop}^3 + N_{sheet}D_d^3 + N_1 d_0^3}{N_{jet}D_{drop}^2 + N_{sheet}D_d^2 + N_1 d_0^2} \tag{4-57}$$

The velocity at which the droplets of size d_{32} flow can be taken to be the number density weighted average of the velocity of the droplets in the three different groups mentioned above. Then, this velocity is obtained as

$$v_{32} = \frac{N_{jet}\bar{w}_{cor} + N_{sheet}\bar{u}_{film} + N_1 v_1}{N_{jet} + N_{sheet} + N_1} \tag{4-58}$$

In the above equation, v_1 represents the velocity of the droplets that escape through the gap between the spacer grid and the fuel rod. If α is the void fraction and S is the slip ratio between the droplets and the steam, the velocity v_1 can be obtained from

$$v_1 = S\left(\frac{u_g}{1-\varepsilon} + \frac{\dot{m}_{EV}(1-\varepsilon)}{\rho_g \alpha A_u}\right) \tag{4-59}$$

In the above equation, u_g is the velocity of steam upstream of a spacer grid. The spacer grid blocks a fraction 'ε' of the flow area as a result of which the steam is accelerated to a velocity '$\frac{u_g}{1-\varepsilon}$'. The first term in the equation signifies this increase in the steam velocity. In addition, as the steam flows through the span of the spacer grid, there is evaporation from the liquid film, adding more mass to the steam phase. The second term in the equation signifies the increase in velocity due to this added mass. Once the velocity v_1 is obtained, the number density of droplets with equivalent diameter d_{32} can be obtained through a simple mass conservation equation given below

$$N_{32} = \frac{N_{jet}\bar{w}_{cor}D_{drop}^3+N_{sheet}\bar{u}_{film}D_d^3+N_1v_1d_0^3}{v_{32}d_{32}^3} \quad (4\text{-}60)$$

The ratio of the sauter mean diameter of the droplets downstream of a wet grid to that upstream of a wet grid is given by

$$(d_{32})_{ratio} = \frac{d_{32}}{d_0} \quad (4\text{-}61)$$

Numerical solution to the above system of governing equations for the equilibrium film thickness can be obtained along with the diameter, velocity and the number density of the droplets immediately downstream of a wet grid. However, it must be noted that this model would still treat the quantity c_1 as a parameter. Hence, it cannot be implemented into a computer code such as COBRA-TF or TRACE directly. Separate effect bench top experiments need to be performed to determine, among other items, the variation of c_1 with the flow conditions in a rod bundle and to validate the proposed model.

4.5 Grid Enhanced Heat Transfer Downstream of a Wet Grid

As postulated in the previous sections, the deposition of the liquid droplets leads to the establishment of a thin liquid film on the surface of a wet spacer grid. The superheated steam

flowing through the gap between the spacer grid and the fuel rod is accelerated due to the flow passage constriction and evaporation from the surface of the liquid film. In addition, the loss of latent heat of vaporization from the superheated steam results in the de – superheating of the same. Thus, downstream of a wet grid, the fuel rod is now exposed to steam that is moving at a much higher velocity (in comparison to the velocity upstream of the grid) and at a much lower temperature. The combination of these two changes in the steam flow properties is expected to cause a significant increase in the heat flux removed from the surface of the fuel rod. Cheung et al [23] proposed a model for the heat transfer augmentation downstream of a dry spacer grid. In a dry grid scenario, the heat transfer augmentation is expected to be due the increase in interfacial surface area (for droplet evaporation) as a result of the shattering of the droplets on hitting the dry spacer grid strap. On the other hand, for a wet grid scenario, the heat transfer augmentation is due to the acceleration of steam, de – superheating of the steam and droplet evaporation downstream of a wet grid.

The droplets downstream of a wet grid have an equivalent diameter d_{32} and flow at a velocity v_{32}. Over a small time interval Δt, these droplets would have traveled a distance $\Delta z = v_{32}\Delta t$. The amount of flow volume in this time interval is $\Delta V_{flow} = A_u \Delta z$. Thus, the interfacial area within this flow volume that is available for droplet evaporation is given by

$$A_i = N_{32} A_u \Delta z \pi d_{32}^2 \tag{4-62}$$

The liquid droplets that are flowing in the continuous steam phase are heated convectively. The convective heat flux to the liquid droplet from the superheated steam is given by

$$q_c^{"} = \frac{k}{d_{32}} Nu_d (T_g - T_{sat}) \tag{4-63}$$

where k is the vapor thermal conductivity, d_{32} is the sauter mean diameter of droplets, Nu_d is the droplet Nusselt number, T_g is the temperature of the vapor. Note that the value of T_g upstream

and downstream of a wet grid is considerably different due to the loss of latent heat of vaporization in the process of evaporation of the liquid film on the surface of the spacer grid. On the contrary, in a dry grid scenario, the value of T_g is expected to be approximately same upstream and downstream of the spacer grid. The reduction in steam temperature as it passes through the span of a wet spacer grid can be obtained through an energy conservation equation as below

$$\Delta T_g = \frac{\dot{m}_{EV} h_{fg} (1-\varepsilon)}{c_p \rho_g \alpha A_u u_g} \tag{4-64}$$

The droplet Nusselt number can be obtained using the correlation for flow over a sphere. This correlation is given by

$$Nu_d = 0.37 \left(\frac{U_r d_{32}}{\nu_g} \right)^{0.6} \tag{4-65}$$

where U_r is the relative velocity between the droplets and the continuous steam phase and ν_g is the kinematic viscosity of the vapor. Then, in terms of the heat flux $q_c^{"}$, the rate of depletion of liquid mass due to evaporation in the flow volume ΔV_{flow} is given by

$$\Delta \dot{m}_f = -\frac{A_i q_c^{"}}{h_{fg}} \tag{4-66}$$

Mass conservation dictates that the rate of consumption of liquid mass is equal to the rate of generation of the vapor mass. Then, the rate of generation of vapor mass in the flow volume is given by

$$\Delta \dot{m}_g = \frac{A_i q_c^{"}}{h_{fg}} \tag{4-67}$$

In the dispersed flow film boiling regime, the void fraction is very close to unity. Thus the rate of convective heat transfer from the rod to the two phase mixture primarily depends on the velocity

and temperature of the vapor flow. The Nusselt number for single phase convective heat transfer from the fuel rod to the steam flow is give by the Weismann correlation as

$$Nu = 0.0317Re^{0.8}Pr^{0.4} \tag{4-68}$$

For steam at a specified temperature and pressure, the above correlation is a function of the velocity of the steam alone (i.e., $Nu \sim u_g^{0.8}$). Then, the heat transfer coefficient at the surface of the fuel rod can be written as

$$h = \frac{Nuk}{D_H} = Cu_g^{0.8} \tag{4-69}$$

The heat flux removed from the surface of the fuel rod is given by

$$q_w^{"} = h(T_w - T_g) = Cu_g^{0.8}(T_w - T_g) \tag{4-70}$$

Droplet evaporation generates additional steam mass thereby increasing the steam velocity. If it is assumed that the temperature change of steam in the droplet evaporation process is minimal, then the droplet induced augmentation in the wall heat flux can be obtained as

$$q_w^{"} = h(T_w - T_g) = C(u_g + \Delta u_g)^{0.8}(T_w - T_g) \tag{4-71}$$

where Δu_g is the increase in the steam velocity due to droplet evaporation. This quantity Δu_g can be obtained from equation (4-67) as

$$\Delta u_g = \frac{\Delta \dot{m}_g}{\rho_g \alpha A_u} = \frac{A_i q_c^{"}}{\rho_g \alpha A_u h_{fg}} \tag{4-72}$$

It is well established that in a dry grid scenario, the process of droplet shattering causes a significant increase in the heat transfer coefficient downstream of the grid. This increase however is only because of the acceleration of the steam due to flow constriction and evaporation of the smaller droplets downstream (droplet shattering process produces smaller droplets with higher number density). Cheung and Bajorek [21] obtained a model for the droplet

sauter mean diameter downstream of a dry grid in terms of the grid blockage ratio and the sauter mean diameter of the droplets upstream of the grid. This equation is given by

$$\frac{d_1}{d_0} = \frac{1}{1+0.1803\varepsilon We_0^{0.558}} \tag{4-73}$$

where d_1 is the sauter mean diameter of the droplets downstream of the grid, d_0 is the sauter mean diameter of the droplets upstream of the grid, ε is the grid blockage ratio and We_0 is the Weber number of the droplets upstream of the grid. If α is the void fraction and S is the slip ratio, then the number density of the droplets upstream of the grid can be obtained by mass balance as

$$N_0 = \frac{6(1-\alpha)}{\pi d_0^3} \tag{4-74}$$

Once again, by mass conservation, the number density of droplets downstream of a dry grid can be obtained as

$$N_1 = (1-\varepsilon)N_0\left(\frac{d_0}{d_1}\right)^3 \tag{4-75}$$

The factor $(1-\varepsilon)$ appears to account for the fact that the steam (and hence droplets) is accelerated as it flows through the grid. In formulating the above equation, it is assumed that the droplets undergo negligible amount of evaporation as they flow through the span of the spacer grid. As mentioned previously, a wet grid is expected to have a greater heat transfer enhancement downstream of the grid in comparison to a dry grid under the same flow and system conditions. In order to compare the relative effectiveness of a wet grid and a dry grid under similar flow conditions, one can consider the ratio of the wall heat flux downstream of a wet grid to that downstream of a dry grid. If $(q_w^{"})_w$ is the wall heat flux downstream of a wet grid and $(q_w^{"})_d$ is the wall heat flux downstream of a dry grid, then

$$eff = \frac{(q_w^{"})_w}{(q_w^{"})_d} \tag{4-76}$$

where '*eff*' is the relative effectiveness of a wet grid in comparison to a dry grid in augmenting the heat transfer immediately downstream. If $(u_g)_w$, $(\Delta u_g)_w$, $(T_g)_w$ represent the velocity of steam, increase in the velocity of steam due to droplet evaporation, steam temperature downstream respectively for a wet grid and $(u_g)_d$, $(\Delta u_g)_d$, $(T_g)_d$ represent these quantities for a dry grid, the equation for '*eff*' can be written as

$$eff = \frac{((u_g)_w+(\Delta u_g)_w)^{0.8}(T_w-(T_g)_w)}{((u_g)_d+(\Delta u_g)_d)^{0.8}(T_w-(T_g)_d)} \tag{4-77}$$

This equation can further be simplified into

$$eff = \frac{\left(R\frac{(u_g)_w}{(u_g)_d}+\frac{(\Delta u_g)_w}{(\Delta u_g)_d}\right)^{0.8}(T_w-(T_g)_w)}{(1+R)^{0.8}(T_w-(T_g)_d)} \tag{4-78}$$

where *R* is the ratio of the steam velocity downstream of a dry gird to the increase in steam velocity due to droplet evaporation downstream of a dry grid. '*R*' is the same quantity that Cheung et al [23] used in their model. Following Cheung et al [23], this quantity will be treated as a parameter in this work. The numerical solution obtained is discussed in the next chapter.

CHAPTER 5

NUMERICAL RESULTS AND DISCUSSION

5.1 Order-of-Magnitude Analysis

In order to obtain an estimate of the thickness of the film on the spacer grid surface, an order-of-magnitude analysis has been performed for two limiting cases:

(1) The flat liquid film extends all along the length of the spacer grid as shown in figure 5-1. The equilibrium thickness of this film is assumed to be 'H'.

(2) The liquid film on the spacer grid consists of the lumped mass at the corner alone as shown in figure 5-2. In this case, all the liquid mass deposited onto the spacer grid is assumed to be driven laterally along the surface of the spacer grid and added onto the lumped mass at the corner. The parameter controlling the size of this film is the polar angle 'θ' measured as shown in the figure 5-2.

For the sake of brevity, the liquid film on a quarter of the unit cell (figure 4-2) alone is shown below

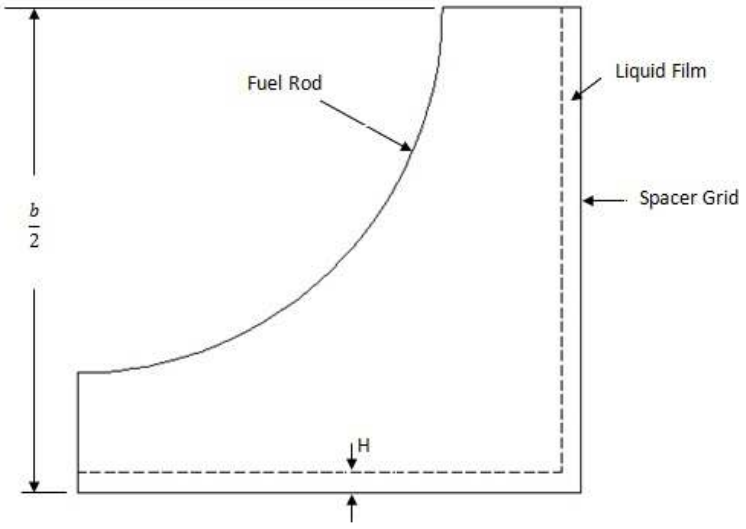

Fig 5-1: Schematic of the Liquid Film, Case 1

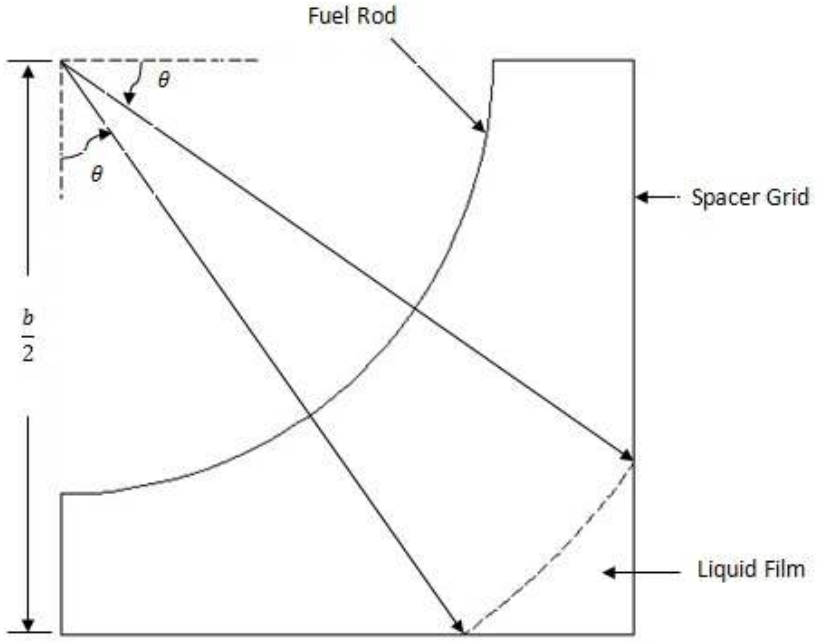

Fig 5-2: Schematic of the Liquid Film, Case 2

The values for various quantities like the spacer grid dimensions, sub-channel dimensions, flow velocities, pressure etc. are taken to be those corresponding to the values of these quantities in the RBHT test facility. The RBHT test facility has a flow housing that provides a flow area of 48.63 cm^2. This flow area can be divided into 36 unit cells, each has the configuration shown in figure 3-2 with four quarter unit cells as shown in figure 3-3. The flow area per unit cell is 0.878 cm^2. The upper plenum pressure can be varied between 20 psia and 60 psia. Consider a flooding rate $(u_f)_0$ of 25.4 mm/s, at a pressure of 20 psia, the mass flow rate through each of the unit cells can readily be calculated by

$$(\dot{m}_f)_0 = (u_f)_0 A_u \rho_f \tag{5-1}$$

As the inlet liquid flows through the rod bundle, it is converted to steam by boiling due to the heat transferred from the rods. The mass quality of the liquid-vapor mixture at any axial location is given by

$$x = \frac{\dot{m}_g}{\dot{m}} = \frac{\dot{m}_g}{(\dot{m}_f)_0} \tag{5-2}$$

Mass balance dictates that at any location, the following relationship must hold

$$\dot{m} = \dot{m}_g + \dot{m}_f = (\dot{m}_f)_0 \tag{5-3}$$

The local void fraction at a given axial location can be related to the local mass quality at that location through a correlation of the form

$$\alpha = f\left(x, \frac{\mu_f}{\mu_g}, \frac{\rho_g}{\rho_f}\right) = \left[1 + B_B \left(\frac{1-x}{x}\right)^{n_1} \left(\frac{\rho_g}{\rho_f}\right)^{n_2} \left(\frac{\mu_f}{\mu_g}\right)^{n_3}\right]^{-1} \tag{5-4}$$

where the coefficient and indices appearing in the above expression are given in Table 5-1 below.

Table 5-1.Coefficient and IndicesEmployed in Different Models and Correlations

Model	B_B	n_1	n_2	n_3
Homogeneous model	1	1	1	0
Zivi model	1	1	0.67	0
Wallis Separate Cylinder model	1	0.72	0.40	0.08
Lockhart &Martinelli model	0.28	0.64	0.36	0.07
Thom correlation	1	1	0.89	0.18
Barcozy correlation	1	0.74	0.65	0.13

Conservation of mass requires that

$$\rho_g \alpha A_u u_g + \rho_f (1-\alpha) A_u u_f = (\dot{m}_f)_0 \tag{5-5}$$

The slip ratio between the liquid and the vapor is defined as

$$S = \frac{u_f}{u_g} \tag{5-6}$$

Assuming that the vapor is at a superheated temperature of 400^{o} C, the local void fraction can be estimated as a function of the mass fraction, and the local liquid and steam velocities can be estimated as a function of the local void fraction using the above expressions.

Assuming that all the liquid flowing through the area of the sub-channel blocked by the spacer grid gets deposited onto the grid while the remaining droplets escape through the gap between the spacer grid and the fuel rod, the mass of liquid deposited is given by

$$\dot{m}_{DE} = \varepsilon(1-x)\left(\dot{m}_f\right)_0 = \varepsilon(1-\alpha)\rho_f A_u S u_g \tag{5-7}$$

where ε is the grid blockage ratio.

This liquid mass that is deposited onto the spacer grid surface forms a thin liquid film on the surface. The liquid film loses mass due to the combined action of shear thinning at the trailing edge and evaporation at the liquid film surface whereas it gains mass through the deposition of liquid droplets. The equilibrium size of the film is governed by the balance between mass depletion and mass addition to the liquid film on the spacer grid. Accordingly, the mass flow rate $\dot{m}_E$ of the liquid ligament shearing off from the liquid film is given by

$$\dot{m}_E = \dot{m}_{DE} - \dot{m}_{EV} \tag{5-8}$$

The mass evaporated can be assumed to be proportional to the mass deposited, i.e.,

$$\dot{m}_{EV} = B\dot{m}_{DE} \qquad 0 < B < 1 \tag{5-9}$$

It follows that

$$\dot{m}_{DE}(1-B) = \dot{m}_E \tag{5-10}$$

Now considering case (1), in terms of the equilibrium thickness of the film, the flow area through which the entrained liquid ligaments leave the spacer grid is given by

$$A_E = 4bH < A_u \tag{5-11}$$

where b is the length of the spacer strap.

If $\bar{u}$ is the average velocity at which the liquid ligaments leave the spacer grid, then from mass conservation, the following relationship must be valid:

$$\dot{m}_E = 4bH\rho_f\bar{u} \tag{5-12}$$

It follows that the average velocity of the liquid ligament is given by

$$\bar{u} = \frac{\dot{m}_E}{4bH\rho_f} \tag{5-13}$$

Assuming a given value for *B*, the variation of $\bar{u}$ with *H* can be determined for different values of the void fraction as shown in figure 5-3.

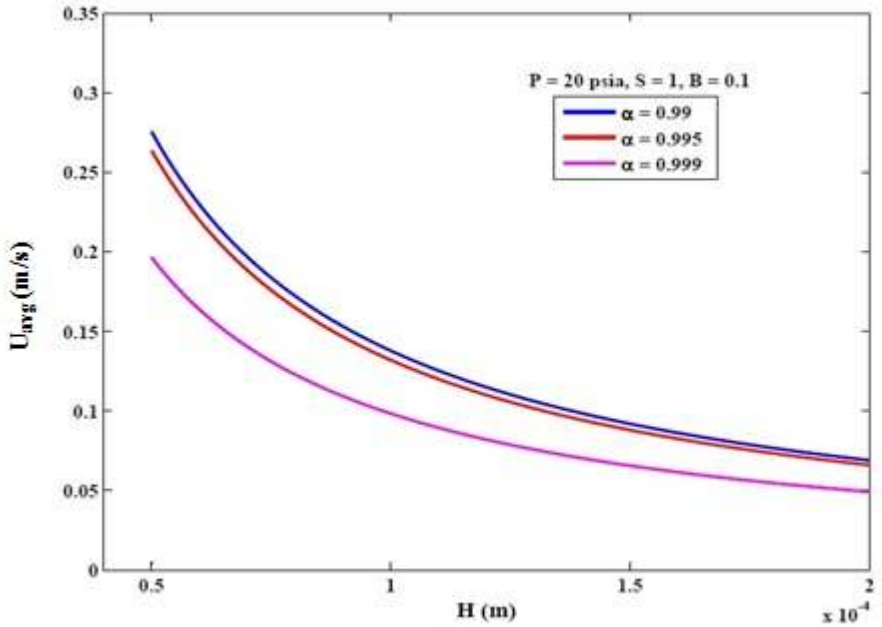

Fig. 5-3.Variations of the Average Film Velocity with the Equilibrium Film Thickness

The shearing action of the two phase mixture would lead to the breakup of the liquid ligaments resulting in the formation of a number of tiny droplets. If this process of breakup results in the formation of *N* droplets of diameter *d*, flowing at an average velocity of u_d, then from mass conservation, the following can be derived:

$$\dot{m}_E = 4bH\rho_f\bar{u} = \rho_f A_u u_d N\frac{\pi}{6}d^3 \tag{5-14}$$

Assuming that the velocity of the droplet is directly proportional to the velocity of the vapor,

$$u_d = au_g \qquad 0 < a < 1 \tag{5-15}$$

the following relationship can be expected

$$\dot{m}_E \sim 4bH\rho_f \bar{u} \sim \rho_f A_u a u_g N \frac{\pi}{6} d^3 \tag{5-16}$$

$$N = \frac{24bH\bar{u}}{A_u a u_g \pi d^3} \tag{5-17}$$

Results are presented in figures 5-4 and 5-5.

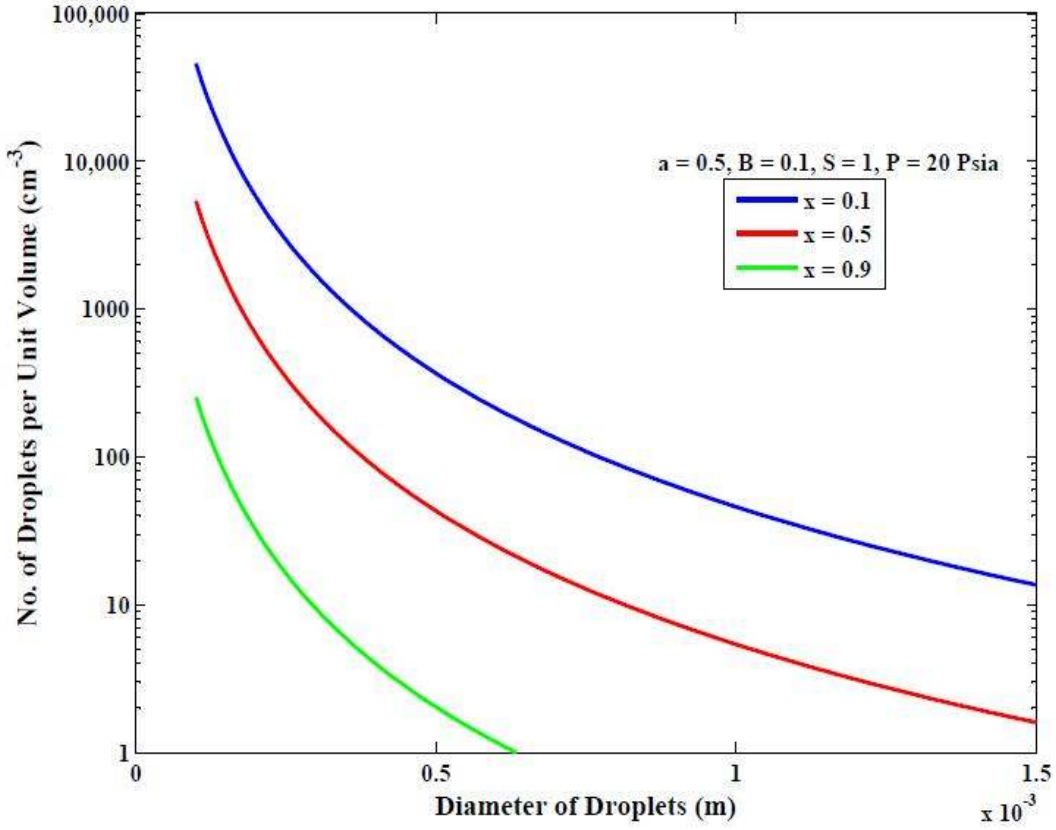

Fig. 5-4.Relationship between the Number of Droplets and the Droplet Size

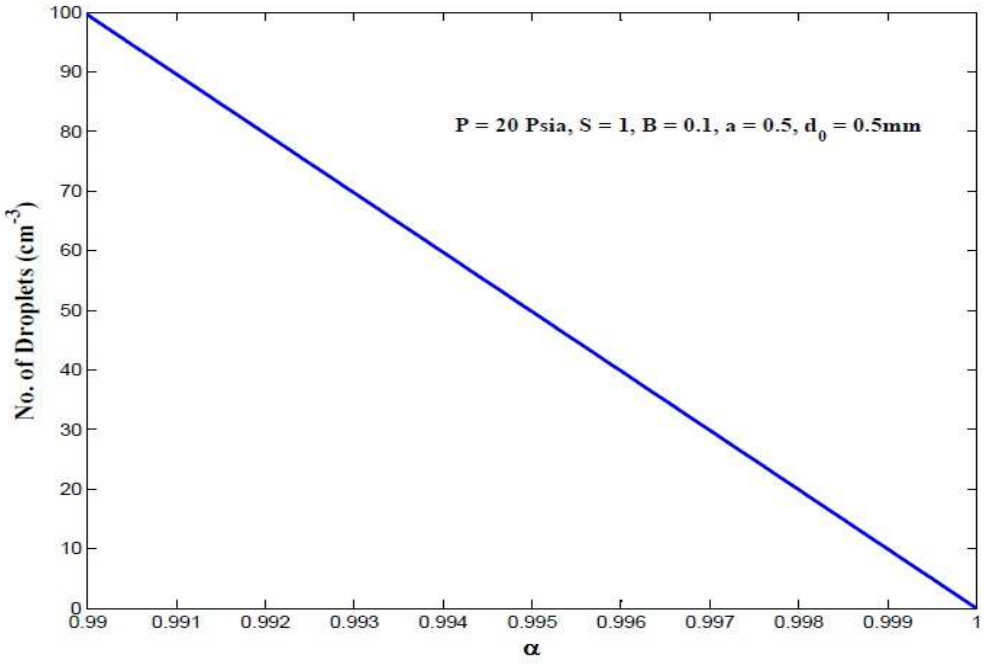

Fig. 5-5.Number of Droplets from the Breakup of Liquid Ligaments

In figure 5-2, the number of droplets for a given mass quality is plotted as a function of the droplet diameter whereas in figure 5-3, the number of droplets resulting from breakup of the liquid ligaments that are entrained from the liquid film is plotted as a function of the local void fraction. As can be seen from these figures, the number of droplets is on the order of 100 for mass fraction more than 0.5 and sizes of droplets on the order of 0.5 mm.

Note that in addition to those droplets formed from the breakup of liquid ligaments, there are liquid droplets escaping through the grid spacer from upstream. The mean flow rate of the latter is given by

$$\dot{m}_0 = (1-\varepsilon)(1-x)\dot{m}_{f_0} \tag{5-18}$$

Assuming that these "escaped" droplets have the same diameter of d_0, the total droplet number N_T will become

$$N_T = N + \frac{6(1-\varepsilon)(1-x)\dot{m}_{f_0}}{A_u a u_g \pi d_0^3 \rho_f} \tag{5-19}$$

Results are shown in figure 5-6.

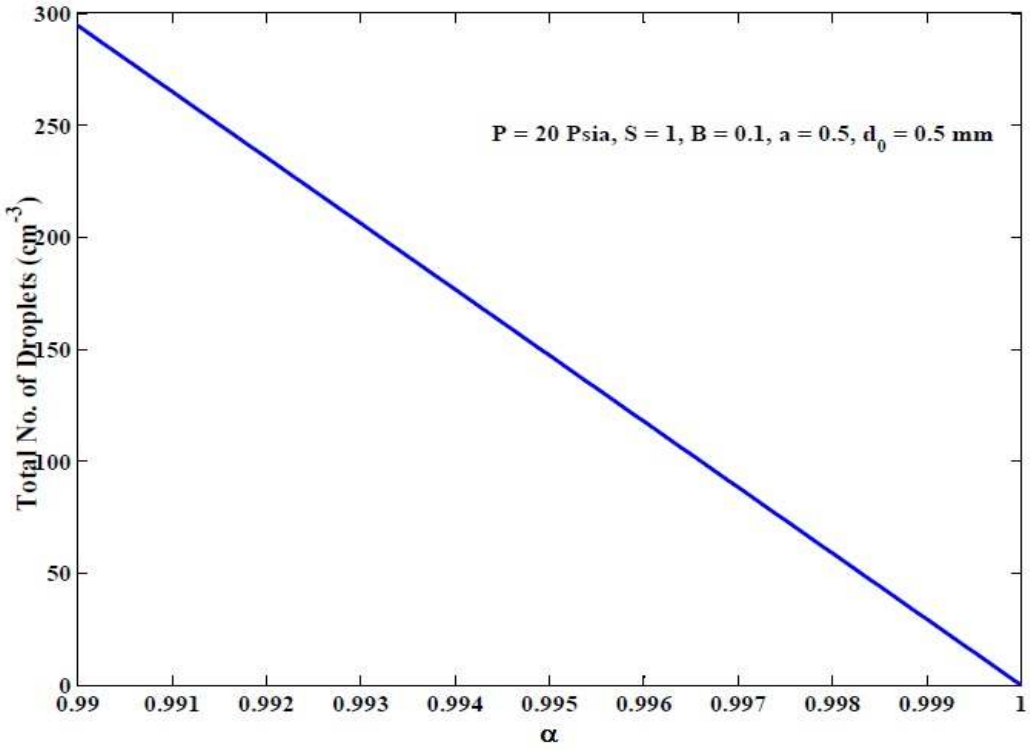

Fig. 5-6.Total Number of Droplets Downstream of a Wet Grid

In case (2), the flow area through which the entrained ligaments leave the trailing edge of the spacer grid is given by

$$A_E = \left(\frac{b}{2}\right)^2 - \left(\frac{b}{2}\right)^2 \tan(\theta) - \frac{\pi-4\theta}{4}\left(\frac{b}{2}\right)^2 sec^2(\theta) \tag{5-20}$$

If $\bar{u}$ is the average velocity at which the liquid ligaments leave the spacer grid, then from mass conservation, the following relationship must be valid

$$\dot{m}_E = 4A_E\rho_f\bar{u} \tag{5-21}$$

It follows that the average velocity of the liquid ligament is given by

$$\bar{u} = \frac{\dot{m}_E}{4A_E\rho_f} \tag{5-22}$$

This corner liquid mass leaves the trailing edge of the spacer grid as a distorted column of liquid.

It is anticipated that the surface tension forces would quickly deform this column into a circular liquid jet. Assuming that the circular liquid jet has the same velocity as that of the distorted column of liquid, conservation of mass yields the diameter of the jet as

$$d_{jet} = \left(\frac{16}{\pi} A_E\right)^{0.5} \tag{5-23}$$

It must be noted that the diameter of the jet cannot exceed a value corresponding to the diameter of a circle that is tangential to all the four fuel rods in the unit cell as shown in figure 5-7 below.

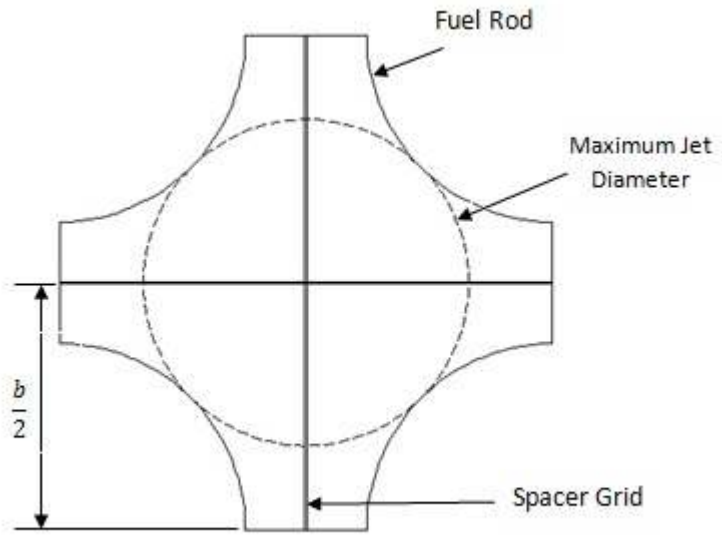

Fig 5-7: Maximum possible Jet Diameter

This diameter is given by

$$(d_{jet})_{max} = b\sqrt{2} - d_{rod} \tag{5-24}$$

This imposes a restriction on the possible angles 'θ' to which the corner liquid mass could extend. For the dimensions of the unit cell as employed in RBHT test facility, this maximum value of jet diameter is obtained as

$$(d_{jet})_{max} = 8.3\ mm \tag{5-25}$$

The variation of the jet diameter with the angle 'θ' is shown in figure 5-8 below

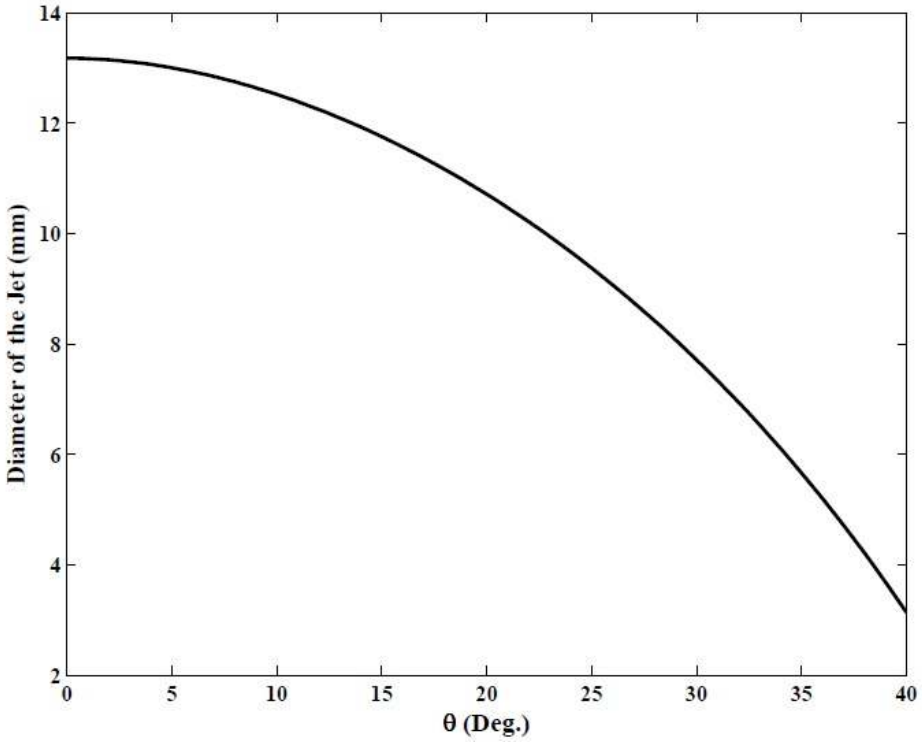

Fig 5-8: Variation of Jet Diameter with θ

From the above figure, it can be seen clearly that the permissible range of values of 'θ' is

$$28.5 < \theta < 45 \tag{5-26}$$

It must be noted that θ = 45 deg. would correspond to no liquid mass which can occur only when the void fraction is unity, i.e. the flow consists of single phase steam entirely. Once again, assuming a value for B, the variation of $\overline{u}$ with θ can be determined for various values of the void fraction as shown below in figure 5-9

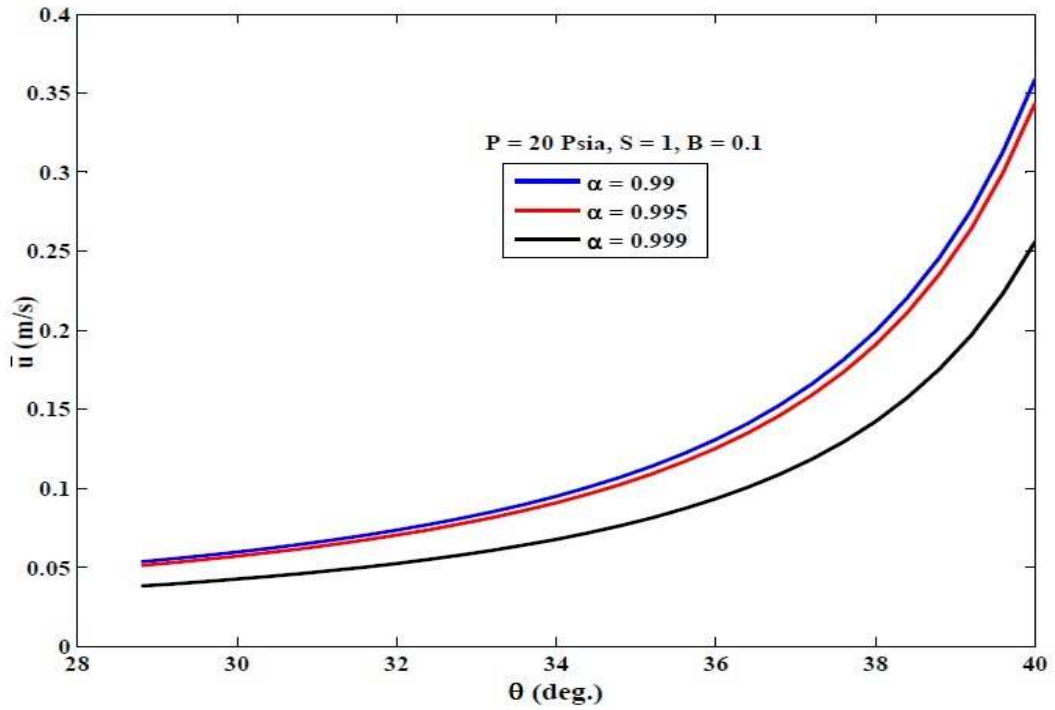

Fig 5-9: Variation of the Average Jet Velocity with 'θ'

5.2 Calculation of the Equilibrium Film Thickness and Droplet Size Downstream of a Wet Grid

The governing equation for the equilibrium film thickness and the fraction of the spacer grid length in the unit cell occupied by the flat portion of the liquid film has been solved numerically in MATLAB. Due to the lack of an additional equation to close the system, c_1 has been treated as a parameter in the numerical calculations with its value varying between 0.7 and 0.8. An inbuilt function *fsolve* available in MATLAB has been utilized to solve the governing equation. The function *fsolve* in MATLAB provides solutions to a non linear system of equations specified by

$$F(X) = 0 \tag{5-27}$$

A function describing the set of equations was written and input to fsolve along with an initial guess value for the equilibrium film thickness. The inbuilt function *fsolve* then outputs the optimal value of the equilibrium film thickness which drives the function *F* to zero. This value of the equilibrium film thickness can then be utilized to obtain the film and the corner mass

velocities. This procedure to determine the film thickness and later the film and corner mass velocities has been carried out for void fractions varying from 0.99 to 0.999 and for each of the void fraction values; two different values of c_1, 0.7 and 0.8, and two different values of the slip ratio (S), 0.9 and 0.8, have been utilized. The results obtained for an upper plenum pressure of 20 Psia and flooding rate of 25.4 mm/s are shown in figures 5-10 to 5-12 below.

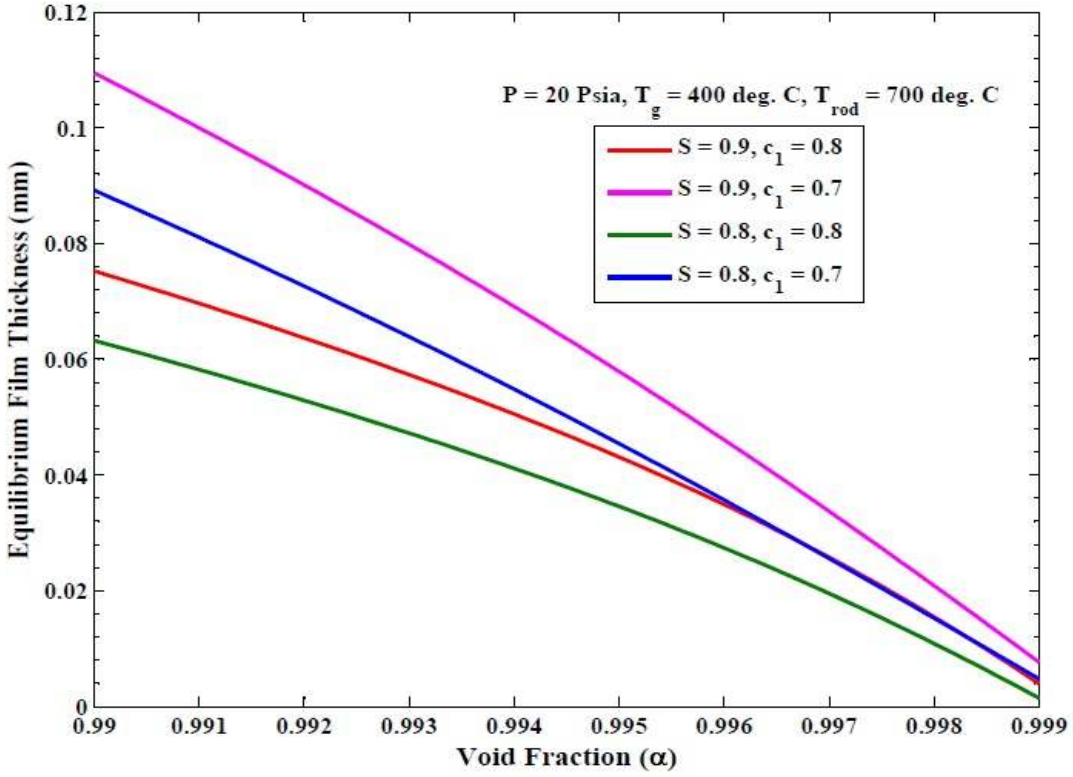

Fig. 5-10.Equilibrium Film Thickness Predicted by the Present Model

As can be seen from figure 5-10, the equilibrium film thickness tends to decrease as the void fraction increases. With an increase in the void fraction, the amount of liquid droplets in the dispersed two-phase mixture reduces resulting in less deposition and consequently a reduced film thickness. The film thickness is found to be higher when the value of c_1 is lower at the same slip ratio. A decrease in the slip ratio results in a decrease in the film thickness. This is because the liquid mass flow rate is a function of the slip ratio. Thus a reduction in the slip ratio causes a

reduction in the liquid deposition rate resulting in a reduced film thickness. This similar trend is reflected in the flat liquid film velocity too, as can be seen from figure 5-11.

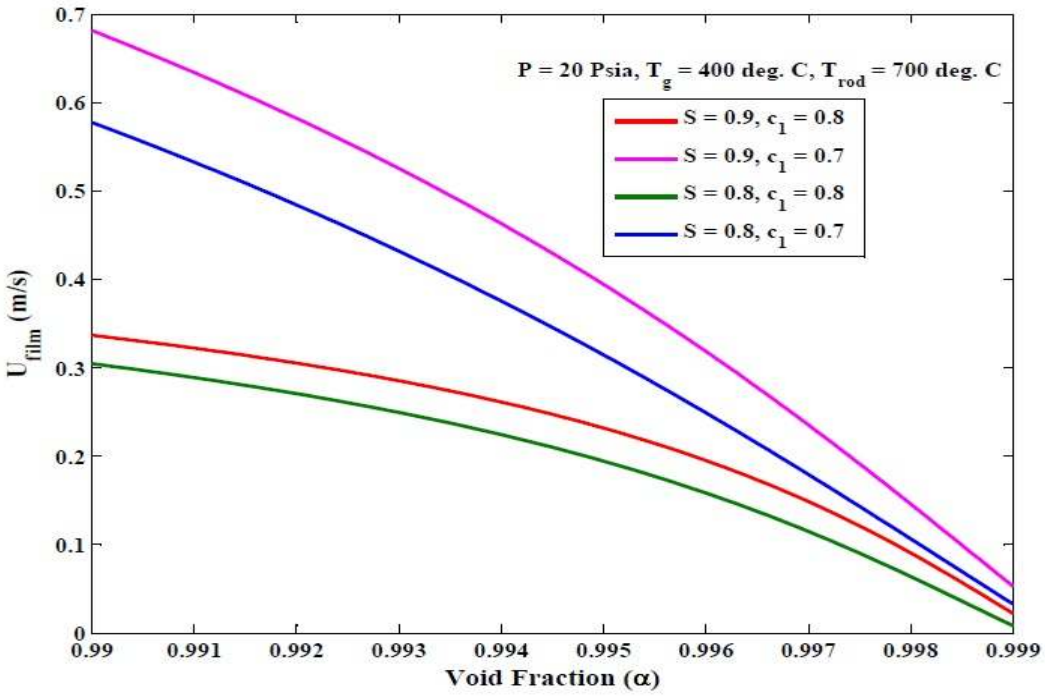

Fig. 5-11.Flat Liquid Film Velocity Predicted by the Present Model

The liquid film velocity reduces as the void fraction increases. Figure 5-12 shows the values of the corner mass velocity obtained for various values of the void fraction, slip ratio and c_1. It can be seen that, not all combinations of the void fraction and c_1 results in a positive film velocity. For any given value of c_1, there is only a certain range of void fractions that would result in the co current flow of the corner liquid mass. For values of void fraction outside this range, the corner liquid mass velocity is found to go negative indicating that the corner mass is flowing in the counter current direction. With an increase in the void fraction, the velocity of the corner mass is found to increase. This is consistent with the observation that the velocity of the flat film decreases with an increase in the void fraction. In order to conserve mass, the corner liquid mass has to flow faster. However, it is interesting to note that there is a maximum in the corner velocity for any combination of c_1 and slip ratio. In addition, for any particular value of

c_1, the corner velocity increases as the slip ratio decreases. This trend is exactly opposite to that observed for the flat film velocity. It can be observed that the velocity of the corner liquid mass obtained from the numerical solution is consistent (both qualitatively and quantitatively) with that obtained through an order of magnitude analysis described previously. From these results, it can be concluded that the velocity of the liquid film (both corner mass and flat film) is strongly dependent on the distribution of liquid mass on the surface of the wet spacer grid. This in turn is a function of the flow and system conditions such as upper plenum pressure, void fraction, fuel rod temperature, grid blockage ratio etc. Data relevant to wet grid phenomenon is presently lacking in the literature. Separate effect bench top experiments need to be carried out to determine the relation of c_1 to the flow and system properties and validate the model under varied flow conditions so that it can be implemented into systems analysis codes like COBRA – TF and TRACE.

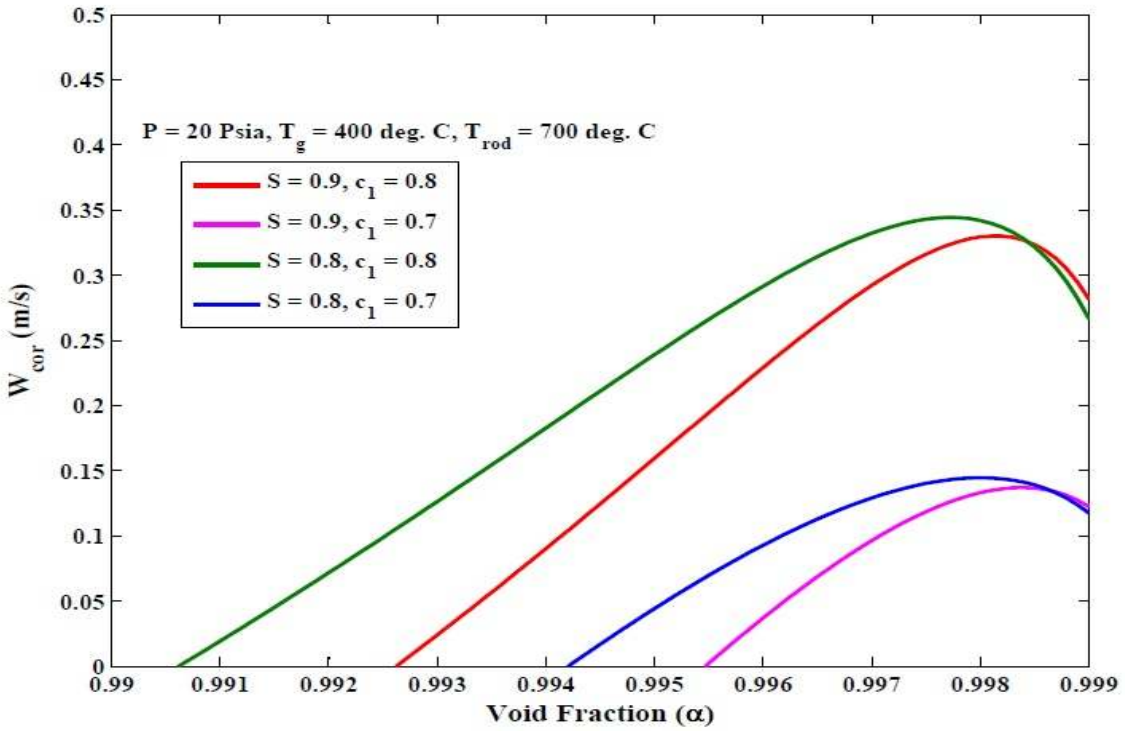

Fig. 5-12.Corner Liquid Jet Velocity Predicted by the Present Model

Once the film thickness, corner liquid mass velocity and the flat film velocity were obtained for various values of the void fraction, c_1 and the slip ratio (S), the sauter mean diameter, velocity and the number density of the droplets formed due to the breakup of the liquid jet and sheet were determined using equations (4-44) to (4-61). For an upstream droplet diameter of 0.5 mm, the downstream to upstream ratio of the sauter mean diameter of the droplets was calculated. Results obtained are shown in the figure 5-13 below.

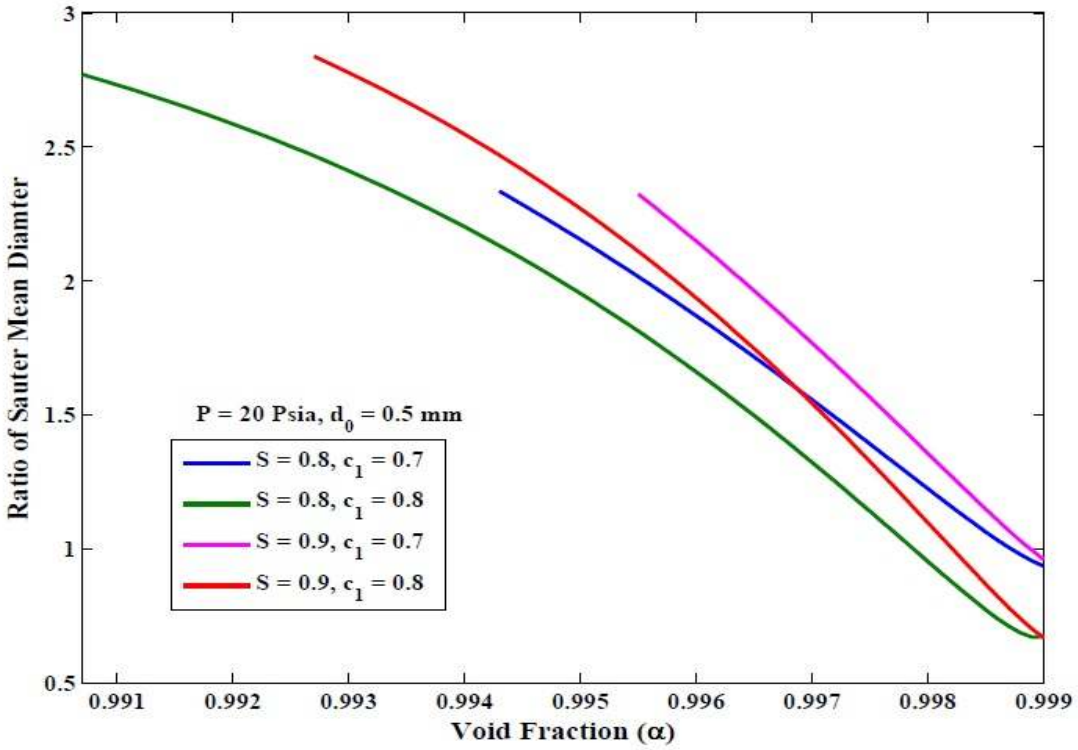

Fig. 5-13. Ratio of Sauter Mean Diameters Predicted by the Present Model

It must be noted that the range of void fractions that are admissible is a strong function of the slip ratio and c_1, as explained above. This is the reason for different curves beginning at different void fraction values in the above plot. The above figure clearly indicates that the sauter mean diameter of the droplets downstream of a wet grid is larger than that upstream of a wet grid, as observed in the RBHT tests. With an increase in the value of c_1 for any particular value of the slip ratio and void fraction, the equilibrium film thickness (H) was found to reduce in magnitude

(see figure 5-10). Consequently, the thickness of the liquid sheet and the diameter of the cylindrical liquid jet issuing from the trailing edge of the spacer grid reduce resulting in droplets of a smaller diameter. As a result, we observe that the increase in the sauter mean diameter of the droplets downstream of a wet grid is lower for a higher value of c_1. As we approach void fractions close to unity (~0.999), the thickness of the film and the diameter of the circular jet reduce to a value less than the diameter of the droplets upstream of the grid. Thus, the droplets formed from the breakup of the sheet and the jet are also smaller in size leading to a reduction in the sauter mean diameter of the droplets downstream of the grid. For values of void fraction other than those very close to unity, a wet grid would result in the generation of larger diameter droplets downstream. To understand the separate effect of the quantities c_1 and S on the sauter mean diameter ratio, calculations for a fixed value of the void fraction and S (or c_1 as the case may be) were carried out. The results obtained are presented in figures 5-14 and 5-15.

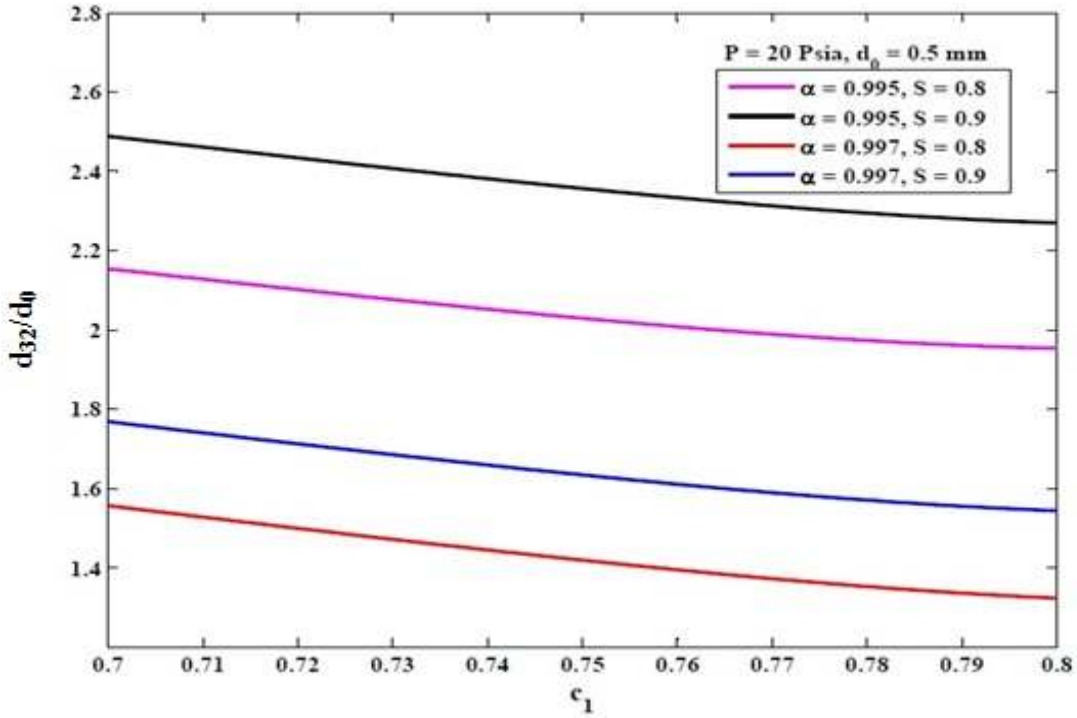

Figure 5-14. Ratio of Sauter Mean Diameters Predicted by the Present Model for a constant S and void fraction

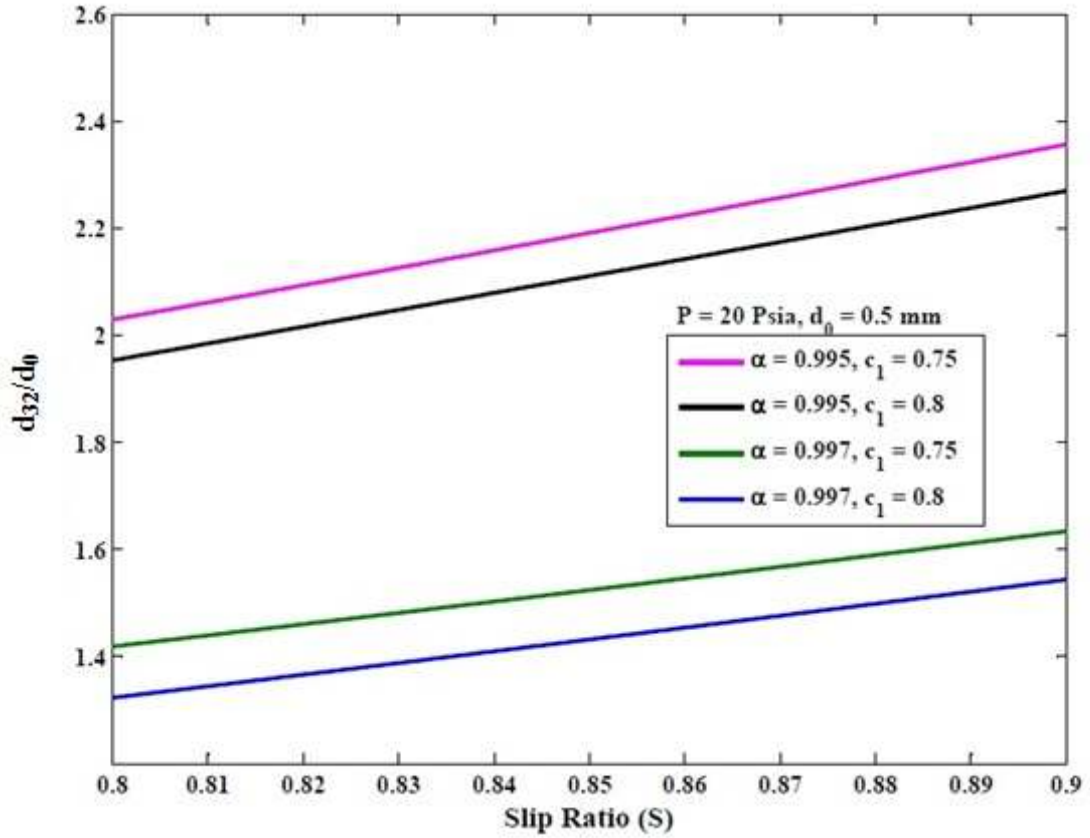

Figure 5-15. Ratio of Sauter Mean Diameters Predicted by the Present Model for a constant c_1 and void fraction

From the above figures, it can be seen that for a given value of the slip ratio and the void fraction, the upstream-to-downstream ratio of the sauter mean diameter of the droplets is a decreasing function of c_1 within the applicable range of the present model. However, for any given value of the void fraction and c_1, the sauter mean diameter ratio is an increasing function of the slip ratio. All the results presented above were obtained by fixing the upstream droplet diameter at 0.5 mm. In order to study the effect of upstream droplet diameter, the calculations were carried out by fixing the value of the slip ratio at 0.8 and using two different values for c_1 (0.7 & 0.8) while the void fraction was varied between 0.995 and 0.999. The results obtained are shown in figures 5-16 and 5-17.

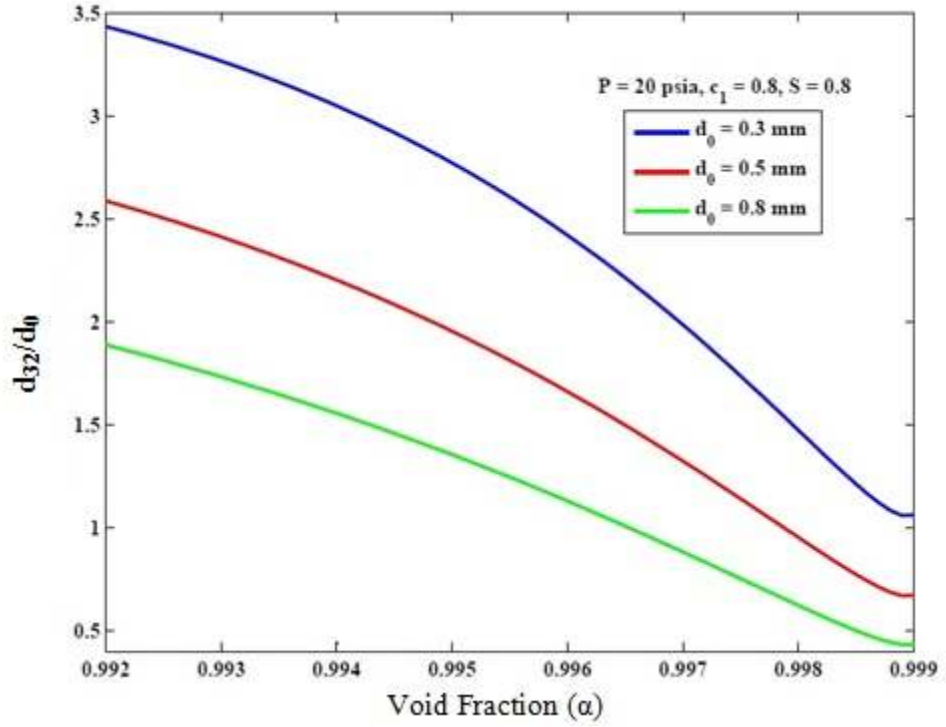

Figure 5-16. Ratio of Sauter Mean Diameters Predicted by the Present Model for different values of the upstream droplet diameter, constant c_1 and S

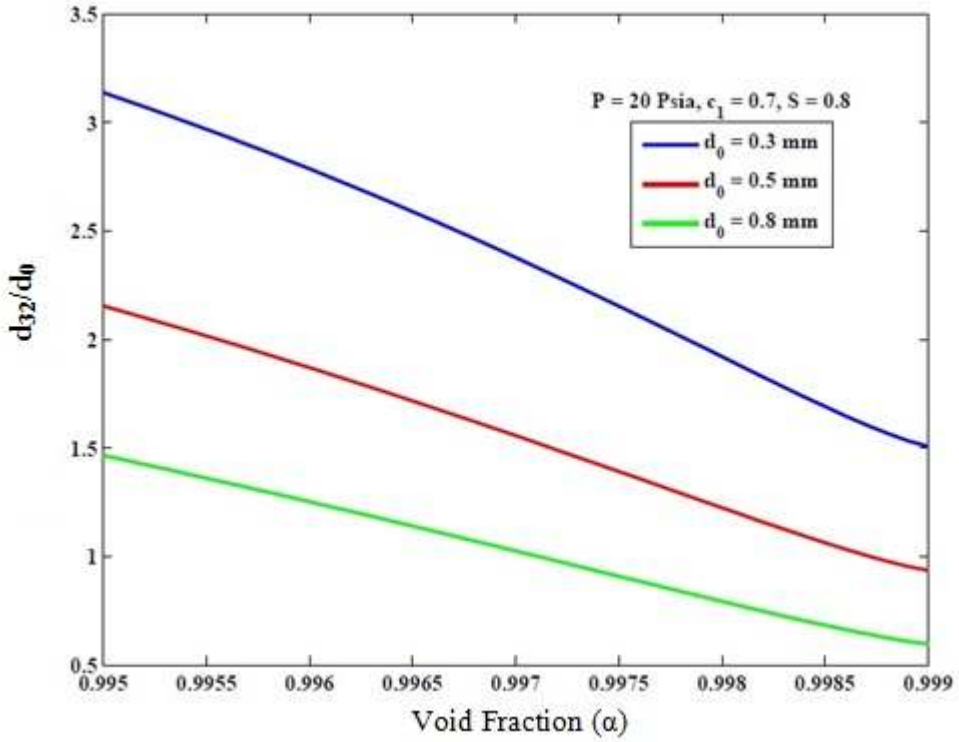

Figure 5-17. Ratio of Sauter Mean Diameters Predicted by the Present Model for different values of the upstream droplet diameter, constant c_1 and S

It can be seen from the above figures that the droplet sauter mean diameter downstream of a wet grid is almost always larger than the droplet diameter upstream of the grid. The ratio of the sauter mean diameters is found to be higher for a smaller value of the droplet diameter upstream of the grid. The Weber number of the droplets represents the ratio of the inertia to surface tension forces acting on the droplet. The Weber number is given by

$$We = \frac{\rho v^2 d}{\sigma} \tag{5-28}$$

The variation of the ratio of the sauter mean diameter is plotted as a function of the upstream droplet Weber number in figure 5-18. The value of slip ratio and c_1 were both fixed at 0.8 while the void fraction was allowed to vary between 0.995 and 0.999. Three different upstream droplet diameters, 0.3 mm, 0.5 mm and 0.8 mm, were used to obtain the results.

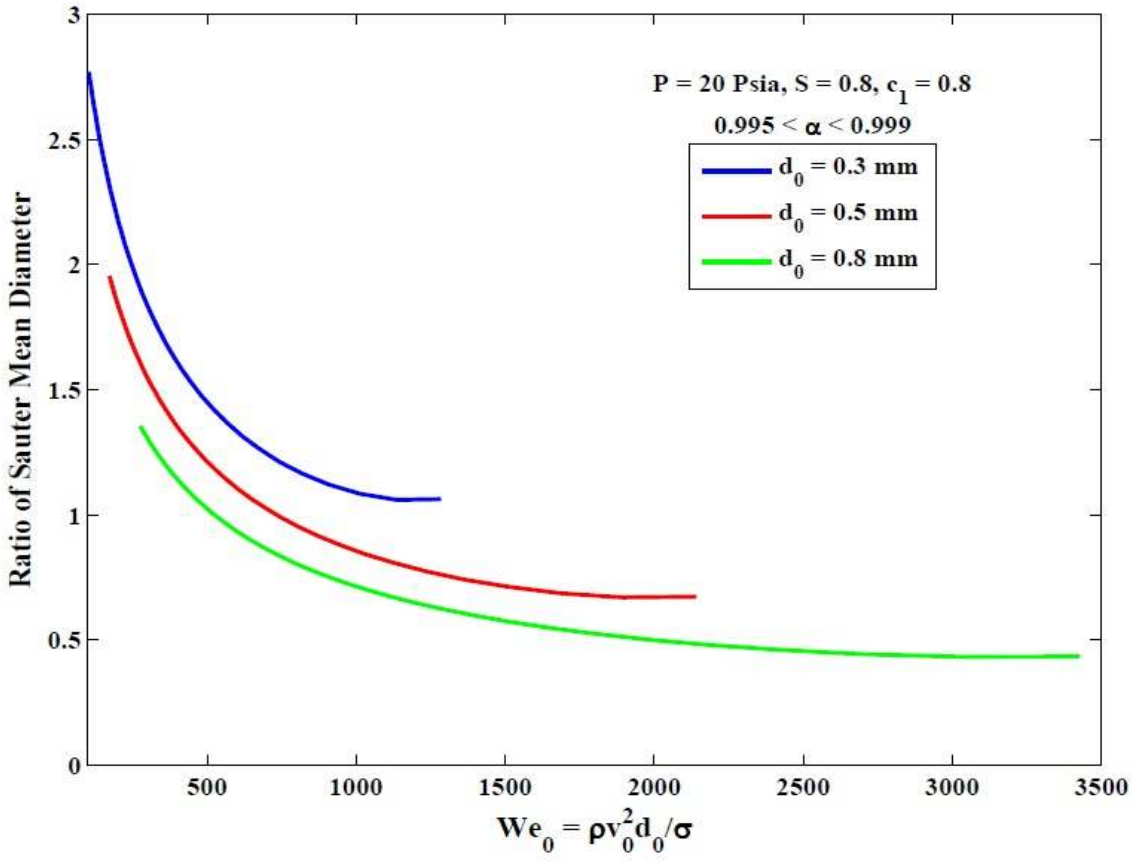

Figure 5-18. Variation of the Ratio of Sauter Mean Diameters with Upstream Droplet Weber Number for constant c_1 and S.

5.3 Development of a Numerical – Based Correlation for the Wet Grid Phenomena

From the results presented in the previous section, it can be concluded that the downstream to upstream ratio of the sauter mean diameters of droplets in a wet grid scenario is a strong function of the void fraction (α), the slip ratio (S), the fraction of the spacer grid length occupied by the flat portion of the liquid film (c_1) and the upstream droplet diameter (d_0). From a practical utility point of view (such as implementation of the model in systems analysis codes like COBRA – TF and TRACE), an empirical correlation to predict the downstream to upstream ratio of the sauter mean diameter was developed. It was found that the numerical data could be collapsed onto a single curve approximately if the quantity $S^{-1.1}We_0^{0.3}\left(\frac{d_{32}}{d_0}\right)^{1/3}$ was plotted against c_1x (x is the mass quality). Then, a correlation for the ratio of the sauter mean diameter of the droplets was obtained by fitting a curve to above data. This correlation is given by

$$\frac{d_{32}}{d_0} = We_0^{-0.9}S^{3.3}f^3$$

$$f = 18.83x_1^{0.188} - 4.573$$

$$x_1 = c_1x = \frac{c_1\alpha\rho_g}{\alpha\rho_g + S(1-\alpha)\rho_f} \tag{5-29}$$

The correlation along with the numerical results obtained for the ratio of sauter mean diameter from the calculations mentioned above are shown in figure 5-19. The green lines in the figure correspond to a value of 10 % above and below that predicted by the correlation. Clearly, the correlation predicts the results obtained for the sauter mean diameter ratio well within the ± 10% bound.

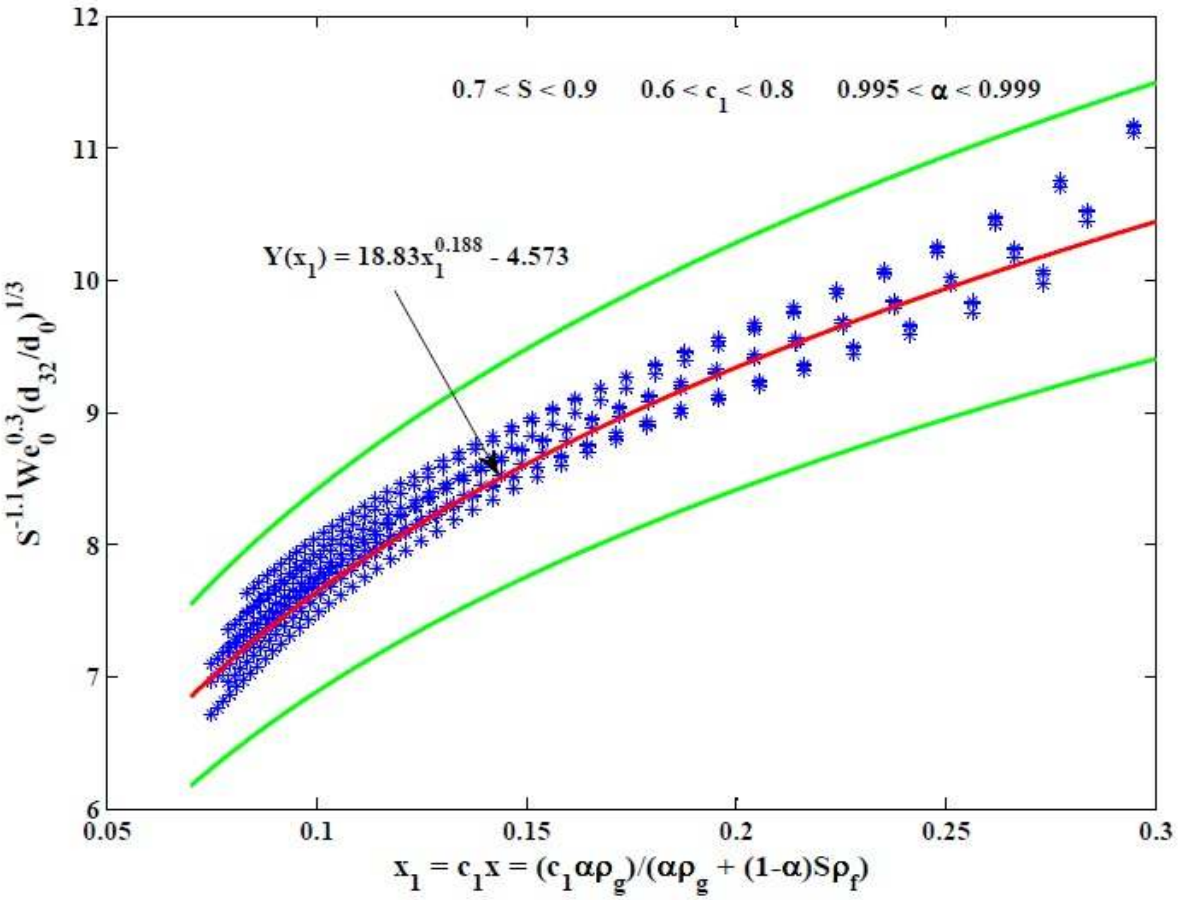

Figure 5-19. Correlation for the Ratio of the Sauter Mean Diameters in a wet grid scenario

5.4 Calculation of the Grid Enhanced Heat Transfer (GHET) Downstream of a Wet Grid

The evaporation of liquid film within a wet grid span results in considerable de – superheating of the steam. The reduction in steam temperature as it flows through the spacer grid is shown in the figure 5-20 below. In order to focus on the effect of a wet grid in enhancing the heat transfer downstream of a wet grid, the droplet size upstream of the grid was fixed at 0.5mm for the calculations.

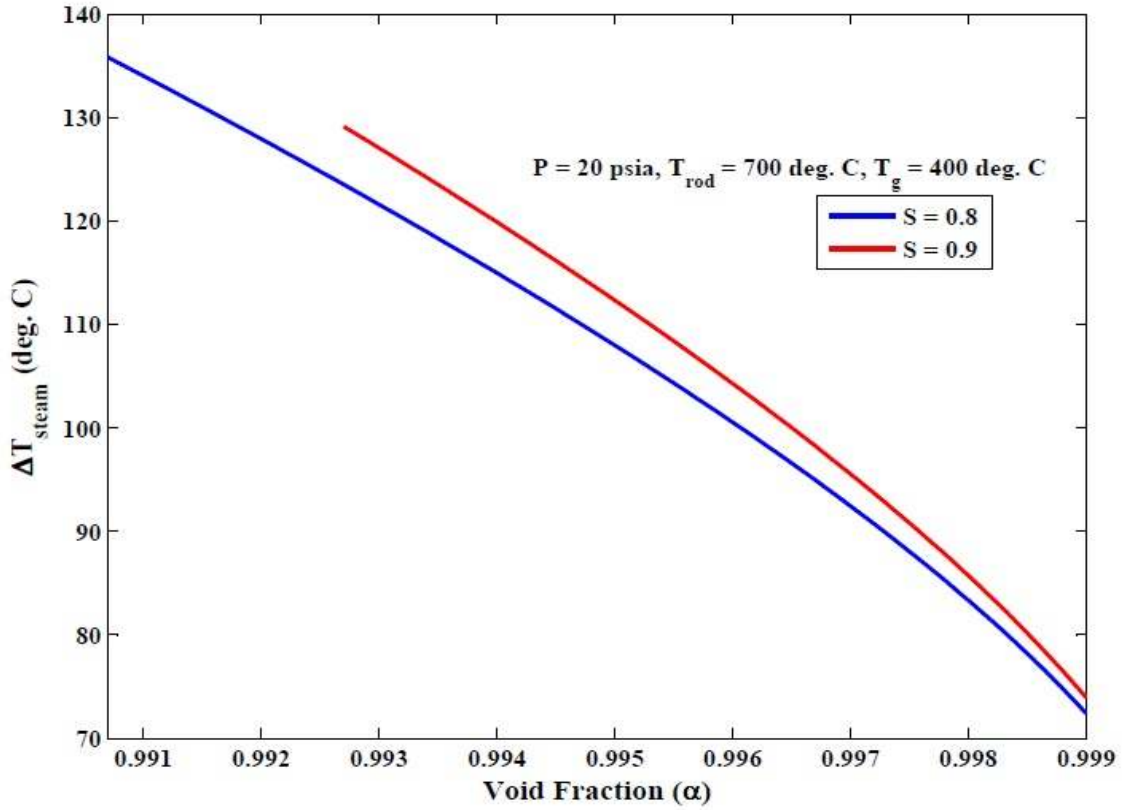

Fig. 5-20. Reduction in Steam Temperature on Flowing through a Wet Spacer Grid

It is now well known that a spacer grid augments heat transfer from the fuel rod during the reflood stage of a LOCA. Dry grid spacers are found to serve as an effective means of breaking large droplets into smaller droplets, thus substantially increasing the interfacial area between the liquid droplets and the steam. The reduction in droplet size is known to be dependent upon the Weber number of the incoming droplets, the blockage ratio of the grid spacer, and the volume fraction of the droplets in the dispersed phase. Increase in the droplet interfacial area promotes the rate of cooling of the rods. A model for the droplet induced heat transfer augmentation downstream of a dry grid was developed by Cheung et al [23] recently. Present systems analysis codes like COBRA – TF and TRACE fail to account for this increase in the heat transfer rate adequately. RBHT tests, however, indicate that at flooding rates equal to or more than 1 in/s, the spacer grids at the top quench earlier than the fuel rod resulting in the formation of a wet grid.

For wet grid spacers, the grids appear to act as a potential source of droplet production resulting in larger diameter droplets downstream as explained above (and observed in RBHT tests). It is of interest to know the effect of a wet grid spacer in comparison to a dry grid spacer in promoting heat transfer downstream of the spacer grid during the reflood stage of a LOCA. A model to predict the relative effectiveness of a wet grid in comparison to a dry grid was described in the previous chapter. Numerical solutions obtained for different values of the slip velocity, c_1 and void fraction are shown in figures 5-21 to 5-24 below.

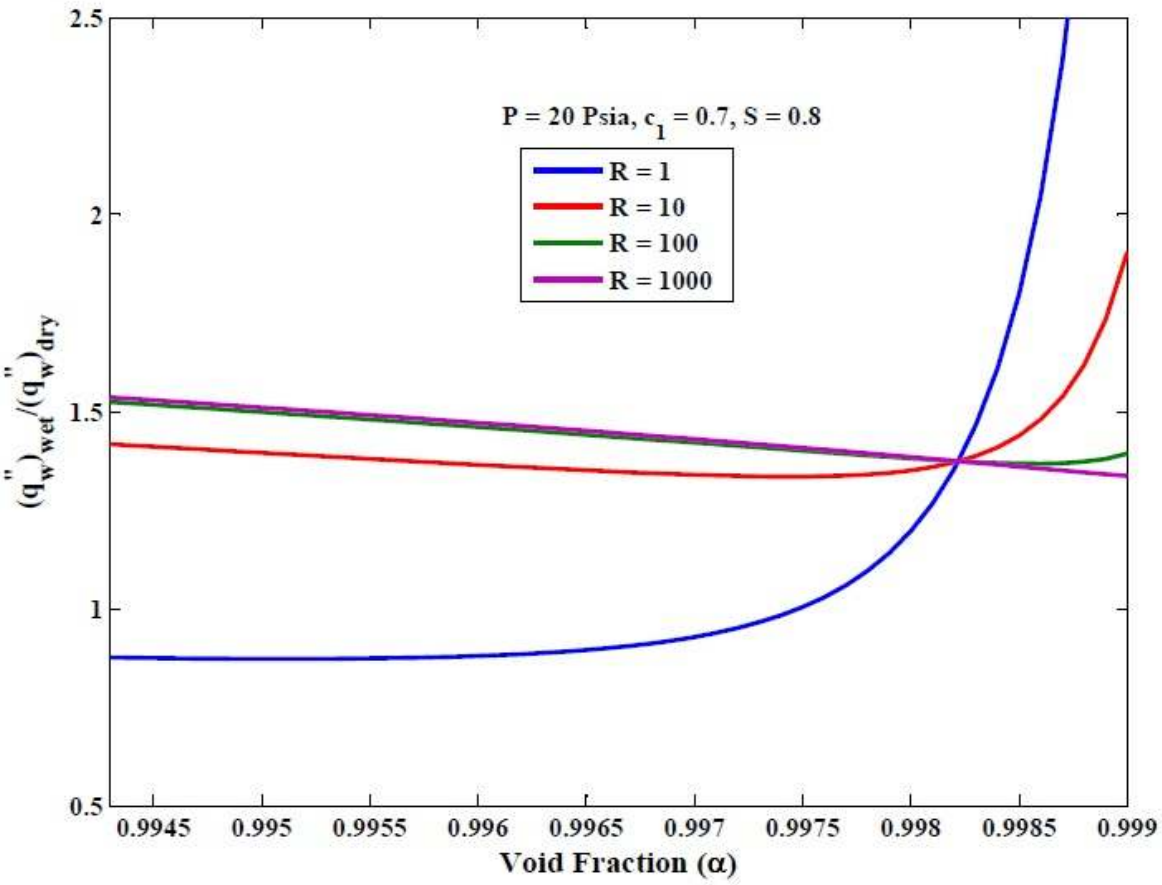

Fig. 5-21. Wet Grid to Dry Grid Wall Heat Flux Ratio

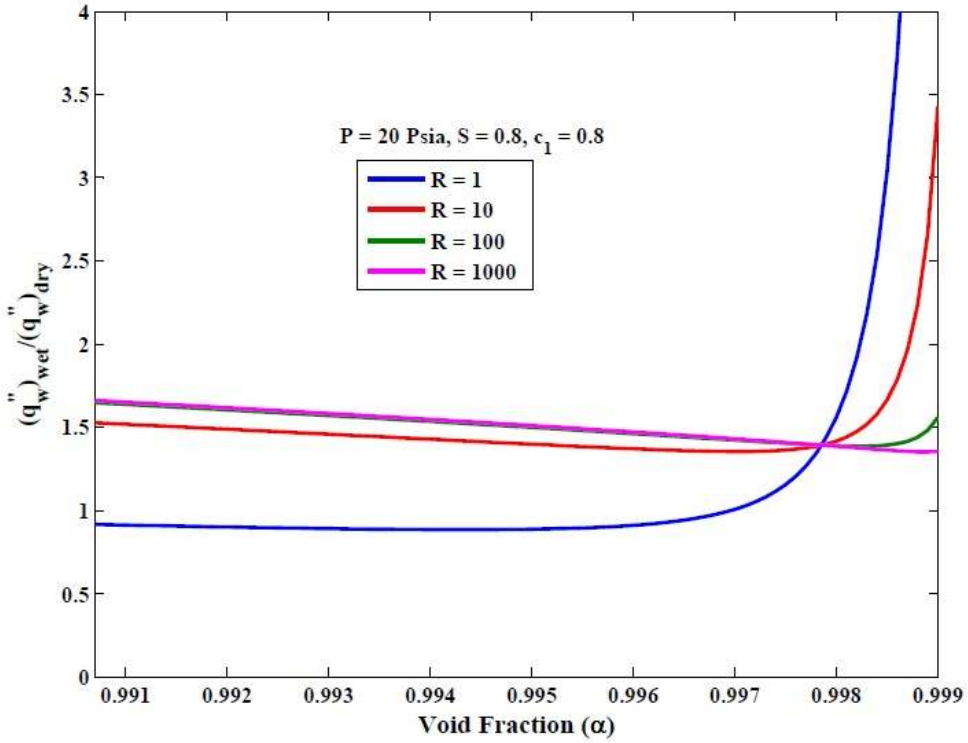

Fig. 5-22. Wet Grid to Dry Grid Wall Heat Flux Ratio

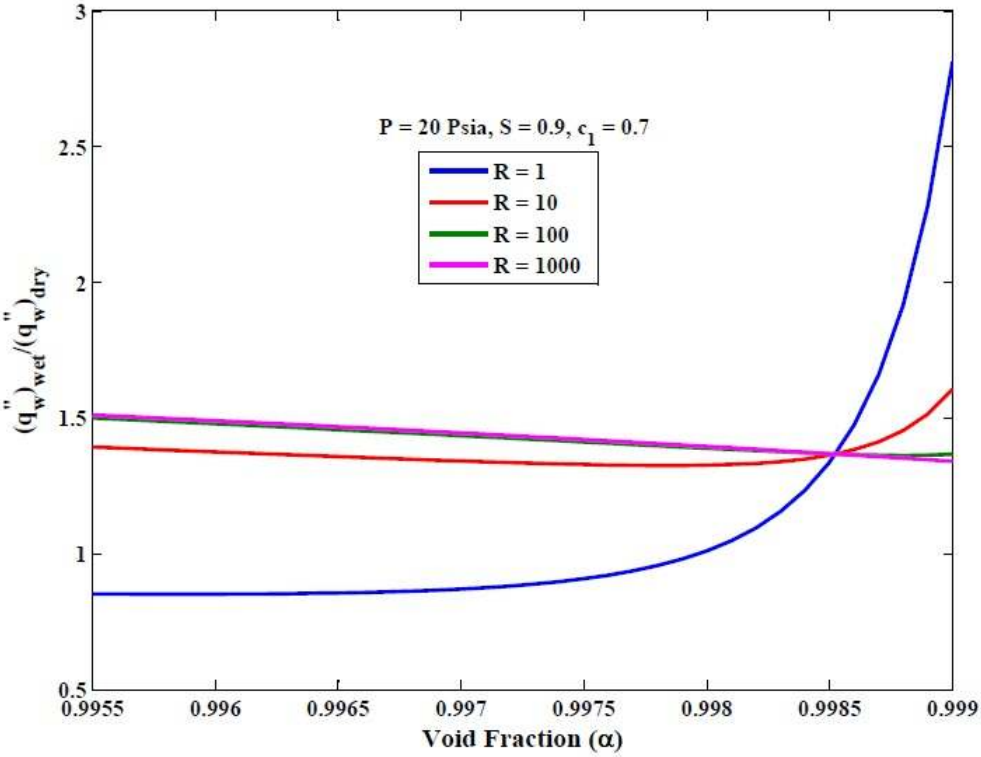

Fig. 5-23. Wet Grid to Dry Grid Wall Heat Flux Ratio

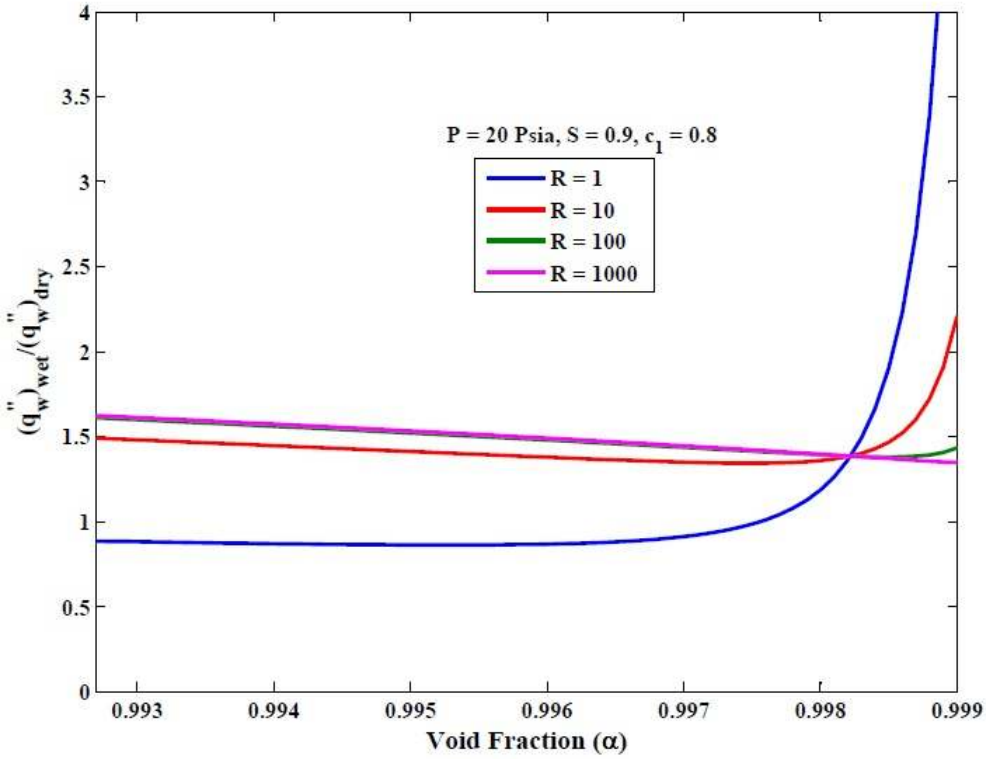

Fig. 5-24. Wet Grid to Dry Grid Wall Heat Flux Ratio

From the above figures, it is clear that a wet grid is more effective than a dry grid in augmenting the heat transfer rate downstream of a spacer grid. The parameter R describes the ratio of the steam velocity downstream of the grid to the increase in the steam velocity due to droplet evaporation downstream of a grid. The value of R is expected to be large (> 100) immediately downstream of the grid. A value of unity for R may not be physically realistic. The sharp increase in the heat flux ratio as the void fraction approaches unity can be explained to be due to the combination of reduction in droplet diameter (as explained above) and the reduction in steam temperature. At such high void fraction values, a wet grid begins to act like a dry grid in the sense that the droplet diameter downstream is smaller than that upstream (though the mechanism of generation of smaller diameter droplets is different from that of a dry grid). In addition to the decrease in droplet diameter, wet grid also results in a rapid de – superheating of

steam which is not present in a dry grid scenario. Consequently, the heat transfer rate increases tremendously in a wet grid situation at void fractions close to unity. For a given slip ratio, the heat transfer augmentation is higher for a higher value of c_1. This is due to the fact that at higher value of c_1 the droplet diameter downstream reduces, thereby increasing the interfacial area. Increased interfacial area results in a greater heat transfer from the steam to the droplets and in turn from the fuel rod to the steam.

It can be seen clearly that the presence of a spacer grid augments heat transfer downstream of the grid during the reflood stage of a LOCA. It is of utmost importance to account for this phenomenon in systems analysis codes like COBRA – TF and TRACE to obtain a precise response of the reactor core during the refold stage. However, it must be emphasized here that there is no experimental data available presently to validate the proposed wet grid model (both the increase in the droplet diameter part and the heat transfer augmentation part of the model). Separate effect bench top experiments need to be performed to obtain much needed data for model validation. Once validated, these models can be directly implemented into codes like COBRA – TF and TRACE.

CHAPTER 6

SUMMARY AND CONCLUSIONS

A physics-based wet grid model has been developed in this work to describe the wet grid phenomenon anticipated during the reflood stage of a large-break LOCA in a nuclear reactor. At moderate-to-high flooding rates, it has been observed in the RBHT and other rod bundle experiments that the spacer grids at elevations above the quench front undergo rewetting much earlier than the heater rods. A consequence of the grid rewetting is the establishment of thin liquid films on the surfaces of the grid spacers. The sizes of liquid droplet downstream of a wet grid are found to be appreciably larger than those found upstream of the grid indicating a distinctly different mechanism of droplet generation as compared to a dry grid scenario for which the droplets decrease in size as they pass through a dry grid.

In the present study, the wet-grid phenomenon is postulated to be consisting of four individual processes. The first process involves the deposition of liquid droplets from the dispersed two-phase flow mixture onto the grid spacer surface. The second process involves the establishment of a liquid film of equilibrium thickness on the surface of the spacer strap. The third process involves the entrainment of liquid ligaments from the liquid film due to the shear action of the steam flow. Finally, the fourth process involves the breakup of the ligaments into a number of fine droplets downstream of the grid. A mathematical model has been formulated for each of these processes which can be used to predict the droplet diameter downstream of a wet grid, given the flow and system conditions upstream of the grid. Results obtained from the model package so developed, however, are still parametric in nature because of insufficient experimental wet-grid data is available in the literature. Future experiments need to be performed to obtain the required database under wet grid conditions for model development and validation.

Once the present model is validated, it can be implemented directly into best estimate systems analysis codes such as COBRA–TF and TRACE for predicting the rate of cooling of the fuel rods during the reflood transients following a LOCA in a nuclear reactor.

After obtaining the droplet sizes downstream of a wet grid, a model has been proposed to compute the heat transfer enhancement in the presence of a wet grid. The heat transfer augmentation downstream of a wet grid is due to the combined action of steam de – superheating (as a result of heat transfer in the form of latent heat of vaporization associated with the evaporation of the liquid film) and steam acceleration (as a result of mass addition from film and droplet evaporation). Results obtained for the heat transfer augmentation due to the presence of a wet spacer grid show that a wet grid is more effective in promoting heat transfer downstream of the grid as compared to a dry grid. It is utmost essential to account for the presence of a wet grid in systems analysis codes like COBRA – TF and TRACE to predict the thermal hydraulic response of the reactor core during a LOCA precisely. However, similar to the wet grid model, lack of experimental data makes it impossible to validate the present model. Heated steam – water experiments need to be carried out to obtain the much needed heat transfer augmentation data under both dry grid and wet grid conditions.

Based on the limited results obtained in the present study, the following preliminary conclusions can be made:

1. Experimental evidence clearly indicates that spacer grids located in the upper portion of a rod bundle could become wet well before the arrival of the quench front even under low-flooding-rate conditions as observed in the RBHT tests. The sizes of liquid droplets downstream of a wet grid are considerably larger than those produced by a dry grid, indicating a distinctly different droplet formation mechanism. In the range of void fractions

considered in the present study (i.e., 0.99 to 0.999) the downstream to upstream ratio of droplet diameters varied between 3.0 and 0.8.

2. Depending on the bundle power and the flooding rate, the spacer grids can be quenched before quenching of the fuel rods because the grids are unpowered. Liquid films would form on the grid spacers following quenching of the grid, which could radically change the subsequent droplet formation mechanism. Wet grid could act as a major source for the generation of new droplets especially in the upper portion of rod bundle where PCT occurs.
3. The equilibrium film thickness was found to be of the order of 0.05 mm (varying between 0.12 mm and 0.01 mm) and tends to decrease as the void fraction is increased. This is because with an increase in the void fraction, the amount of liquid droplets in the dispersed two-phase mixture reduces resulting in less deposition and consequently a reduced film thickness. The velocity in the liquid film was in the range of 0.7 to 0.1 m/s. Similar to the equilibrium film thickness, the flat liquid film velocity tends to decrease as the void fraction is increased. However, the velocity of the corner liquid mass is found to increase with an increase in the void fraction.
4. The velocity of the liquid film is strongly dependent on the distribution of the liquid mass (including both the corner mass and the flat film) on the surface of the grid spacer. This in turn is a function of the flow and system conditions including the upper plenum pressure, void fraction, fuel rod temperature, and grid blockage ratio. Data relevant to wet grid phenomenon is presently lacking in the literature. Separate effect bench top experiments need to be carried out in order to validate the model under various flow conditions so that it can be implemented into systems analysis codes.

5. The spacer-grid models currently employed in transient system analysis codes such as COBRA-TF and TRACE which are applicable only for dry grids, cannot be applied under wet-grid conditions. The droplet field downstream of a wet grid could be appreciably different than those described by the existing correlations employed in transient system analysis codes. Without incorporating an appropriate wet-grid model in these codes, the steam and cladding temperatures could not be accurately predicted during numerical simulations of the reflood transients.
6. A wet spacer grid is found to provide a greater heat transfer augmentation downstream of a spacer grid than a dry spacer grid. This is because in a wet grid scenario, the heat transfer augmentation occurs due to the strong effect of steam de – superheating and steam acceleration. The superheated steam is found to lose as much as 100 deg. C on flowing through the span of a wet spacer grid. On the other hand, in a dry grid scenario, the heat transfer augmentation is primarily due to the acceleration of steam. The augmentation in heat transfer under a wet grid scenario is found to be as much as three times that due to a dry grid for void fractions very close to unity.
7. A physics-based wet-grid model package such as the one being developed in the present study that adequately accounts for the droplet generation mechanism downstream of a wet grid and the grid-enhanced heat transfer (GEHT) due to the wet grid effect should be implemented into TRACE and other transient system analysis codes so as to improve the PCT predictions under wet-grid conditions.

CHAPTER 7

RECCOMENDATIONS FOR FUTURE WORK – EXPERIMENTAL NEEDS

Although a physics-based model package for the wet grid phenomena and Grid Enhanced Heat Transfer (GEHT) has been developed in this study, the various components of the model package cannot be fine-tuned and validated because of the absence of experimental data. At the present time, very little data relevant to the wet-grid phenomenon occurring during reflood transients is available that can be used for model development and code validation. Separate-effect bench-top experiments need to be conducted to simulate the entrainment of liquid ligaments by a shear flow of superheated steam over a thin liquid film on a grid spacer strap and the subsequent formation of a new droplet field. More importantly, wet-grid-focused tests need to be performed subjected to prescribed flow conditions in the RBHT facility to obtain confirmatory data for assessment of models and validation of TRACE.

To gather new droplet data in a rod bundle setting covering a suitable range of grid blockage ratios, it is recommended that a shorter section of rod bundle with interchangeable spacer grids be designed and fabricated. The section should be designed such that spacer grids with distinctly different blockage ratios can be easily installed for use in a prescribed series of wet-grid-focused tests. Hydrophilic coating (Wang et al. [33]) should be used to promote wetting of the grid spacer straps. To facilitate the construction and operation of such a test assembly, dummy heater rods without power should be used in the test section and the housing should be made of transparent material for flow visualization. The tests should be focusing on the hydrodynamic aspects of the equilibrium film on a simulated grid space strap, the shearing off of the film to form liquid ligaments, and the subsequent breakup of the ligaments to generate new droplets. Measurements of the drop size distribution and the droplet velocities should be made at two separate locations

immediately upstream and downstream of a spacer grid using the upgraded VisiSizer system from Oxford Lasers.

The above adiabatic test setup, when operated under wet-grid conditions, should provide useful data for fine-tuning and validation of the various components of the model package pertinent to the wet-grid phenomena presented in this work. Moreover, the adiabatic test setup could readily be modified and upgraded using actual heater rods rather than dummy rods to obtain heat transfer data under wet-grid conditions to determine the GEHT due to wet grids and dry grids, respectively.

REFERENCES

[1] Keeyes et al,1970,"Liquid entrainment in adiabatic steam–water flow at 500 and 1000 psia", *UKAEA Report AERE-R6293*

[2] Wurtz J, 1978, "An experimental and theoretical investigation of annular steam water in tubes and annuli at 30 and 90 bar", *Riso Report 372*

[3] Singh et al, 1969, "Liquid film flow rates in two-phase flow of steam and water at 1000 psia", *AIChE J*, Vol 15, pp 51 – 56.

[4] Dallman J C, 1978, "Investigation of Seperated Flow Model in Annular Gas Liquid Two Phase Flows", *Phd Thesis*, University of Illinois at Urbana Chanpaign.

[5] Ishii M., Grolmes M. A., 1975, "Inception Criteriafor Droplet Entrainment in Two – Phase Co – current Film Flow", *AIChE J*, Vol 21, pp 308 – 318.

[6] Ishii M, Kataoka I, Kocamastafougullari G., 1981, "Phenomenological modeling of Two Phase Flow in Water Reactor at ANL", *9th Water Reactor Safety Research Information Meeting*, Gaithersburg.

[7] Sugawara S.,1990, "Droplet deposition and Entrainment Modeling based on Three Fluid model", *Nucl Eng. Des.*, Vol 122, pp 67 – 84.

[8] Hewitt G. F., Govan A., 1990, "Phenomenological Modeling of Non Equilibrium flows with Phase Change", *Int J Heat Mass Transfer*, Vol 33, pp 229 – 242.

[9] Nigmatulin et al, 1996, "Entrainment and Deposition rates in a Dispersed Film Flow", *Int J Multiphase Flow*, Vol 22, pp 19 – 30.

[10] Lopez de Bertodano M. A., Assad A., Beus S. G., 2001, "Experiments for Entrainment rate of Droplets in the Annular Regime", *Int J Multiphase Flow*, Vol 27, pp685 – 699.

[11] Sawant P, Ishii M, Mori M, 2009, "Prediction of the Amount of Entrained Droplets in Vertical Annular Two Phase Flow", *Int J Heat Fluid Flow*, Vol 30, pp 715 – 728.

[12] Paleev II, Filipovich B S, 1966, "Phenomena of liquid transfer in two phase dispersed annular flow", *Int. J Heat Mass Transfer*, Vol 9, pp 1089 – 1093.

[13] Namie S, Ueda T, 1972, "Droplet Transfer in Two Phase Annular Mist Flow, Part 1: Experiment of Droplet Transfer Rate and Distributions of Droplet Concentration and Velocity", *Bulletin JSME*, Vol 15, pp 1568 – 1580.

[14] Namie S, Ueda T, 1973, "Droplet Transfer in Two Phase Annular Mist Flow, Part 2: Prediction of Droplet Transfer Rate", *Bulletin JSME*, Vol 16, pp 752 – 764.

[15] Issapour I, Lee S L, 1990, "Droplet Deposition from Mist Flow on a Paralle Vertical Wall", *Part. Part. SystCharact.*, Vol 7, pp 70 – 73.

[16] Trela M., Zembik J., Durkiewicz B., 1982, "Droplet Deposition on a Flat Plate from an Air – Water Turbulent Mist Flow", *Int J Multiphase Flow*, Vol 8, pp 227 – 238.

[17] Okawa T., KataokaI., 2005, "Correlations for mass transfer rate of droplets in vertical upward annular flow", *Int J Heat Mass Transfer*, Vol 48, pp 4766 – 4778.

[18] Schadel S A, Leman G W, Binder J L, Hanratty T J, 1990, "Rates of Atomization and Deposition in Vertical Annular Flow", *Int J Multiphase Flow,*Vol 16, pp 363 – 374.

[19] Ganic E N, Mastanaiah K, 1981, "Investigation of Droplet Deposition from a Turbulent Gas Stream", *Int J Multiphase Flow*, Vol 7, pp 401 – 422.

[20] El – Kassaby M M, Ganic E N, 1986, "Droplet Deposition in Two Phase Turbulent Flow", *Int J Heat Mass Transfer*, Vol 29, pp 1149 – 1158.

[21] Cheung, F. B. and Bajorek, S. M.,"Dynamics of Droplet Breakup Through a Grid Spacer in a Rod Bundle". To appear in *Nucl. Eng.Des.*, (2010).

[22] Cheung F B, Goverapet Srinivasan S, 2010, "Droplet Breakup on Dry Spacer Grids", *NRC – 04 – 07 – 094 Letter Report.*

[23] Cheung F B, Bajorek S M, Goverapet Srinivasan S, 2010, "Droplet-Induced Heat Transfer Augmentation Downstream of a Spacer GridDuring Dispersed Flow Film Boiling", To appear in *Proc. NUTHOS – 8*, Shangai, China.

[24] Carey Van P, 2008, "Liquid Vapor Phase Change Phenomena",*Taylor & FrancisGroup*, New York.

[25] Collier J G, Thome J R, 1994, "Convective Boiling and Condensation", *Oxford Press*

[26] Rosal E R, Lin T F, Mclellan I F, Brewer R C, 2002, "RBHT Test Facility Description Report", *PSU – ARL NRC-04-01 Report.*

[27] Hochreiter et al, 2007, "RBHT Reflood Heat Transfer Experiments Data Analysis"

[28] Timotika H, 1935, "Breaking up of a Drop of Viscous Liquid Immersed in Another Viscous Fluid which is Extending at a Uniform Rate", *Proc. Roy. Soc. London*, Vol 153, pp 302–318.

[29] Teng H, Kinoshita C M, Masutani S M, 1995, "Prediction of Droplet Size from the Breakup of Cylindrical Liquid Jet", *Int J Multiphase Flow*, Vol 21, pp 129 – 136.

[30] Faeth G M, 1995, "Spray Combustion: A Review", *Proc. 2nd Intl. Conf. Multiphase Flow*, Japan

[31] Kolev N I, 2005, "Multiphase Flow Dynamics 2", *Springer*, Germany

[32] Dombrowski N, Johns W R, 1963, "The Aerodynamic Instability and Disintegration of Viscous Liquid Sheets", *Chem. Eng. Sci.,* Vol 18, pp 203 – 214.

[33] Wang C C, Lee W S, Sheu W J, Chang Y J, 2002, "A Comparison of the Air-Side Performance of the Fin-and-Tube Heat Exchangers in Wet Conditions with and without Hydrophilic Coating", *Applied Thermal Engineering*, Vol 22, 267-278